

EUROPEAN ORGANISATION FOR NUCLEAR RESEARCH (CERN)



JHEP 10 (2019) 203
DOI: [10.1007/JHEP10\(2019\)203](https://doi.org/10.1007/JHEP10(2019)203)



CERN-EP-2019-136
13th November 2019

Measurement of the inclusive isolated-photon cross section in pp collisions at $\sqrt{s} = 13$ TeV using 36 fb^{-1} of ATLAS data

The ATLAS Collaboration

The differential cross section for isolated-photon production in pp collisions is measured at a centre-of-mass energy of 13 TeV with the ATLAS detector at the LHC using an integrated luminosity of 36.1 fb^{-1} . The differential cross section is presented as a function of the photon transverse energy in different regions of photon pseudorapidity. The differential cross section as a function of the absolute value of the photon pseudorapidity is also presented in different regions of photon transverse energy. Next-to-leading-order QCD calculations from JETPHOX and SHERPA as well as next-to-next-to-leading-order QCD calculations from NNLOJET are compared with the measurement, using several parameterisations of the proton parton distribution functions. The predictions provide a good description of the data within the experimental and theoretical uncertainties.

Contents

1	Introduction	2
2	ATLAS detector	3
3	Data sample and Monte Carlo simulations	4
4	Event selection	5
5	Background evaluation and signal extraction	6
6	Fiducial phase space and unfolding	8
7	Systematic uncertainties	9
8	Theoretical predictions	11
8.1	Theoretical uncertainties in the NLO QCD predictions	15
8.2	Theoretical uncertainties in the NNLO QCD prediction	16
9	Results	20
10	Summary and conclusions	28

1 Introduction

Prompt photons with large transverse momenta constitute colourless probes of the hard interaction and their production in proton–proton collisions, $pp \rightarrow \gamma + X$, provides a testing ground for perturbative QCD (pQCD). Prompt photons are defined as those that are not secondaries from hadron decays. Prompt-photon production is understood to proceed via two processes: the one in which the photon arises directly from the hard interaction (the direct-photon process) and the one in which the photon is emitted in the fragmentation of a high transverse momentum (p_T) parton (the fragmentation-photon process) [1, 2].

In proton–proton collisions, due to the abundance of photons from neutral-hadron decays and the contribution from the fragmentation process, prompt-photon production is studied by requiring the photons to be isolated. Measurements of inclusive isolated-photon production in pp collisions at centre-of-mass energies (\sqrt{s}) of 7, 8 and 13 TeV are available from the ATLAS [3–5] and CMS [6, 7] collaborations.

At the LHC the dominant contribution to prompt-photon production arises from the $qg \rightarrow q\gamma$ process. As a consequence, the production is sensitive to the gluon density in the proton [8–10] even at leading order (LO) in pQCD. A recent study [11] has included the ATLAS measurement of inclusive isolated-photon production at 8 TeV [4] in a next-to-next-to-leading-order (NNLO) QCD fit to obtain the parton distribution functions (PDF) of the proton. The inclusion of the ATLAS data leads to a reduction in the gluon density uncertainties [11].

Measurements of inclusive prompt-photon production also provide benchmarks to use in investigating novel approaches to parton radiation [12], next-to-leading-order (NLO) QCD corrections with matched parton showers [13], the relevance of threshold logarithms in QCD and electroweak corrections [14] and

NNLO QCD corrections [15–17]. More specifically, the production of prompt photons, which is less sensitive to hadronisation effects than that of jets, can be used to pursue an alternative QCD description based on the k_T factorisation approach combining off-shell amplitudes and transverse-momentum-dependent parton densities [12]. The prompt-photon data allow the investigation of the fragmentation contribution, which can be done either via fragmentation functions or through the inclusion of parton showers [13]. Electroweak corrections are likely to play an important role at the TeV scale and, thereby, measurements at photon transverse energies in that region would help to unveil such phenomena [14]. The prompt-photon measurements at the LHC are characterised by small uncertainties that demand precise theoretical predictions, e.g. those from NNLO QCD calculations [15–17], in order to fully exploit these data. Measurements involving isolated photons have also been used to constrain the contributions from new light scalar particles decaying into a photon pair [18].

This paper presents a measurement of isolated prompt-photon production in pp collisions at $\sqrt{s} = 13$ TeV with the ATLAS detector at the LHC using an integrated luminosity of 36.1 fb^{-1} . The differential cross section as a function of the photon transverse energy¹ (E_T^γ) is measured in different regions of the photon pseudorapidity (η^γ) for $E_T^\gamma > 125\text{ GeV}$ and $|\eta^\gamma| < 2.37$, excluding the region $1.37 < |\eta^\gamma| < 1.56$. In addition, the double-differential cross section as a function of $|\eta^\gamma|$ in different regions of E_T^γ is also presented. The results are based on a data sample with a more than ten-fold increase in statistics relative to the previous study [5]. The measurement presented here is found to be consistent with the previous one in the overlapping kinematic regions. This increase in statistics allows improvements in the calibration of the photon energy and reductions in the experimental systematic uncertainties affecting the cross-section measurement, as well as an extension of the coverage in E_T^γ to higher values than previously measured. In this analysis, the region where the measurement is limited by systematic uncertainties is extended to $E_T^\gamma \sim 1\text{ TeV}$, beyond what was achieved in the previous measurement. The NLO QCD predictions of JETPHOX [19, 20] and SHERPA [21] based on several parameterisations of the PDFs are compared with the measurement. The NNLO QCD prediction of NNLOJET [16], which has significantly reduced uncertainties due to fewer missing higher-order terms, is also confronted with the data.

2 ATLAS detector

The ATLAS detector [22–24] is a multipurpose detector with a forward–backward symmetric cylindrical geometry. It consists of an inner tracking detector surrounded by a thin superconducting solenoid, electromagnetic and hadronic calorimeters, and a muon spectrometer incorporating three large superconducting toroid magnets. The inner-detector system is immersed in a 2 T axial magnetic field and provides charged-particle tracking in the range $|\eta| < 2.5$. The high-granularity silicon pixel detector is closest to the interaction region and provides four measurements per track. The pixel detector is followed by the silicon microstrip tracker, which typically provides four three-dimensional space point measurements per track. These silicon detectors are complemented by the transition radiation tracker, which enables radially extended track reconstruction up to $|\eta| = 2$. The calorimeter system covers the range $|\eta| < 4.9$. Within the region $|\eta| < 3.2$, electromagnetic (EM) calorimetry is provided by barrel and endcap high-granularity lead/liquid-argon (LAr) calorimeters, with an additional thin LAr presampler covering $|\eta| < 1.8$ to correct

¹ ATLAS uses a right-handed coordinate system with its origin at the nominal interaction point (IP) in the centre of the detector and the z -axis along the beam pipe. The x -axis points from the IP to the centre of the LHC ring, and the y -axis points upwards. Cylindrical coordinates (r, ϕ) are used in the transverse plane, ϕ being the azimuthal angle around the z -axis. The transverse energy is defined as $E_T = E \sin \theta$, where E is the energy and θ is the polar angle. The pseudorapidity is defined as $\eta = -\ln \tan(\theta/2)$ and the angular distance is measured in units of $\Delta R \equiv \sqrt{(\Delta\eta)^2 + (\Delta\phi)^2}$.

for energy loss in material upstream of the calorimeters; for $|\eta| < 2.5$, the EM calorimeter is divided into three layers in depth. Hadronic calorimetry is provided by a steel/scintillator-tile calorimeter, segmented into three barrel structures within $|\eta| < 1.7$, and two copper/LAr hadronic endcap calorimeters, which cover the region $1.5 < |\eta| < 3.2$. The solid-angle coverage is completed out to $|\eta| = 4.9$ with forward copper/LAr and tungsten/LAr calorimeter modules, which are optimised for EM and hadronic measurements, respectively. Events are selected using a first-level trigger implemented in custom electronics, which reduces the maximum bunch crossing rate of 40 MHz to a design value of 100 kHz using a subset of detector information. Software algorithms with access to the full detector information are then used in the high-level trigger to yield a recorded event rate of about 1 kHz [25].

3 Data sample and Monte Carlo simulations

The data used in this analysis were collected with the ATLAS detector during the proton–proton collision running periods of 2015 and 2016, when the LHC operated at a centre-of-mass energy of $\sqrt{s} = 13$ TeV. Only events taken during stable beam conditions and satisfying detector- and data-quality requirements, which include the calorimeters and inner tracking detectors being in nominal operation, are considered. In the collected data sample the average number of pp interactions per bunch crossing is 24, while the total integrated luminosity is $36.1 \pm 0.8 \text{ fb}^{-1}$ out of which $3.22 \pm 0.07 \text{ fb}^{-1}$ corresponds to the 2015 running period. The uncertainty in the combined 2015–2016 integrated luminosity is 2.1% [26], obtained using the LUCID-2 detector [27] for the primary luminosity measurements.

The simulated events were produced using MC event generators and were passed through the GEANT4-based [28] ATLAS detector and trigger simulation programs [29]. They are reconstructed and analysed with the same programs chain as the data.

Simulated signal samples. Samples of prompt-photon events were generated using the programs PYTHIA 8.186 [30] and SHERPA 2.1.1 [21] to study the characteristics of signal events. In both cases, the event generation was performed using tree-level matrix elements, with the inclusion of initial- and final-state parton showers. Fragmentation into hadrons is described by the Lund string model [31] in the case of PYTHIA and by a modified version of the cluster model [32] in the case of SHERPA. The proton’s structure was parameterised by the LO NNPDF2.3 [33] PDF set for PYTHIA and by the NLO CT10 [34] PDF set for SHERPA. All samples include a simulation of the underlying event (UE), with parameter values set according to the ATLAS 2014 tune series (A14 tune) for PYTHIA [35] or to the tune developed by the authors of SHERPA for use in conjunction with the NLO CT10 PDF set. The PYTHIA simulation of the signal includes LO photon-plus-jet events from direct processes (the hard subprocesses $qg \rightarrow q\gamma$ and $q\bar{q} \rightarrow g\gamma$, called the ‘hard’ component) and photon bremsstrahlung in LO QCD dijet events (called the ‘bremsstrahlung’ component). The bremsstrahlung component is modelled by final-state QED radiation arising from calculations of all $2 \rightarrow 2$ QCD processes. The SHERPA samples were generated with LO matrix elements for photon-plus-jet final states with up to three additional partons ($2 \rightarrow n$ processes with n from 2 to 5); the matrix elements were merged with the SHERPA parton shower using the ME+PS@LO prescription [36]. The bremsstrahlung component is accounted for in SHERPA through the matrix elements of $2 \rightarrow n$ processes with $n \geq 3$. In the generation of the SHERPA samples, a requirement on the photon isolation at the matrix-element level is imposed using the criterion defined in Ref. [37]. This criterion, commonly called Frixione’s criterion, requires the total transverse energy inside a cone of size r in the η – ϕ plane around the generated final-state photon, excluding the photon itself, to be below a certain threshold, $E_T^{\max}(r) = \epsilon E_T^\gamma ((1 - \cos r)/(1 - \cos R))^n$, for all $r < R$, where R is the maximal cone size, n is the power

and ϵ is a constant such that ϵE_T^γ represents the threshold for $r = \mathcal{R}$. The parameters for the threshold are chosen to be $\mathcal{R} = 0.3$, $n = 2$ and $\epsilon = 0.025$. The criterion is applied to avoid divergencies in the matrix elements when the photon is collinear with a parton.

Simulated background samples. The main background to isolated-photon events arises from jets misidentified as photons. This background is subtracted using a data-driven technique, which is described in Section 5; thus, no MC sample is used to simulate this background. The background from electrons or positrons misidentified as photons is evaluated using MC samples generated with the program SHERPA 2.2.1 [21, 38–42]. The $pp \rightarrow Z/\gamma^* \rightarrow e^+e^- + X$ and $pp \rightarrow W \rightarrow ev + X$ processes were generated with matrix elements calculated for up to two additional partons at NLO and up to four partons at LO. The NNLO NNPDF3.0 PDF set [43] was used in conjunction with a dedicated set of parton-shower-generator parameter values (tune) developed by the SHERPA authors.

Simulation of pile-up. Pile-up from additional pp collisions in the same and neighbouring bunch crossings was simulated by overlaying each MC event with a variable number of simulated inelastic pp collisions generated using PYTHIA 8.186 with the ATLAS set of tuned parameters for minimum-bias events (A2 tune) [44] and the MSTW2008LO PDF set [45]. The MC events are weighted ('pile-up reweighting') to reproduce the distribution of the average number of interactions per bunch crossing observed in the data.

4 Event selection

Events were recorded using a single-photon trigger with a transverse energy threshold of 120 GeV (140 GeV) for the 2015 (2015 and 2016) data-taking period² and ‘loose’ photon identification requirements [25, 46].³ Events are required to contain at least one reconstructed proton–proton interaction vertex. The vertex with the highest sum of the p_T^2 of the associated tracks is selected as the primary vertex.

Photon candidates are reconstructed from clusters of energy deposited in the EM calorimeter and classified [46] as unconverted photon candidates (clusters without a matching track or without a matching reconstructed conversion vertex in the inner detector) or converted photon candidates (clusters with a matching reconstructed conversion vertex or a matching track consistent with originating from a photon conversion). The main background in the prompt-photon production measurement comes from an energetic π^0 or η meson which is misidentified as a photon because it decays into an almost collinear photon pair. Such energetic π^0 or η mesons are produced copiously inside jets. This background is reduced by the photon identification criteria and by requiring the photon candidate to be isolated. Photon candidates are identified by using variables that characterise the lateral and longitudinal electromagnetic shower development in the EM calorimeter and the energy fraction leaking into the hadronic calorimeter. Tight requirements are imposed on the shower shapes in the second layer and in the finely segmented first layer of the EM calorimeter as well as on the energy deposited in the hadronic calorimeter [46]. These requirements are optimised separately for unconverted and converted photon candidates and ensure the compatibility of the measured shower profile with that originating from a single photon impacting the calorimeter. Small differences in the average values of the shower-shape variables between data and simulation are observed and corrected for in simulated events prior to the application of the photon identification criteria. Three data-driven methods based on radiative Z decays, electron extrapolation and an inclusive sample of photon

² The single-photon trigger with the threshold of 120 GeV was kept unprescaled during 2015 whereas it had to be prescaled during 2016 due to the increase in instantaneous luminosity.

³ The discriminating variables used for ‘loose’ and ‘tight’ photon identification can be found in Table 1 of Ref. [46].

candidates [46] are used to measure the efficiency of the tight identification criteria. The results of the three methods agree in the overlapping kinematic regions and the measured efficiencies are above 90% (95%) for unconverted (converted) photon candidates with $E_T^\gamma > 125$ GeV. Efficiency scale factors are evaluated as the ratios of the measured efficiencies to the efficiencies obtained in simulation and are applied to photon candidates in simulated events. The resulting efficiency scale factors are compatible with unity and have uncertainties in the range 1%–3%, depending on E_T^γ and η^γ .

The photon isolation requirement is based on the amount of transverse energy (E_T^{iso}) inside a cone of size $\Delta R = 0.4$ around the photon candidate, excluding an area of size $\Delta\eta \times \Delta\phi = 0.125 \times 0.175$ centred on the barycentre of the photon cluster. The measured value of E_T^{iso} is computed from topological clusters of calorimeter cells [47] and is corrected for the expected leakage of the photon energy into the isolation cone as well as for the contributions from the UE and pile-up [48, 49]. The correction to E_T^{iso} from the combined effect of the UE and pile-up is evaluated using the jet-area method [50, 51] on an event-by-event basis and is typically 3.5 GeV (1.3 GeV) in the region $|\eta^\gamma| < 1.37$ ($1.56 < |\eta^\gamma| < 2.37$). In simulated events, E_T^{iso} is adjusted so that the peak position in the E_T^{iso} distribution coincides in data and simulation. After the corrections, E_T^{iso} is required to be less than $E_{T,\text{cut}}^{\text{iso}} \equiv 4.2 \times 10^{-3} \times E_T^\gamma + 4.8$ GeV [4].

The calibration of the photon energy in the calorimeter accounts for upstream energy loss as well as lateral and longitudinal leakages. The procedure used for photon energy calibration in Run 1 [52] is employed here, optimised for the detector configuration in Run 2 [53]. The energy of the cluster of calorimeter cells associated with the photon candidate is corrected using a combination of simulation-based and data-driven calibration factors determined from $Z \rightarrow e^+e^-$ events collected during the 2015 and 2016 data-taking periods. The calibration is performed separately for converted and unconverted candidates. The uncertainty in the photon energy scale at $E_T^\gamma = 125$ GeV varies in the range 0.4%–3.1% (0.4%–2.7%) for unconverted (converted) candidates depending on $|\eta^\gamma|$.

Events with at least one photon candidate with calibrated E_T^γ above 125 GeV and $|\eta^\gamma| < 2.37$ are selected. Candidates in the region $1.37 < |\eta^\gamma| < 1.56$, which includes the transition region between the barrel and endcap calorimeters, are not considered. Photon candidates with $125 < E_T^\gamma < 150$ GeV ($E_T^\gamma > 150$ GeV) are selected from the 2015 (2015 and 2016) data-taking period.

If an event contains more than one photon candidate satisfying the selection criteria above, only the highest- E_T^γ (leading) photon is considered for further study. The total number of selected events with a photon candidate with $E_T^\gamma > 150$ GeV ($125 < E_T^\gamma < 150$ GeV) is 7 012 797 (650 410). The kinematic requirements and the number of selected events in data in each $|\eta^\gamma|$ region are summarised in Table 1. Each region in $|\eta^\gamma|$ is divided into 16 bins of E_T^γ starting at $E_T^\gamma = 125$ GeV and ending at 2500 GeV. The binning is given by the following array of values of E_T^γ (in units of GeV): 125, 150, 175, 200, 250, 300, 350, 400, 470, 550, 650, 750, 900, 1100, 1500, 2000 and 2500. Some of the high- E_T^γ bins are not measured depending on the $|\eta^\gamma|$ region.

5 Background evaluation and signal extraction

After the event selection described above, there is a residual background contribution from jets misidentified as photons. This background is evaluated bin-by-bin using a data-driven technique [4, 5] and subtracted to obtain the signal yield. For this purpose, a two-dimensional sideband method is applied, based on a plane formed by the variable E_T^{iso} and the photon identification criteria. A photon candidate that fulfils the tight identification criteria is classified as ‘tight’; the requirements are described in Ref. [46]. A

Table 1: Definition of the phase-space region for the measurement and predictions. The (next-to) last row indicates the number of data events selected in each $|\eta^\gamma|$ region for $E_T^\gamma > 150$ GeV ($125 < E_T^\gamma < 150$ GeV). For $125 < E_T^\gamma < 150$ GeV only data from the 2015 running period are used while for $E_T^\gamma > 150$ GeV data from the 2015 and 2016 running periods are used.

	Phase-space region				
Requirement on E_T^γ	$E_T^\gamma > 125$ GeV				
Isolation requirement	$E_T^{\text{iso}} < 4.2 \times 10^{-3} \times E_T^\gamma + 4.8$ GeV				
Requirement on $ \eta^\gamma $	$ \eta^\gamma < 0.6$	$0.6 < \eta^\gamma < 1.37$	$1.56 < \eta^\gamma < 1.81$	$1.81 < \eta^\gamma < 2.37$	
Number of events with $125 < E_T^\gamma < 150$ GeV	182 754	248 538	74 405	144 713	
Number of events with $E_T^\gamma > 150$ GeV	2 030 144	2 696 077	814 623	1 471 953	

photon candidate is classified as ‘non-tight’ if it satisfies a modified set of requirements, but fails the tight identification. The modified set of requirements is built from the full list of tight requirements by removing four⁴ of the selections associated with the shower-shape variables computed from the energy deposits in the first layer of the EM calorimeter. The variables that are removed from the list of tight requirements are those that are least correlated with E_T^{iso} . Four regions are defined in the E_T^{iso} -tightness plane: a signal region (A) containing isolated ($E_T^{\text{iso}} < E_{T,\text{cut}}^{\text{iso}}$) tight photons; a background control region B consisting of non-isolated ($E_{T,\text{cut}}^{\text{iso}} + 2$ GeV $< E_T^{\text{iso}} < 50$ GeV) tight photons; a background control region C containing isolated non-tight photons; and a background control region D consisting of non-isolated non-tight photons.

The signal yield N_A^{sig} in region A is extracted by solving the equation

$$N_A^{\text{sig}} = N_A - R^{\text{bg}} \cdot (N_B - f_B N_A^{\text{sig}}) \cdot \frac{(N_C - f_C N_A^{\text{sig}})}{(N_D - f_D N_A^{\text{sig}})}, \quad (1)$$

where N_K , with $K = A, B, C, D$, is the number of events in region K and $R^{\text{bg}} = N_A^{\text{bg}} \cdot N_D^{\text{bg}} / (N_B^{\text{bg}} \cdot N_C^{\text{bg}})$ is the so-called background correlation, where N_K^{bg} with $K = A, B, C, D$, is the a priori unknown number of background events in each region. The number of signal events in each of the three background control regions (N_K^{sig}) is taken into account in Eq. (1) via the signal leakage fractions $f_K \equiv N_K^{\text{sig}} / N_A^{\text{sig}}$ with $K = B, C, D$. MC simulations of the signal are used to evaluate the signal leakage fractions. Equation (1) with $R^{\text{bg}} = 1$ can be understood as the relationship arising from the application of the standard ABCD method [48] taking into account the contributions from signal events in each region.

⁴ The four variables are $w_{s,3}$, f_{side} , ΔE_s and E_{ratio} [46]. These variables make use of the first layer of the EM calorimeter; this layer is segmented into high-granularity strips in the η direction. The variable $w_{s,3}$ is the lateral shower width calculated from three strips around the strip with maximum energy deposit. The variable f_{side} is the energy outside the core of the three central strips but within seven strips divided by the energy within the three central strips. The variable ΔE_s is the difference between the energy associated with the second maximum in the strip layer and the energy reconstructed in the strip with the minimum value found between the first and second maxima. The variable E_{ratio} is the ratio of the energy difference between the maximum energy deposit and the energy deposit in the secondary maximum in the cluster to the sum of these energies.

The ratio of the signal yield to the number of photon candidates in region A is used to estimate the signal purity and is above 90% in all bins of the measured distributions. The signal yield is extracted using leakage fractions from MC simulations and, hence, depends on the modelling of the final state. This dependence is studied by comparing the results obtained using either PYTHIA or SHERPA simulations. The calculations using the two generators lead to similar signal yields and the differences are taken as systematic uncertainties. The signal yields obtained using PYTHIA for the signal leakage fractions are taken as the nominal ones. The distributions of the signal yields as functions of E_T^γ in different regions of $|\eta^\gamma|$ are well described by the PYTHIA and SHERPA MC simulations, except for $E_T^\gamma \gtrsim 900$ GeV in the range $|\eta^\gamma| < 1.37$. The impact of this mismodelling in the measured cross section, which is estimated by reweighting the MC simulations so that the distributions have the same shape as the data and re-evaluating the unfolding correction factors (see Section 6), is found to be negligible.

For the nominal results it is assumed that the photon isolation and identification variables are uncorrelated for background events, i.e. $R^{\text{bg}} = 1$. The dependence of the signal yield on this assumption is investigated in validation regions, which are defined within the background control regions B and D . Region B is subdivided into two regions: region B' of tight photon candidates with $E_{\text{T},\text{cut}}^{\text{iso}} + 2$ GeV $< E_{\text{T}}^{\text{iso}} < E_{\text{T},\text{cut}}^{\text{iso}} + 10$ GeV and region B'' of tight photon candidates with $E_{\text{T}}^{\text{iso}} > E_{\text{T},\text{cut}}^{\text{iso}} + 10$ GeV. Likewise, region D is subdivided into two regions, D' and D'' , using the same separation in $E_{\text{T}}^{\text{iso}}$ as above. The four regions B' , B'' , D' and D'' are used to extract values of R^{bg} from the data after accounting for the signal leakage fractions in those regions using either PYTHIA or SHERPA MC simulations. The dependence on the signal leakage is investigated by increasing the lower limits on $E_{\text{T}}^{\text{iso}}$ for the validation regions, $E_{\text{T},\text{cut}}^{\text{iso}} + 2$ GeV ($E_{\text{T},\text{cut}}^{\text{iso}} + 10$ GeV), each time by 1 GeV up to $E_{\text{T},\text{cut}}^{\text{iso}} + 7$ GeV ($E_{\text{T},\text{cut}}^{\text{iso}} + 15$ GeV) for regions B' and D' (B'' and D''), keeping the width in $E_{\text{T}}^{\text{iso}}$ fixed to 8 GeV for the regions B' and D' . The maximum deviations of R^{bg} from unity in the validation regions vary in the range 15%–40% depending on E_T^γ and η^γ . The differences between the nominal signal yields and those obtained using the maximum deviations of R^{bg} from unity observed in the validation regions are taken as systematic uncertainties.

Electrons or positrons can be misidentified as photons and represent an additional source of background. This background is largely suppressed by the photon selection. The residual background contribution is evaluated using MC simulations of the Drell–Yan processes $Z/\gamma^* \rightarrow e^+e^-$ and $W \rightarrow e\nu$ and is found to be sub-percent in the phase-space region of the analysis. Accordingly, no subtraction is performed and a systematic uncertainty of the size of the evaluated background is assigned.

6 Fiducial phase space and unfolding

The measured differential cross section is unfolded from the distribution in E_T^γ separately for each of the four regions in $|\eta^\gamma|$ after the selection explained in Section 4 and after background subtraction, as discussed in Section 5. The phase-space region of the measurement closely follows the applied event selection and is indicated in Table 1. The fiducial phase-space region is defined at particle level for all particles with a decay length of $c\tau > 10$ mm; these particles are referred to as ‘stable’. The isolation requirement on the photon at particle level is based on the total transverse energy of all stable particles, excluding muons and neutrinos, in a cone of size $\Delta R = 0.4$ around the photon direction after the contributions from the photon itself and the UE are subtracted. The same subtraction procedure of the UE used at detector level is applied at the particle level. The particle-level requirement on $E_{\text{T}}^{\text{iso}}$ is also the same as the one used at detector level, i.e. $E_{\text{T}}^{\text{iso}} < E_{\text{T},\text{cut}}^{\text{iso}}$.

The distributions of the background-subtracted signal yields as functions of E_T^γ in different regions of $|\eta^\gamma|$ are unfolded to the particle level using the MC samples of events via a bin-by-bin technique which corrects for resolution effects and the efficiency of the photon selection through the formula

$$\frac{d\sigma}{dE_T^\gamma}(i) = \frac{N_A^{\text{sig}}(i) C^{\text{MC}}(i)}{\mathcal{L} \Delta E_T^\gamma(i)},$$

where $d\sigma/dE_T^\gamma(i)$ is the differential cross section in bin i , $N_A^{\text{sig}}(i)$ is the signal yield in bin i , $C^{\text{MC}}(i)$ is the unfolding correction factor in bin i , \mathcal{L} is the integrated luminosity and $\Delta E_T^\gamma(i)$ is the width of bin i . The unfolding correction factors are computed using the MC samples as $C^{\text{MC}}(i) = N_{\text{part}}^{\text{MC}}(i)/N_{\text{det}}^{\text{MC}}(i)$, where $N_{\text{part}}^{\text{MC}}(i)$ ($N_{\text{det}}^{\text{MC}}(i)$) is the number of events generated (reconstructed) in bin i at the particle (detector) level. The PYTHIA MC simulation is used in the evaluation of the unfolding correction factors to obtain the nominal cross section. The unfolding correction factors vary approximately between 1.1 and 1.3 depending on E_T^γ and $|\eta^\gamma|$. The dependence of the results on the modelling of the final state, namely the inclusion of higher-order tree-level matrix elements, the parton shower approach and the hadronisation model, is studied with the SHERPA MC simulation. The differences between the results obtained by using either the PYTHIA or SHERPA MC simulations are taken as systematic uncertainties. The cross section is also obtained using an iterative Bayesian unfolding method [54] and compared with the nominal result; the two results are consistent with each other independently of whether the PYTHIA or SHERPA MC simulations are used for the unfolding.

7 Systematic uncertainties

The sources of systematic uncertainty that affect the measurement are discussed below. These sources include the signal modelling, the background subtraction, the photon identification and isolation, the unfolding procedure, the modelling of pile-up, the trigger efficiency, the luminosity measurement and the photon energy scale and resolution. For some of the systematic uncertainties, the Bootstrap technique [55] is used to evaluate the data statistical influence on the uncertainties. The results are then used in a fit to smooth the systematic uncertainties.

Model dependence of the signal leakage fractions. The nominal signal leakage fractions used in the extraction of the signal yield are evaluated with the PYTHIA simulation. The effect of the implementation of the matrix-element calculation in the generator as well as the models used for the parton shower and hadronisation are evaluated by comparing the nominal results with those obtained using the SHERPA simulation for the determination of the signal leakage fractions (see Section 5). The differences are taken as systematic uncertainties. The resulting uncertainty in the measured cross section is always less than 2% and typically less than 1%.

Background subtraction. The data-driven background subtraction depends on the choice of background control regions. This dependence is studied by varying the lower limit on E_T^{iso} for regions B and D by ± 1 GeV, removing the upper limit on E_T^{iso} for regions B and D , as well as changing the choice of inverted photon identification variables. For the last variation, the analysis is repeated increasing or decreasing the number of the shower-shape variables computed from the energy deposits in the first layer of the EM calorimeter that are removed from the list of tight requirements used in the classification of non-tight photon candidates. For each variation, the differences between the nominal signal yields and those extracted using the modified background control regions are taken as systematic uncertainties. The

resulting uncertainties in the measured cross section due to the first two variations mentioned above are less than 0.2%. The third variation leads to uncertainties in the measured cross section that are less than 2% and typically less than 1%. As described in Section 5, a systematic uncertainty is assigned to the assumption $R^{\text{bg}} = 1$. The resulting uncertainty in the measured cross section is less than 2.5% and typically less than 1%. The background contribution from electrons or positrons misidentified as photons is sub-percent and a systematic uncertainty is included by assigning the full size of this background; as an example, the background from W (Z) decays is 0.22% (0.07%) for $|\eta^\gamma| < 0.6$.

Photon identification and isolation. The uncertainties in the efficiency scale factors, which are applied to simulated events to match the tight photon identification efficiency measured in data [46], are propagated to the measured cross section. The resulting uncertainty in the measured cross section is in the range 1%–3%. The uncertainties in the cross section due to the modelling of $E_{\text{T}}^{\text{iso}}$ in simulated events are evaluated by comparing the nominal results with those obtained using MC samples of events in which the data-driven correction to $E_{\text{T}}^{\text{iso}}$ is not applied (see Section 4). The resulting uncertainty in the measured cross section is less than 2% except for $E_{\text{T}}^\gamma > 500$ GeV in the regions $0.6 < |\eta^\gamma| < 1.37$ and $1.56 < |\eta^\gamma| < 1.81$, where it increases to 3%.

Model dependence of the unfolding. The nominal unfolding correction factors are computed using the PYTHIA simulation. As discussed in Section 6, the effects on the unfolding correction factors due to the matrix elements and the parton shower and hadronisation models employed in the generators are investigated. The difference in the cross section between the nominal result and that obtained using the SHERPA simulation for the determination of the unfolding correction factors is taken as a systematic uncertainty. The uncertainties in the measured cross section are less than 2% and typically less than 1%. The uncertainty in the cross section due to the statistical uncertainty of the MC samples is propagated into the measured cross section and typically amounts to less than 0.5%.

Pile-up. A variation in the pile-up reweighting of simulated events is included to cover the uncertainty in the ratio of the predicted to measured inelastic cross sections [56]. The resulting uncertainty in the measured cross section is less than 1.5%.

Trigger efficiency. The uncertainty in the trigger efficiency is estimated using the same methodology as in Ref. [25] and is propagated into the measured cross section. The uncertainty in the measured cross section is at most 0.4%.

Luminosity measurement. The uncertainty in the integrated luminosity is 2.1%. It is fully correlated between all bins with $E_{\text{T}}^\gamma > 150$ GeV of the cross section. For the bin with $125 < E_{\text{T}}^\gamma < 150$ GeV only data from the 2015 running period is used and the uncertainty in the luminosity measurement is not fully correlated with the uncertainty in the combined integrated luminosity corresponding to the 2015 and 2016 running periods. However, the impact of the uncorrelated part can be safely neglected.

Photon energy scale and resolution. A detailed analysis of the sources of uncertainty in the energy scale and resolution for photons was made with Run 1 data [52]. The same model is implemented and updated for Run 2 data [53]. The sources of uncertainty include: the uncertainty in the overall energy scale adjustment using $Z \rightarrow e^+e^-$ decays; the uncertainty in the non-linearity of the energy measurement at the cell level; the uncertainty in the relative calibration of the different calorimeter layers; the uncertainty in the amount of material in front of the calorimeter; the uncertainty in the modelling of the reconstruction of photon conversions; the uncertainty in the modelling of the lateral shower shape; the uncertainty in

the modelling of the sampling term;⁵ the uncertainty in the measurement of the constant term in Z -boson decays. The sources of uncertainty are modelled using independent components to account for their η dependence. A total of 76 individual components influencing the energy scale and resolution of the photon are identified to assess the overall uncertainty in the energy measurement. All the uncertainty components are propagated separately through the analysis to keep track of the information about the correlations between different bins. The systematic uncertainty in the measured cross section is evaluated by varying each individual source of uncertainty separately by $\pm 1\sigma$ in the MC simulations and then adding the uncertainty contributions in quadrature. The resulting uncertainties in the measured cross section are typically less than 0.5% for the energy resolution and in the range 1%–16% for the energy scale.

Total systematic uncertainty. The total experimental systematic uncertainty is calculated by adding in quadrature the uncertainties listed above. The total systematic uncertainty is in the range 3%–17%, depending on E_T^γ and the $|\eta^\gamma|$ region. The dominant sources of uncertainty arise from the photon energy scale, the photon identification efficiency and the integrated luminosity. Figure 1 shows the total systematic uncertainty for each measured cross section together with the dominant components. The systematic uncertainty dominates the total experimental uncertainty for $E_T^\gamma \lesssim 1$ TeV and $|\eta^\gamma| < 1.37$, whereas for higher E_T^γ values, the statistical uncertainty of the data limits the precision of the measurement, as can be seen in Figure 2. This represents an improvement relative to the previous measurement [5], where the region dominated by the systematic uncertainties was $E_T^\gamma \lesssim 600$ GeV.

8 Theoretical predictions

The NLO pQCD predictions are computed using two programs, namely JETPHOX 1.3.1_2 and SHERPA 2.2.2. The JETPHOX program provides NLO QCD calculations of the direct and fragmentation contributions to the prompt-photon cross section. The number of massless quark flavours is set to five. The renormalisation (μ_R), factorisation (μ_F) and fragmentation (μ_f) scales are chosen to be $\mu_R = \mu_F = \mu_f = E_T^\gamma$. Variations of these scales are considered to get an estimate of the uncertainties due to missing higher-order terms in the perturbative expansion (see Section 8.1). The nominal prediction is obtained using the MMHT2014 [57] PDF set and the BFG set II of parton-to-photon fragmentation functions [58], both of which are determined at NLO. The strong coupling constant is set to $\alpha_s(m_Z) = 0.120$ since it is the value assumed in the MMHT2014 PDF fit. For the electromagnetic coupling (α_{EM}), the low-energy limit of 1/137.036 is used. A parton-level isolation criterion is used which requires the total transverse energy from the partons inside a cone of size $\Delta R = 0.4$ around the photon direction to be below the same $E_{T,\text{cut}}^{\text{iso}}$ applied at particle and detector level; this isolation prescription is referred to as ‘fixed-cone isolation’. Predictions based on other PDF sets, namely CT14 [59], ABMP16 [60], HERAPDF2.0 [61] and NNPDF3.0 [43], are also compared with the data; in each case $\alpha_s(m_Z)$ is set to the value assumed in the PDF fit.

The SHERPA 2.2.2 program consistently combines parton-level calculations of $\gamma + (1, 2)$ -jet events at NLO in pQCD and $\gamma + (3, 4)$ -jet events at LO [39, 40] supplemented with a parton shower [41] while avoiding double-counting effects [42]. The sample of events generated with SHERPA 2.2.2 is different from the sample of events from SHERPA 2.1.1 described in Section 3. The former includes the higher-order virtual corrections for $\gamma + (1, 2)$ -jet and is not passed through the ATLAS detector simulation programs since the goal is to compare the SHERPA 2.2.2 prediction with the measured cross section. Photon isolation at the matrix-element level is applied by using Frixione’s criterion with $\mathcal{R} = 0.1$, $n = 2$ and $\epsilon = 0.1$ (see

⁵ The relative energy resolution is parameterised as $\sigma(E)/E = a/\sqrt{E} \oplus b/E \oplus c$, where a is the sampling term, b is the noise term and c is the constant term.

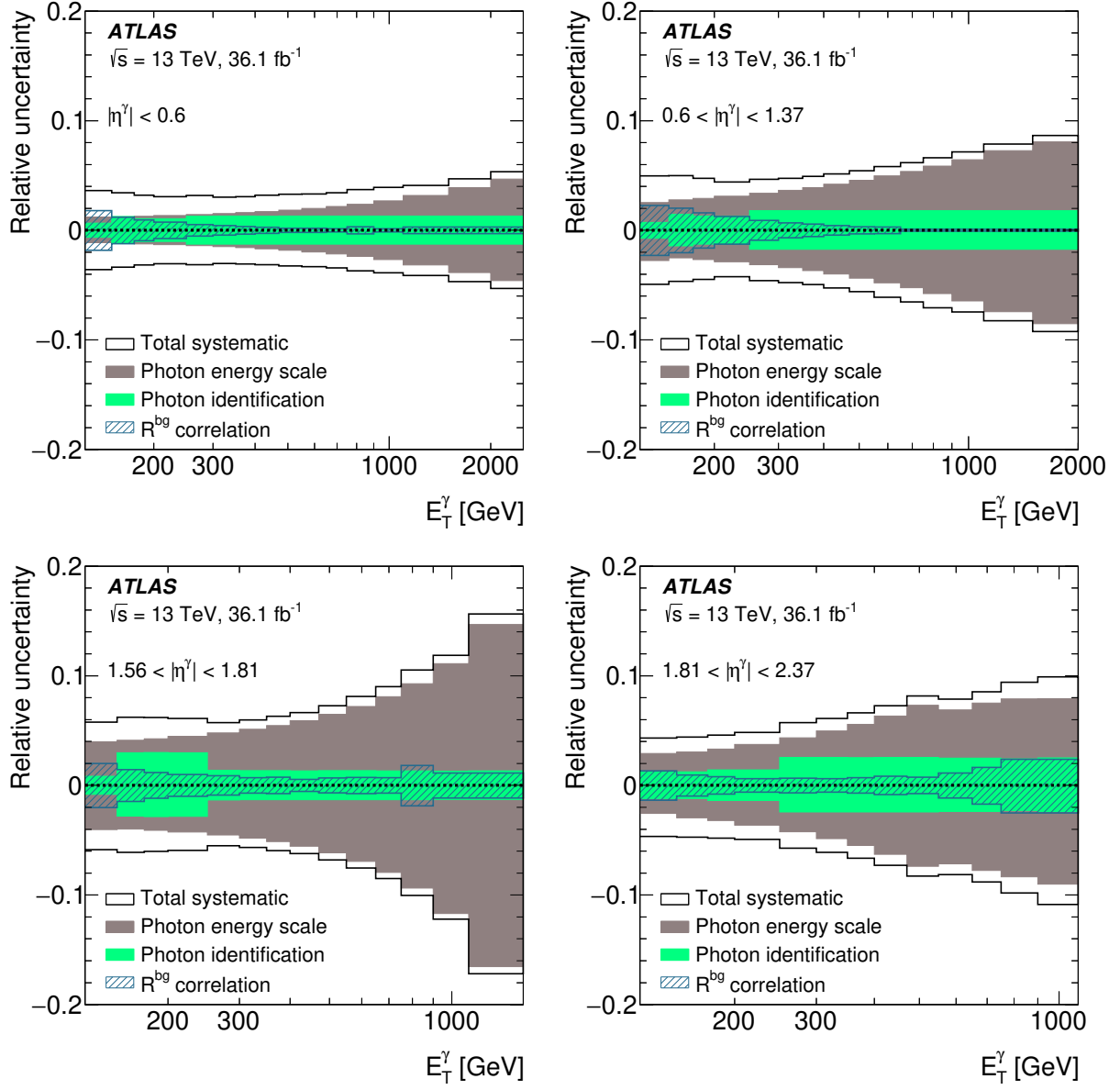


Figure 1: The relative total systematic uncertainty in the cross section (white areas) as a function of E_T^γ in different $|\eta^\gamma|$ regions. The relative uncertainty due to the photon energy scale (grey areas), the relative uncertainty due to the photon identification efficiency (green areas) and the relative uncertainty due to R^{bg} (blue hatched areas) are also shown.

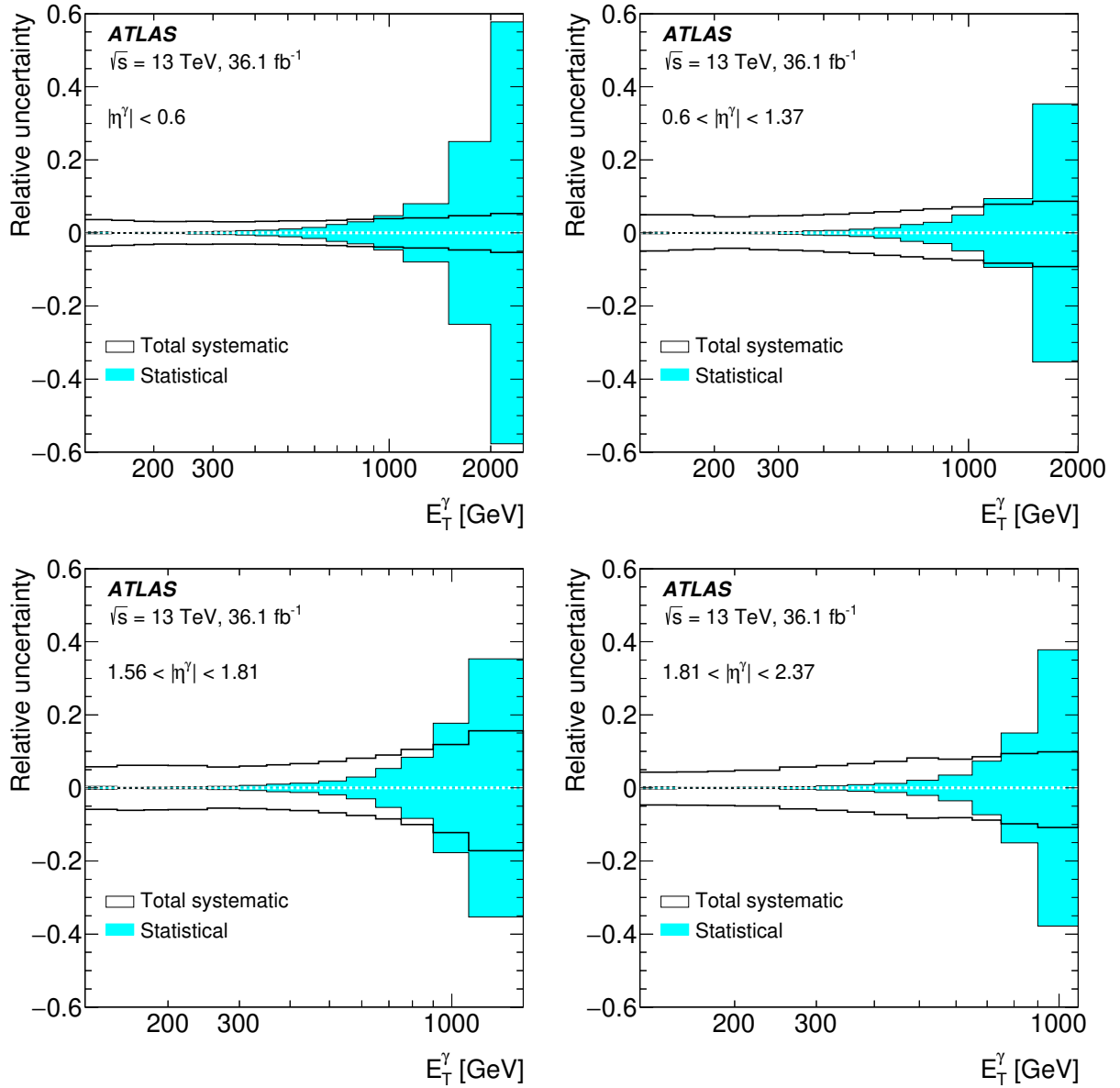


Figure 2: The relative total systematic uncertainty in the cross section (white areas) as a function of E_T^γ in different $|\eta^\gamma|$ regions. The relative statistical uncertainty from the data is also shown (cyan areas).

Section 3). The parameters are chosen to be as loose as possible to minimise a bias from the application of the photon isolation requirement at particle level. Since Frixione’s criterion requires the upper limit on the transverse energy isolation to be exactly zero at $r = 0$, the criterion cannot be strictly looser than any non-zero photon isolation requirement at detector or particle level for all $r < \mathcal{R}$. The photon isolation requirement is applied (see Table 1) using the procedure described in Section 6; the prescription employed is referred to as ‘hybrid-cone isolation’ [16, 62] since it includes the application of the Frixione’s criterion at a small value of ΔR ($\mathcal{R} = 0.1$) and the fixed-cone isolation at $\Delta R = 0.4$ used for the fiducial region of the measurement. Dynamic factorisation and renormalisation scales are adopted (E_T^γ) as well as a dynamical merging scale with $\bar{Q}_{\text{cut}} = 20$ GeV [62]. The strong coupling constant is set to $\alpha_s(m_Z) = 0.118$. The same prescription for the electromagnetic coupling as for the JETPHOX prediction is used. Fragmentation into hadrons and simulation of the UE are performed using the same models as for the SHERPA samples of simulated events presented in Section 3. The NNLO NNPDF3.0 PDF set is used in conjunction with the corresponding SHERPA tuning.

The NNLO QCD prediction is calculated [16] in the Nnlojet framework. The NNLO corrections include three types of parton-level contributions, namely the two-loop corrections to photon-plus-one-parton production, the virtual corrections to photon-plus-two-parton production and the tree-level photon-plus-three-parton production. Only direct-photon processes are included; fragmentation processes are circumvented by the application of the Frixione’s criterion at small ΔR using the same parameter settings as for the SHERPA 2.2.2 prediction. The photon transverse energy is used as the baseline choice for the renormalisation and factorisation scales. The NNPDF3.1 PDF set [63] at NNLO is used. The electromagnetic coupling is taken in the G_μ -scheme [64] as $\alpha_{\text{EM}}^{G_\mu} = 1/132.232$. Photon isolation is implemented following the ‘hybrid-cone isolation’ prescription described above. For the Nnlojet prediction the fixed-cone isolation at $\Delta R = 0.4$ is applied at the parton level using the same requirement as for the particle level. The prediction at NLO pQCD in the Nnlojet framework is also calculated to illustrate the improvements achieved by including the NNLO QCD corrections. The NLO QCD prediction of Nnlojet differs from that of JETPHOX in the fragmentation contribution, the photon isolation prescription, the value of α_{EM} and the PDF set.

There are several differences between the calculations using JETPHOX, SHERPA 2.2.2 and Nnlojet: the calculations from Nnlojet include NNLO QCD corrections; the calculations using SHERPA 2.2.2 include higher-order contributions as well as parton showers; the application of the Frixione’s criterion (SHERPA 2.2.2 and Nnlojet) at matrix-element level allows the fragmentation contribution to be ignored; and the prediction for the cross section using SHERPA 2.2.2 is at particle level and include UE effects. A compilation of the major features of the three different approaches is shown in Table 2.

Table 2: Major features of the three predictions used for inclusive isolated-photon production.

Program	Order in α_s	Fragmentation	Parton shower	Isolation	α_{EM}	Particle Level
JETPHOX	NLO	Yes	No	Fixed cone	1/137.036	No
SHERPA 2.2.2	NLO for $\gamma + (1, 2)$ -jet LO for $\gamma + (3, 4)$ -jet	No	Yes	Hybrid cone	1/137.036	Yes
Nnlojet	NNLO	No	No	Hybrid cone	1/132.232	No

Electroweak corrections are not included in the calculations of JETPHOX, SHERPA 2.2.2 or Nnlojet. As mentioned earlier, the corrections are likely to play an important role at the TeV scale. Electroweak Sudakov corrections for single photon production are available [65]. However, these constitute only

part of the full electroweak corrections since the real corrections are not included. The full electroweak corrections can differ significantly from the Sudakov corrections because the latter corrections and the real corrections partially cancel out when the presence of W or Z bosons in the final state is not vetoed. The measurement presented here does not preclude the presence of massive gauge bosons in addition to the high-transverse-momentum photon.

8.1 Theoretical uncertainties in the NLO QCD predictions

The major source of uncertainty affecting the predictions is due to terms beyond NLO in QCD. In the case of JETPHOX it is evaluated by repeating the calculations using values of μ_R , μ_F and μ_f scaled by the factors 0.5 and 2. The three scales are either varied simultaneously or independently; in addition, configurations in which one scale is fixed and the other two are varied simultaneously are also considered. In all cases, the condition $0.5 \leq \mu_A/\mu_B \leq 2$ is imposed, where $A, B = R, F, f$. The final uncertainty is taken as the largest deviation from the nominal value among the 14 possible variations; this is done separately for the positive and negative contributions, so the final uncertainty is not necessarily symmetric. In the case of SHERPA 2.2.2, which does not include the fragmentation contribution, μ_R and μ_F are varied as above and the largest deviation from the nominal prediction among the six possible variations is taken as the uncertainty. The resulting uncertainties in the prediction are 10%–15% (20%–30%) for JETPHOX (SHERPA 2.2.2). The fact that the uncertainties are larger for SHERPA than for JETPHOX is attributed to multi-jet configurations which are accounted for only in the case of SHERPA.

The uncertainty in the prediction of JETPHOX due to the uncertainty in the proton PDFs is estimated by repeating the calculations using the 50 sets from the MMHT2014 error analysis and applying the Hessian method [66]. In the case of SHERPA 2.2.2, it is estimated using the 100 replicas from the NNPDF3.0 analysis. The resulting uncertainties in the prediction is in the range 1%–6% for JETPHOX and 1%–9% for SHERPA 2.2.2, depending on E_T^γ and the $|\eta^\gamma|$ region.

The uncertainty in the prediction of JETPHOX (SHERPA 2.2.2) due to the uncertainty in α_s is evaluated by repeating the calculations using two additional sets of proton PDFs from the MMHT2014 (NNPDF3.0) analysis for which different values of α_s at m_Z are assumed in the fits, namely 0.118 (0.117) and 0.122 (0.119); in this way, the correlation between α_s and the PDFs is preserved. The uncertainties in JETPHOX associated with α_s are evaluated as the differences between the varied and the nominal cross sections scaled by a factor 1.5/2. This scaling factor accounts for the difference in $\alpha_s(m_Z)$ between the nominal and the $\alpha_s(m_Z)$ -varied calculations (0.002) and the uncertainty in $\alpha_s(m_Z)$ (0.0015) recommended by the authors of MMHT2014 [67]. The uncertainties in SHERPA 2.2.2 due to α_s are evaluated as the differences between the varied and the nominal cross sections scaled by a factor 1.5 to match the prescription used for MMHT2014. The resulting uncertainties in the prediction of JETPHOX (SHERPA 2.2.2) are less than 3% (6% except for the highest measured E_T^γ point in the region $1.81 < |\eta^\gamma| < 2.37$, where it increases to 12%).

Since the NLO pQCD prediction from JETPHOX is at the parton level while the measurement is at the particle level, correction factors for the non-perturbative (NP) effects of hadronisation and the underlying event are needed for the former to match the data. However, the data are corrected for pile-up and UE effects and the distributions are unfolded to a phase-space definition in which the requirement on E_T^{iso} at particle level is applied after subtraction of the UE. Therefore, corrections for NP effects are expected to be close to unity. They are evaluated by computing the ratio of the particle-level cross section for a PYTHIA sample with UE effects to the parton-level cross section without UE effects. The resulting corrections are consistent with unity within $\pm 1\%$. Thus, no correction is applied to the NLO QCD prediction of

JETPHOX and an uncertainty of 1% is assigned. The SHERPA 2.2.2 prediction is based on particle-level observables after applying the requirements listed in Table 1 and, therefore, can be compared directly with the measurement. Although no tunes are available to assess the impact of hadronisation and UE in the SHERPA 2.2.2 prediction, it is expected that the associated uncertainty is of a similar size as that evaluated using PYTHIA and, therefore, can be neglected in comparison to the other uncertainties.

The total theoretical uncertainty is obtained by adding in quadrature the individual uncertainties listed above (see Figures 3 and 4). The dominant theoretical uncertainty for the prediction using JETPHOX or SHERPA 2.2.2 is that arising from the variation of the scales. The uncertainty arising from the PDFs ($\alpha_s(m_Z)$) is the second dominant uncertainty for the prediction of JETPHOX (SHERPA 2.2.2). A prediction from JETPHOX using as scales $\mu_R = \mu_F = \mu_f = E_T^\gamma/2$ is also made and the associated theoretical uncertainties are calculated using the same procedure as above, including variations of the scales by the factors 0.5 and 2 with respect to $E_T^\gamma/2$.

8.2 Theoretical uncertainties in the NNLO QCD prediction

The uncertainty in the NNLO QCD prediction due to higher-order terms is evaluated by varying the renormalisation and factorisation scales as is done for the SHERPA 2.2.2 prediction (see Section 8.1). The resulting uncertainties are compared with those of the NLO QCD prediction from Nnlojet in Figure 5. The uncertainties in the NNLO QCD prediction arising from the scale variations are in the range 0.6%–5% and are smaller than those in the NLO QCD prediction by a factor in the range 2–20, depending on E_T^γ and η^γ . The uncertainties due to the PDFs and α_s are not available, but they are expected to be similar to, or smaller than, those affecting the JETPHOX prediction. For the comparison with the data in Section 9, the ‘total’ uncertainty associated with the Nnlojet prediction is taken as the sum in quadrature of the scale uncertainties, the statistical uncertainties of the calculations, the uncertainty of 1% assigned to the non-perturbative corrections (see Section 8.1) and, as an approximation, the uncertainties due to the PDFs and α_s as estimated from JETPHOX at NLO.

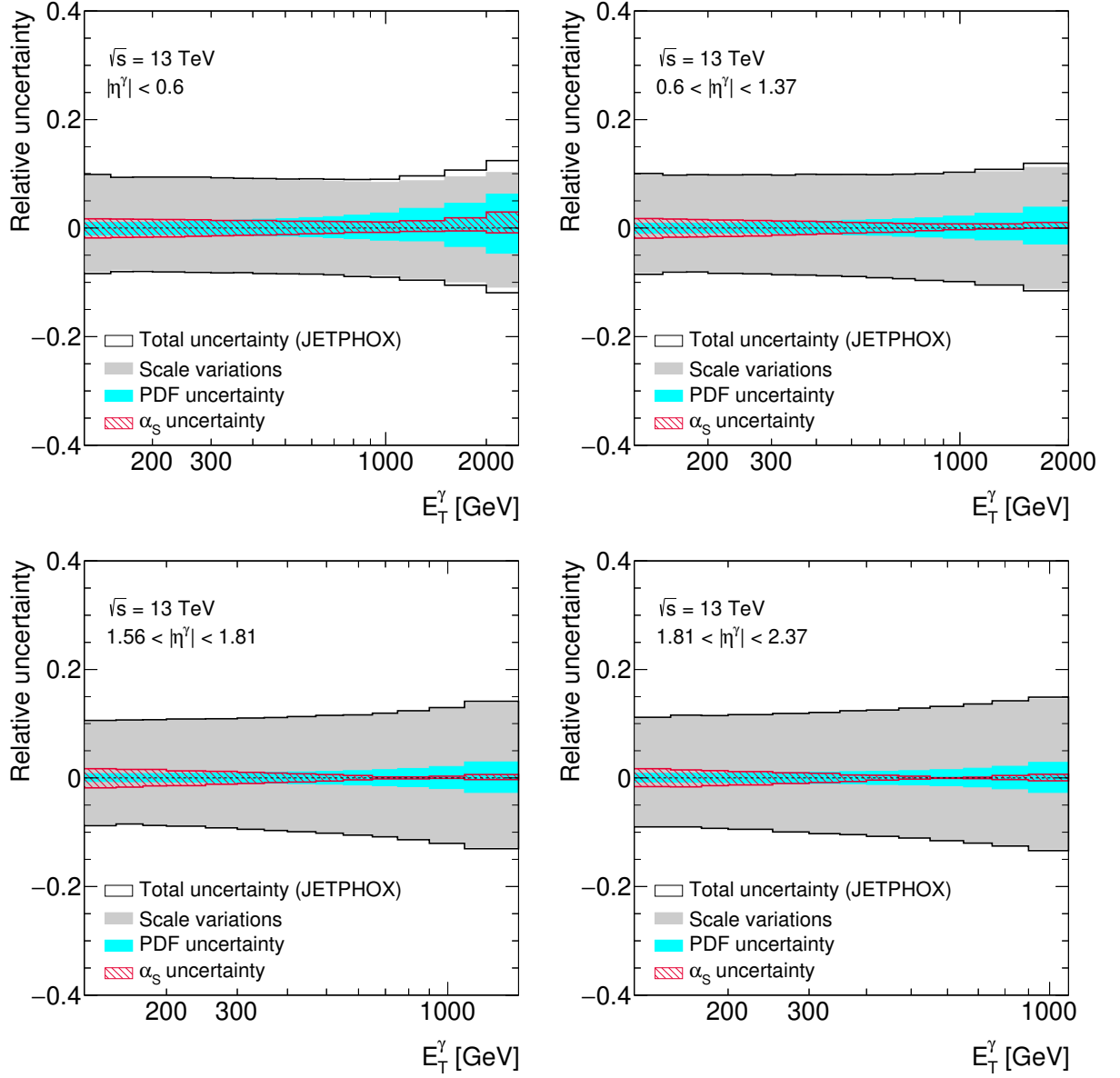


Figure 3: The relative total theoretical uncertainty in the cross-section prediction of JETPHOX as a function of E_T^γ in different regions of $|\eta^\gamma|$. The uncertainty from the scale variations, the uncertainty from the PDFs and the uncertainty from the value of α_s are also included.

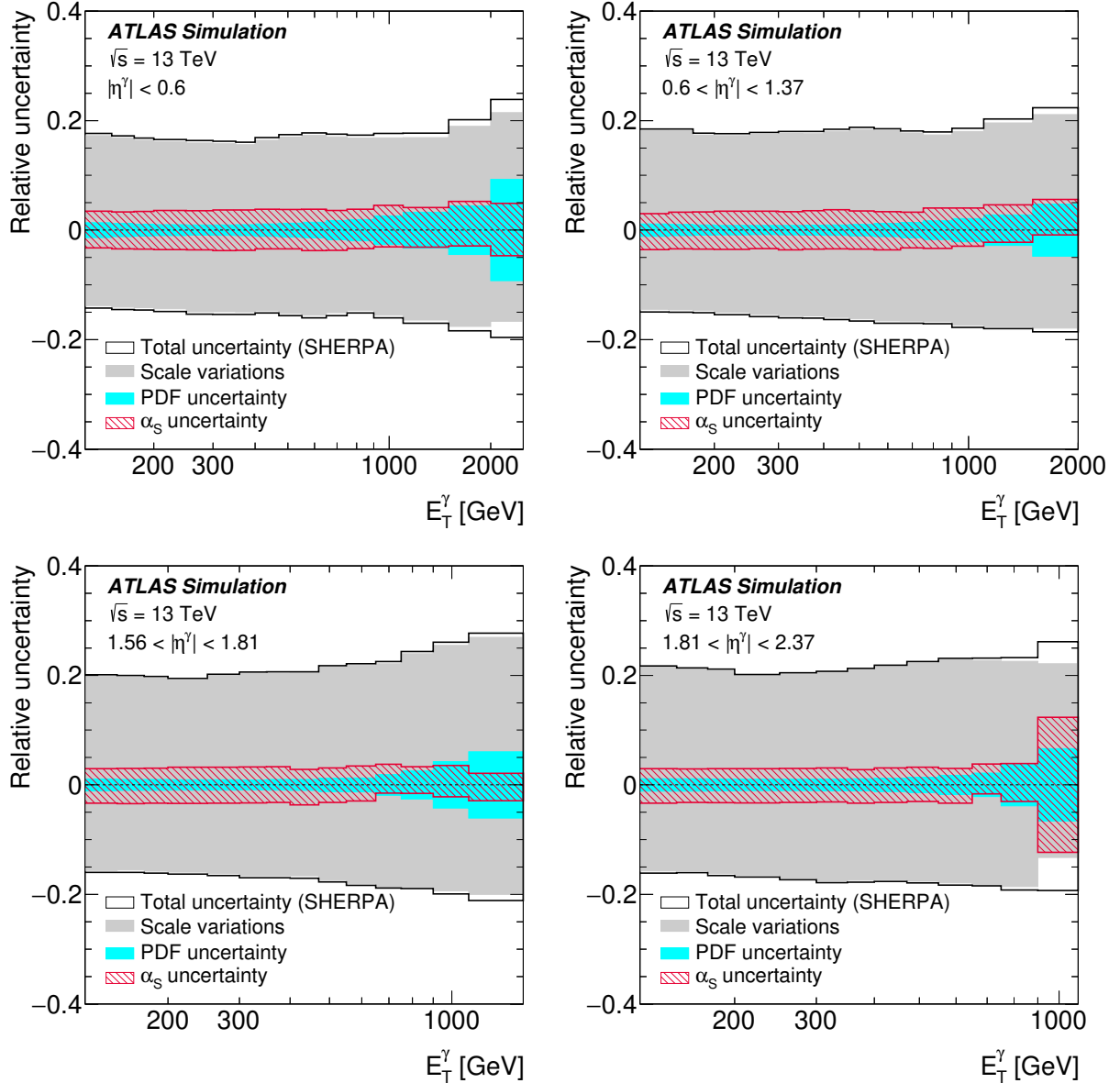


Figure 4: The relative total theoretical uncertainty in the cross-section prediction of SHERPA 2.2.2 as a function of E_T^γ in different regions of $|\eta^\gamma|$. The uncertainty from the scale variations, the uncertainty from the PDFs and the uncertainty from the value of α_s are also included.

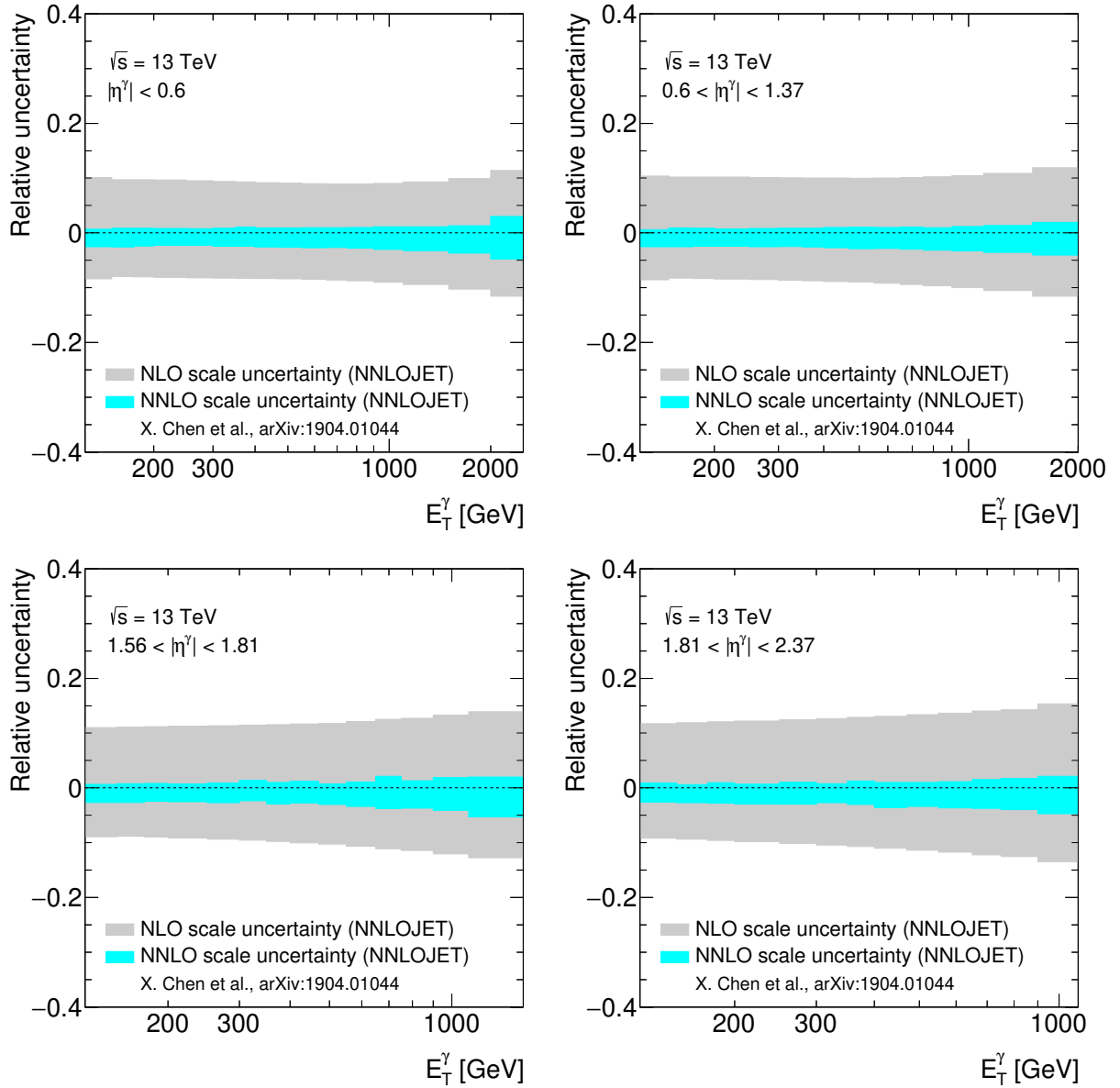


Figure 5: The relative theoretical uncertainty in the cross-section prediction of Nnlojet arising from the scale variations as a function of E_T^γ in different regions of $|\eta^\gamma|$: for NLO and NNLO QCD predictions.

9 Results

The measurement of the inclusive isolated-photon differential cross section as a function of E_T^γ in different regions of $|\eta^\gamma|$ is shown in Figure 6. In the region $|\eta^\gamma| < 0.6$ ($0.6 < |\eta^\gamma| < 1.37$) the cross section decreases by seven orders of magnitude in the measured range $125 < E_T^\gamma < 2500$ GeV ($125 < E_T^\gamma < 2000$ GeV). In the forward regions $1.56 < |\eta^\gamma| < 1.81$ and $1.81 < |\eta^\gamma| < 2.37$, the measured ranges are $125 < E_T^\gamma < 1500$ GeV and $125 < E_T^\gamma < 1100$ GeV, respectively, and the cross section spans approximately six orders of magnitude.

Figure 7 shows the inclusive isolated-photon double-differential cross section $d^2\sigma/d|\eta^\gamma|dE_T^\gamma$ as a function of $|\eta^\gamma|$ in different regions of E_T^γ . At high E_T^γ , the decrease of the double-differential cross section with increasing $|\eta^\gamma|$ is more prominent. Whereas the measured double-differential cross section decreases by 12% from the most central point to the most forward point for the lowest E_T^γ range, the decrease is 98% for the highest E_T^γ range.

The NLO QCD prediction of JETPHOX is compared with the measurement in Figures 6 and 7. The NLO QCD prediction from SHERPA 2.2.2 is also reported in Figures 6 and 7 and is denoted by ‘ME+PS@NLO QCD’ to highlight the differences relative to the predictions from JETPHOX discussed in Section 8. The nominal prediction of SHERPA 2.2.2 is above that of JETPHOX; this is attributed to the fact that the former includes contributions from parton showers, virtual corrections for $\gamma + 2$ -jet and higher-order tree-level matrix elements for the processes $2 \rightarrow n$ with $n = 4$ and 5, which are not present in the prediction of JETPHOX. Both types of predictions adequately reproduce the dependence of the single- and double-differential cross section on E_T^γ and $|\eta^\gamma|$ as observed in the data.

Although the predictions are overall consistent with the measurement within the uncertainties, a detailed comparison is presented in terms of the ratios of theory predictions to data. The ratios of the predictions of JETPHOX with $\mu_R = \mu_F = \mu_f = E_T^\gamma$ using different PDF sets to the measured cross section as a function of E_T^γ are shown in Figures 8 and 9; the full theoretical uncertainty, including the variations of the scales, is shown for the prediction based on the MMHT2014 PDF set. The predictions based on the MMHT2014, CT14 and NNPDF3.0 PDF sets are similar and closest to the data for $|\eta^\gamma| < 1.37$ for most of the range in E_T^γ . For $1.56 < |\eta^\gamma| < 2.37$, the prediction based on the HERAPDF2.0 PDF set is closest to the data. The prediction based on the ABMP16 PDF set is further away from the data than that based on the MMHT2014 PDF set for $E_T^\gamma \lesssim 1$ TeV in the region $|\eta^\gamma| < 1.37$. The prediction of JETPHOX with $\mu_R = \mu_F = \mu_f = E_T^\gamma$ exhibits a tendency to underestimate the data over most of the measured range in E_T^γ . However, the prediction of JETPHOX with a different choice for the scales, namely $\mu_R = \mu_F = \mu_f = E_T^\gamma/2$, provides an improved description of the normalisation of the data, as can be seen in Figure 10; the full theoretical uncertainty, including the variations of the scales with respect to $E_T^\gamma/2$, is shown for the prediction based on the MMHT2014 PDF set. The ratio of the prediction of SHERPA 2.2.2 to the measured cross section as a function of E_T^γ is also shown in Figure 10. Good agreement is observed between this prediction and the data distribution. In general, the NLO pQCD predictions are consistent with the measurement within the experimental and theoretical uncertainties.

The NNLO QCD prediction from Nnlojet, which represent a significant step forward in precision, is compared with the data in Figures 6, 7, 11 and 12. The inclusion of the NNLO QCD corrections increases the normalisation of the prediction and significantly reduces the uncertainties due to the scale variations, which are dominant for NLO QCD calculations. With the described choice of the input parameters, the NNLO QCD prediction provides an excellent description of the data except in the region $1.56 < |\eta^\gamma| < 1.81$,

where there is a tendency in the theory to underestimate the data. The improvements in the description of the data by the NNLO QCD prediction relative to that of NLO QCD are shown in Figures 11 and 12.

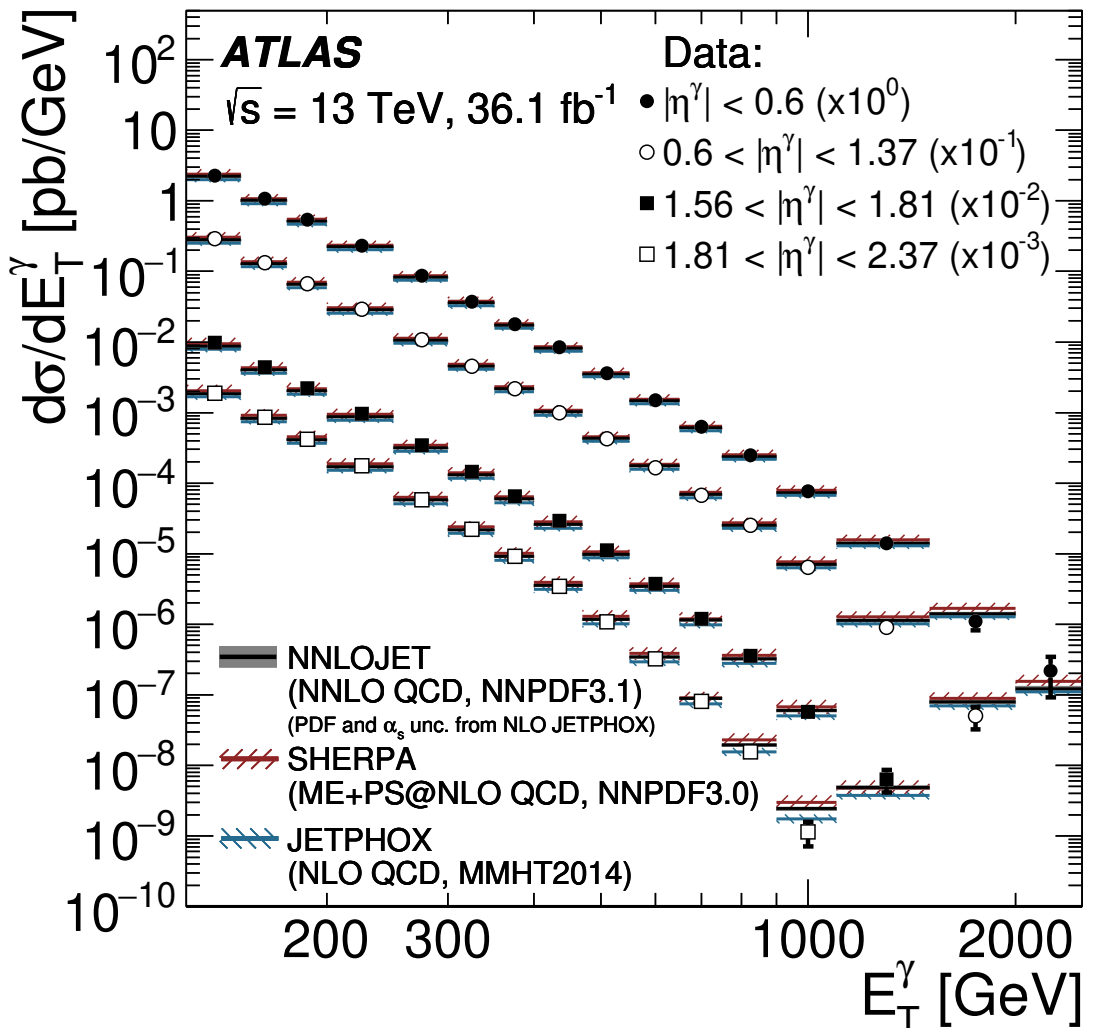


Figure 6: The measured differential cross section for isolated-photon production as a function of E_T^γ in $|\eta^\gamma| < 0.6$ (black dots), $0.6 < |\eta^\gamma| < 1.37$ (open circles), $1.56 < |\eta^\gamma| < 1.81$ (black squares) and $1.81 < |\eta^\gamma| < 2.37$ (open squares). The NLO pQCD prediction from JETPHOX, the ME+PS@NLO QCD prediction from SHERPA 2.2.2 and the NNLO QCD prediction from NNLOJET are also shown. The measurement and the predictions are normalised by the factors shown in parentheses to aid visibility. The error bars represent the data statistical uncertainties and systematic uncertainties added in quadrature. For most of the points, the error bars are smaller than the marker size and, thus, not visible. The bands represent the theoretical uncertainty associated with the predictions; in the case of NNLOJET, the uncertainties due to the PDFs and α_s are estimated at NLO with JETPHOX.

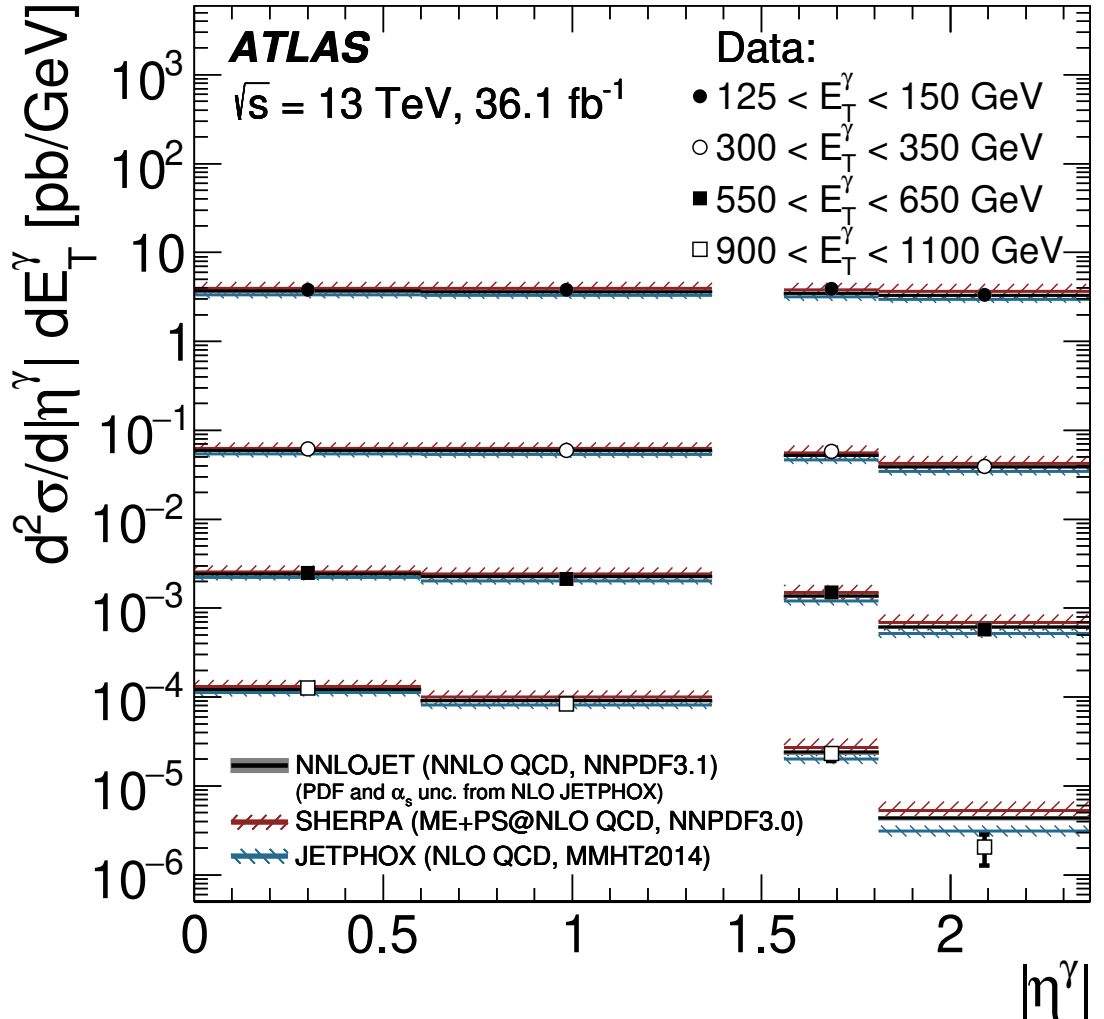


Figure 7: The measured double-differential cross section for isolated-photon production as a function of $|\eta^\gamma|$ in $125 < E_T^\gamma < 150$ GeV (black dots), $300 < E_T^\gamma < 350$ GeV (open circles), $550 < E_T^\gamma < 650$ GeV (black squares) and $900 < E_T^\gamma < 1100$ GeV (open squares). The NLO pQCD prediction from JETPHOX, the ME+PS@NLO QCD prediction from SHERPA 2.2.2 and the NNLO QCD prediction from NNLOJET are also shown. The error bars represent the data statistical uncertainties and systematic uncertainties added in quadrature. For most of the points, the error bars are smaller than the marker size and, thus, not visible. The bands represent the theoretical uncertainty associated with the predictions; in the case of NNLOJET, the uncertainties due to the PDFs and α_s are estimated at NLO with JETPHOX.

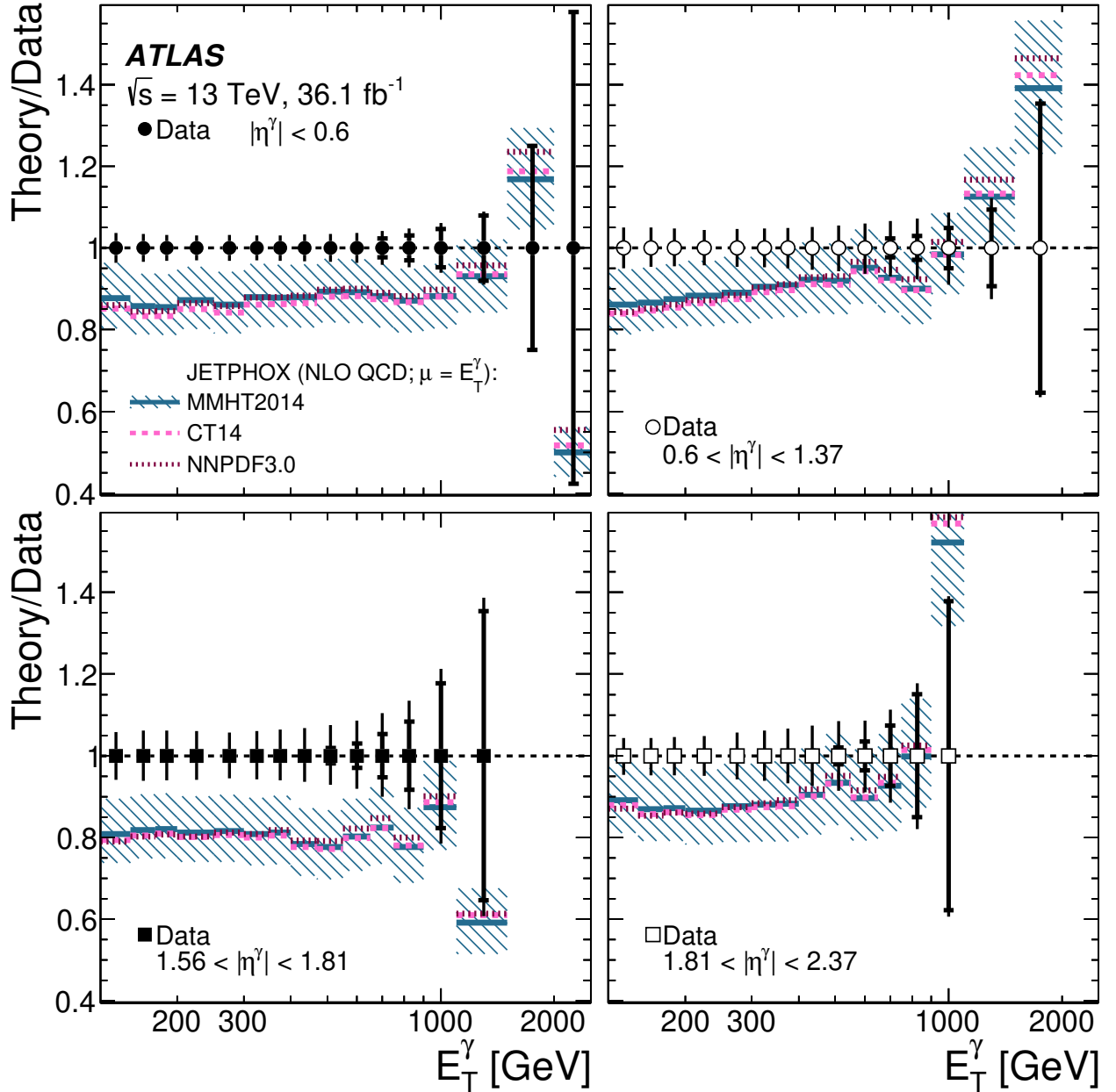


Figure 8: The ratio of the NLO pQCD prediction of JETPHOX with $\mu_R = \mu_F = \mu_f = E_T^\gamma$ using the MMHT2014 PDF set to the measured differential cross section for isolated-photon production (solid lines) as a function of E_T^γ in different regions of $|\eta^\gamma|$. The symbols for the data are centred at unity and the inner (outer) error bars represent the relative data statistical uncertainties (statistical and systematic uncertainties added in quadrature). The hatched bands represent the full theoretical uncertainty associated to the prediction based on the MMHT2014 PDF set, including the variations of the scales. For comparison, the predictions using the CT14 (dashed lines) and NNPDF3.0 (dotted lines) PDF sets are also included.

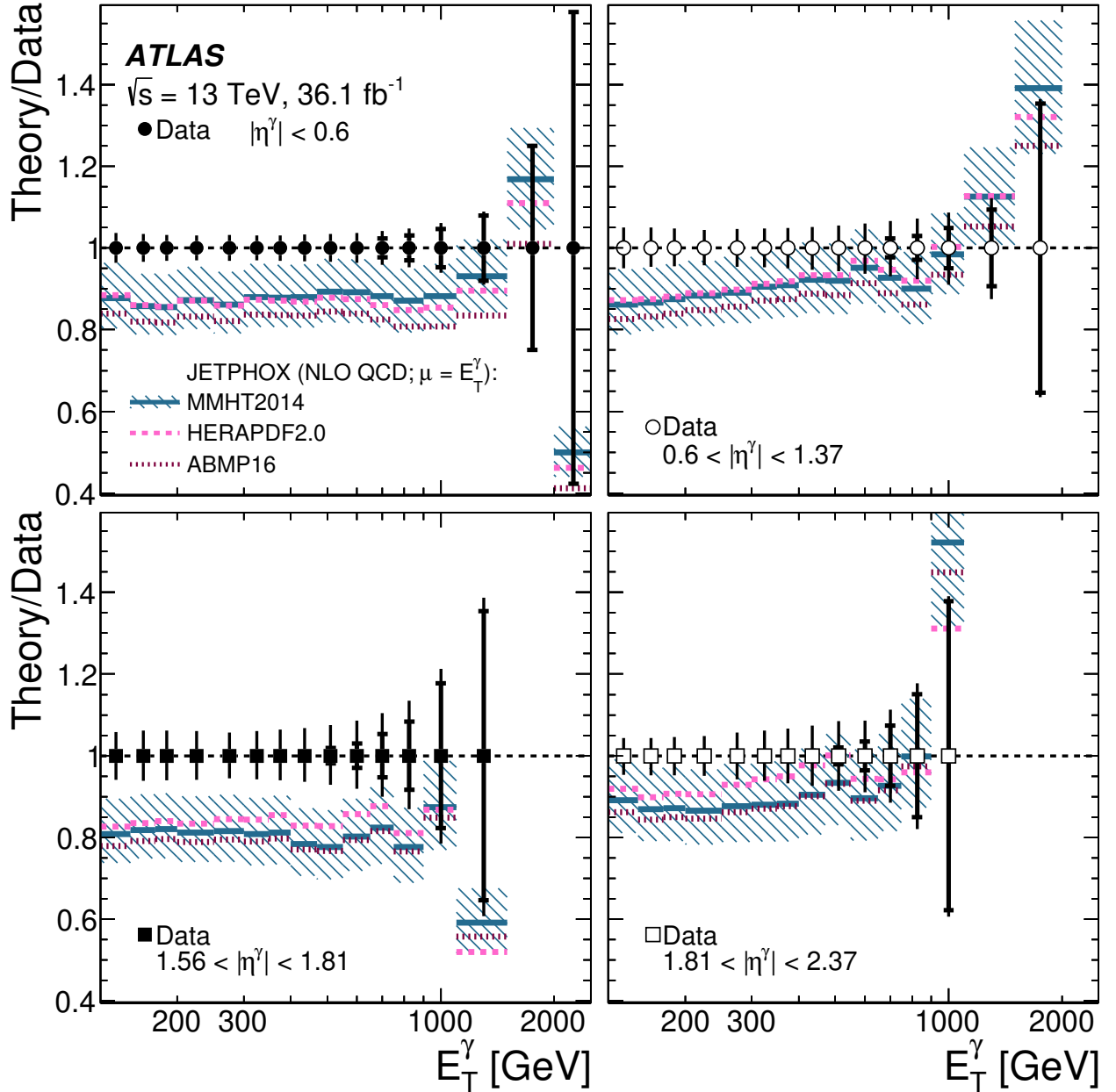


Figure 9: The ratio of the NLO pQCD prediction of JETPHOX with $\mu_R = \mu_F = \mu_f = E_T^\gamma$ using the MMHT2014 PDF set to the measured differential cross section for isolated-photon production (solid lines) as a function of E_T^γ in different regions of $|\eta^\gamma|$. The symbols for the data are centred at unity and the inner (outer) error bars represent the relative data statistical uncertainties (statistical and systematic uncertainties added in quadrature). The hatched bands represent the full theoretical uncertainty associated to the prediction based on the MMHT2014 PDF set, including the variations of the scales. For comparison, the predictions using the HERAPDF2.0 (dashed lines) and ABMP16 (dotted lines) PDF sets are also included.

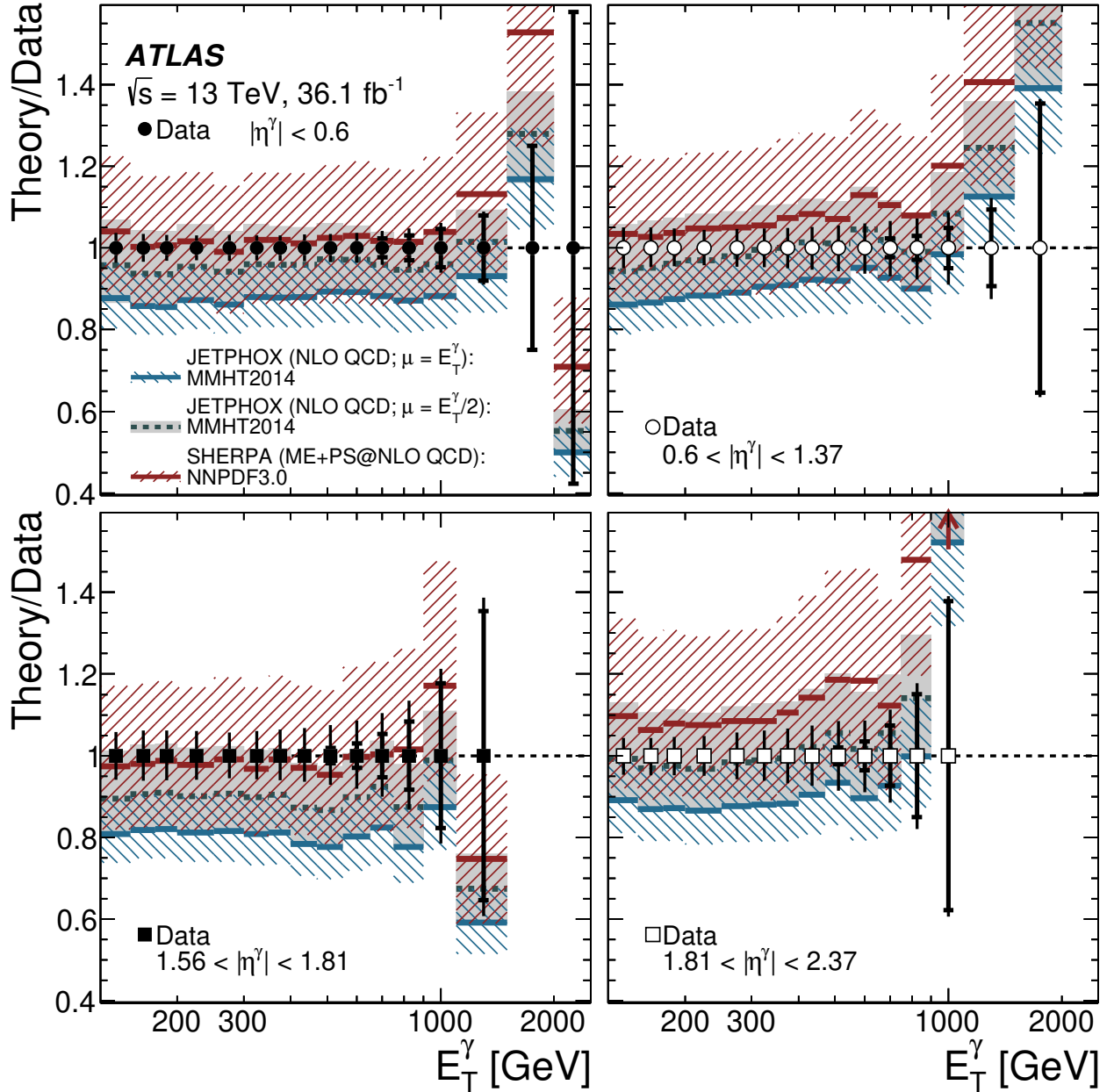


Figure 10: The ratio of the NLO pQCD prediction of JETPHOX with $\mu_R = \mu_F = \mu_f = E_T^\gamma$, the ratio of the NLO pQCD prediction of JETPHOX with $\mu_R = \mu_F = \mu_f = E_T^\gamma/2$ and the ratio of the ME+PS@NLO QCD prediction of SHERPA 2.2.2 to the measured differential cross section for isolated-photon production as a function of E_T^γ in different regions of $|\eta^\gamma|$. The symbols for the data are centred at unity and the inner (outer) error bars represent the relative data statistical uncertainties (statistical and systematic uncertainties added in quadrature). The bands represent the full theoretical uncertainty, which includes the variations of the scales.

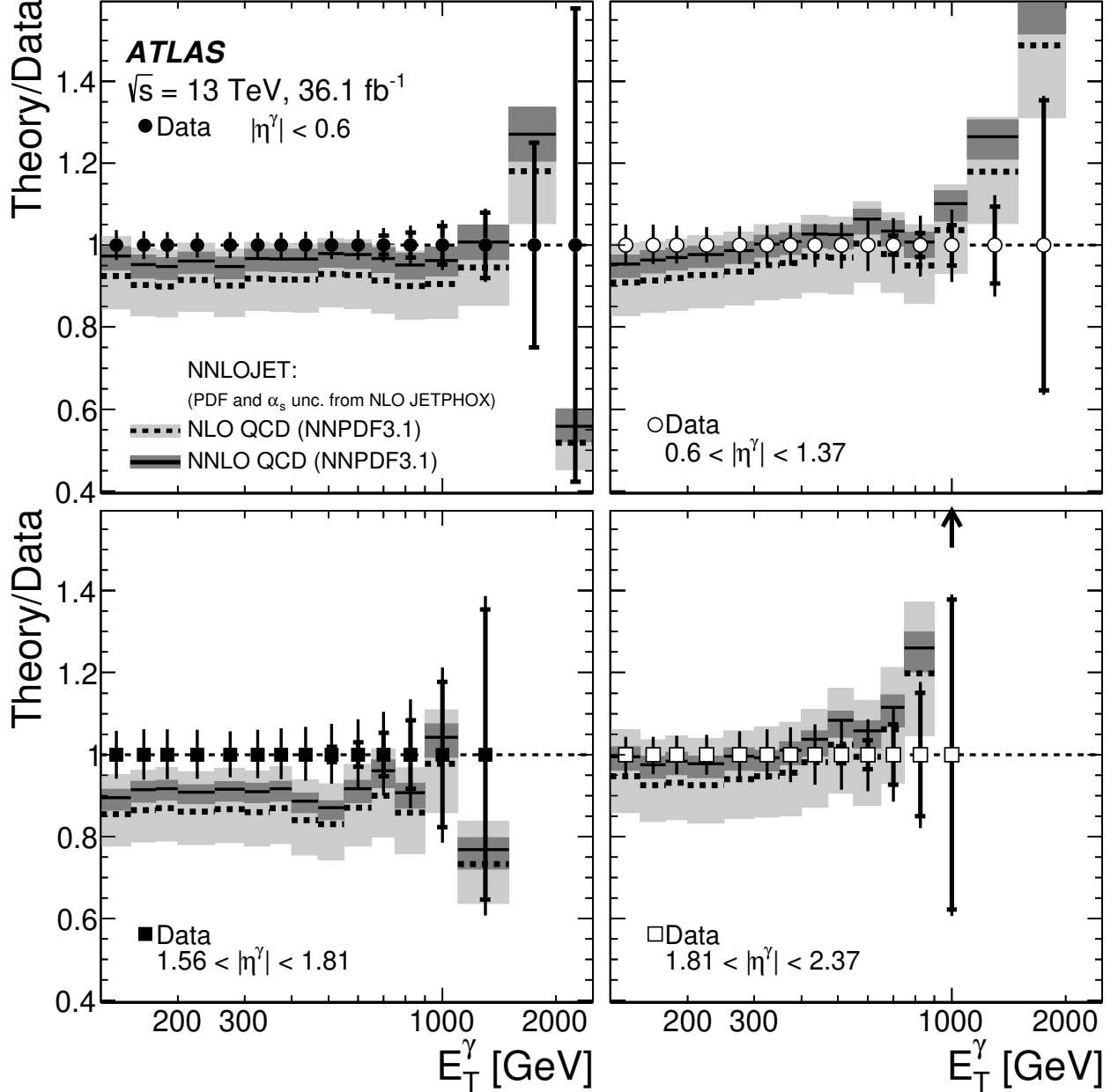


Figure 11: The ratio of the NNLO (NLO) QCD prediction of NNLOJET using the NNPDF3.1 PDF set to the measured differential cross section for isolated-photon production as a function of E_T^γ in different regions of $|\eta^\gamma|$ is shown as a solid (dashed) line. The symbols for the data are centred at unity and the inner (outer) error bars represent the relative data statistical uncertainties (statistical and systematic uncertainties added in quadrature). The shaded bands represent the theoretical uncertainties, which include those due to the PDFs and α_s as estimated at NLO with JETPHOX.

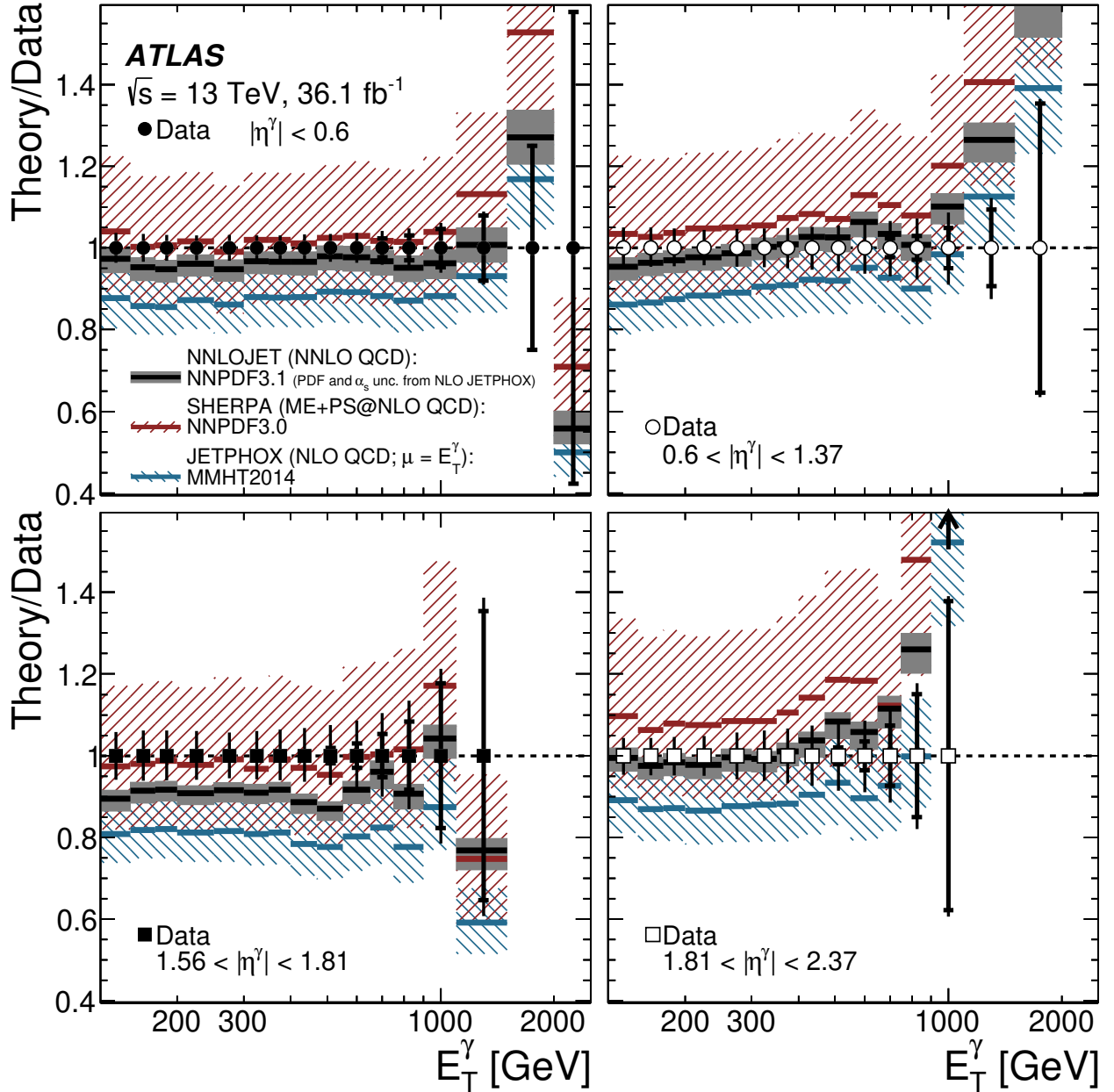


Figure 12: The ratio of the NLO pQCD prediction of JETPHOX with $\mu_R = \mu_F = \mu_f = E_T^\gamma$, the ratio of the ME+PS@NLO QCD prediction of SHERPA 2.2.2 and the ratio of the NNLO QCD prediction of Nnlojet to the measured differential cross section for isolated-photon production as a function of E_T^γ in different regions of $|\eta^\gamma|$. The symbols for the data are centred at unity and the inner (outer) error bars represent the relative data statistical uncertainties (statistical and systematic uncertainties added in quadrature). The bands represent the theoretical uncertainty; in the case of NNLOJET, the uncertainties due to the PDFs and α_s are estimated at NLO with JETPHOX.

10 Summary and conclusions

The cross section for inclusive isolated-photon production in pp collisions at $\sqrt{s} = 13$ TeV is measured using data with an integrated luminosity of 36.1 fb^{-1} collected by the ATLAS detector at the LHC. The differential cross section as a function of E_T^γ is measured in different regions of $|\eta^\gamma|$ for photons with $E_T^\gamma > 125 \text{ GeV}$ and $|\eta^\gamma| < 2.37$, excluding the region $1.37 < |\eta^\gamma| < 1.56$.

The measurement presented here constitutes an improvement in terms of statistical and systematic uncertainties relative to that published earlier thanks to the ten-fold increase in the integrated luminosity. In the new measurement, the reach in E_T^γ is extended upwards by 1000, 500, 400 and 200 GeV for $|\eta^\gamma| < 0.6$, $0.6 < |\eta^\gamma| < 1.37$, $1.56 < |\eta^\gamma| < 1.81$ and $1.81 < |\eta^\gamma| < 2.37$, respectively, relative to the previous measurement at $\sqrt{s} = 13$ TeV. The range in which the measurement is limited by systematic uncertainties is extended upwards to 1 TeV for $|\eta^\gamma| < 1.37$, where previously the limitation was at 600 GeV.

Next-to-leading-order QCD predictions using several PDF sets are compared with the measurement and found to provide an adequate description of the data within the experimental and theoretical uncertainties. The comparison of data and theory is limited by the theoretical uncertainties due to terms beyond NLO in QCD. Experimental systematic uncertainties are smaller than the theoretical uncertainties over the full investigated phase space. The inclusion of higher-order matrix elements and parton showers, as provided by the `SHERPA 2.2.2` program, improves the description of the normalisation of the data by the prediction.

Recently, a next-to-next-to-leading-order QCD prediction was calculated in which the uncertainties due to the scale variations are reduced by a factor in the range 2–20 relative to those of a NLO QCD calculation. Overall, the NNLO QCD prediction gives an excellent description of the data. The comparison of the NNLO QCD prediction with the measured cross section represents a precise test of the theory at $O(\alpha_{\text{EM}}\alpha_s^3)$ in the range of photon transverse energies from 125 GeV up to and beyond 1 TeV. The measurement has the potential to further constrain the PDFs, particularly the gluon density in the proton, within a global NNLO QCD fit.

Acknowledgements

We thank CERN for the very successful operation of the LHC, as well as the support staff from our institutions without whom ATLAS could not be operated efficiently.

We acknowledge the support of ANPCyT, Argentina; YerPhI, Armenia; ARC, Australia; BMWFW and FWF, Austria; ANAS, Azerbaijan; SSTC, Belarus; CNPq and FAPESP, Brazil; NSERC, NRC and CFI, Canada; CERN; CONICYT, Chile; CAS, MOST and NSFC, China; COLCIENCIAS, Colombia; MSMT CR, MPO CR and VSC CR, Czech Republic; DNRF and DNSRC, Denmark; IN2P3-CNRS, CEA-DRF/IRFU, France; SRNSFG, Georgia; BMBF, HGF, and MPG, Germany; GSRT, Greece; RGC, Hong Kong SAR, China; ISF and Benoziyo Center, Israel; INFN, Italy; MEXT and JSPS, Japan; CNRST, Morocco; NWO, Netherlands; RCN, Norway; MNiSW and NCN, Poland; FCT, Portugal; MNE/IFA, Romania; MES of Russia and NRC KI, Russian Federation; JINR; MESTD, Serbia; MSSR, Slovakia; ARRS and MIZŠ, Slovenia; DST/NRF, South Africa; MINECO, Spain; SRC and Wallenberg Foundation, Sweden; SERI, SNSF and Cantons of Bern and Geneva, Switzerland; MOST, Taiwan; TAEK, Turkey; STFC, United Kingdom; DOE and NSF, United States of America. In addition, individual groups and members have received support from BCKDF, CANARIE, CRC and Compute Canada, Canada; COST, ERC, ERDF, Horizon 2020, and Marie Skłodowska-Curie Actions, European Union; Investissements d'

Avenir Labex and Idex, ANR, France; DFG and AvH Foundation, Germany; Herakleitos, Thales and Aristeia programmes co-financed by EU-ESF and the Greek NSRF, Greece; BSF-NSF and GIF, Israel; CERCA Programme Generalitat de Catalunya, Spain; The Royal Society and Leverhulme Trust, United Kingdom.

The crucial computing support from all WLCG partners is acknowledged gratefully, in particular from CERN, the ATLAS Tier-1 facilities at TRIUMF (Canada), NDGF (Denmark, Norway, Sweden), CC-IN2P3 (France), KIT/GridKA (Germany), INFN-CNAF (Italy), NL-T1 (Netherlands), PIC (Spain), ASGC (Taiwan), RAL (UK) and BNL (USA), the Tier-2 facilities worldwide and large non-WLCG resource providers. Major contributors of computing resources are listed in Ref. [68].

References

- [1] T. Pietrycki and A. Szczurek, *Photon-jet correlations in pp and pp collisions*, *Phys. Rev. D* **76** (2007) 034003, arXiv: [0704.2158 \[hep-ph\]](#).
- [2] Z. Belghobsi et al., *Photon-jet correlations and constraints on fragmentation functions*, *Phys. Rev. D* **79** (2009) 114024, arXiv: [0903.4834 \[hep-ph\]](#).
- [3] ATLAS Collaboration, *Measurement of the inclusive isolated prompt photons cross section in pp collisions at $\sqrt{s} = 7$ TeV with the ATLAS detector using 4.6 fb^{-1}* , *Phys. Rev. D* **89** (2014) 052004, arXiv: [1311.1440 \[hep-ex\]](#).
- [4] ATLAS Collaboration, *Measurement of the inclusive isolated prompt photon cross section in pp collisions at $\sqrt{s} = 8$ TeV with the ATLAS detector*, *JHEP* **08** (2016) 005, arXiv: [1605.03495 \[hep-ex\]](#).
- [5] ATLAS Collaboration, *Measurement of the cross section for inclusive isolated-photon production in pp collisions at $\sqrt{s} = 13$ TeV using the ATLAS detector*, *Phys. Lett. B* **770** (2017) 473, arXiv: [1701.06882 \[hep-ex\]](#).
- [6] CMS Collaboration, *Measurement of the differential cross section for isolated prompt photon production in pp collisions at 7 TeV*, *Phys. Rev. D* **84** (2011) 052011, arXiv: [1108.2044 \[hep-ex\]](#).
- [7] CMS Collaboration, *Measurement of differential cross sections for inclusive isolated-photon and photon+jets production in proton-proton collisions at $\sqrt{s} = 13$ TeV*, *Eur. Phys. J. C* **79** (2019) 20, arXiv: [1807.00782 \[hep-ex\]](#).
- [8] D. d'Enterria and J. Rojo, *Quantitative constraints on the gluon distribution function in the proton from collider isolated-photon data*, *Nucl. Phys. B* **860** (2012) 311, arXiv: [1202.1762 \[hep-ph\]](#).
- [9] L. Carminati et al., *Sensitivity of the LHC isolated- γ +jet data to the parton distribution functions of the proton*, *Europhys. Lett.* **101** (2013) 61002, arXiv: [1212.5511 \[hep-ph\]](#).
- [10] J. Gao, L. Harland-Lang and J. Rojo, *The Structure of the Proton in the LHC Precision Era*, *Phys. Rep.* **742** (2018) 1, arXiv: [1709.04922 \[hep-ph\]](#).
- [11] J.M. Campbell, J. Rojo, E. Slade, C. Williams, *Direct photon production and PDF fits reloaded*, *Eur. Phys. J. C* **78** (2018) 470, arXiv: [1802.03021 \[hep-ph\]](#).
- [12] A.V. Lipatov and M.A. Malyshev, *Reconsideration of the inclusive prompt photon production at the LHC with k_T -factorization*, *Phys. Rev. D* **94** (2016) 034020, arXiv: [1606.02696 \[hep-ph\]](#).

- [13] M. Klasen, C. Klein-Bösing and H. Poppenborg, *Prompt photon production and photon-jet correlations at the LHC*, JHEP **03** (2018) 081, arXiv: [1709.04154 \[hep-ph\]](#).
- [14] M.D. Schwartz, *Precision direct photon spectra at high energy and comparison to the 8 TeV ATLAS data*, JHEP **09** (2016) 005, arXiv: [1606.02313 \[hep-ph\]](#).
- [15] J.M. Campbell, R.K. Ellis, C. Williams, *Direct Photon Production at Next-to-Next-to-Leading Order*, Phys. Rev. Lett. **118** (2017) 222001, arXiv: [1612.04333 \[hep-ph\]](#).
- [16] X. Chen, T. Gehrmann, N. Glover, M. Höfer and A. Huss, *Isolated photon and photon+jet production at NNLO QCD accuracy*, (2019), arXiv: [1904.01044 \[hep-ph\]](#).
- [17] X. Chen, T. Gehrmann, N. Glover, M. Höfer and A. Huss, *Isolated photon and photon+jet production at NNLO QCD accuracy and the ratio $R_{13/8}^{\gamma}$* , (2019), arXiv: [1905.08577 \[hep-ph\]](#).
- [18] G. Brooijmans et al., *Les Houches 2017: Physics at TeV Colliders New Physics Working Group Report, contribution 20*, FERMILAB-CONF-17-664-PPD (2018), arXiv: [1803.10379 \[hep-ex\]](#).
- [19] S. Catani, M. Fontannaz, J. Ph. Guillet and E. Pilon, *Cross section of isolated prompt photons in hadron-hadron collisions*, JHEP **05** (2002) 028, arXiv: [hep-ph/0204023](#).
- [20] P. Aurenche, M. Fontannaz, J. Ph. Guillet, E. Pilon and M. Werlen, *A new critical study of photon production in hadronic collisions*, Phys. Rev. D **73** (2006) 094007, arXiv: [hep-ph/0602133](#).
- [21] T. Gleisberg et al., *Event generation with SHERPA 1.1*, JHEP **02** (2009) 007, arXiv: [0811.4622 \[hep-ph\]](#).
- [22] ATLAS Collaboration, *The ATLAS Experiment at the CERN Large Hadron Collider*, JINST **3** (2008) S08003.
- [23] ATLAS Collaboration, *ATLAS Insertable B-Layer Technical Design Report*, CERN-LHCC-2010-013, ATLAS-TDR-19, 2010,
URL: <https://cds.cern.ch/record/1291633>, *ATLAS Insertable B-Layer Technical Design Report Addendum*, ATLAS-TDR-19-ADD-1, 2012, URL: <https://cds.cern.ch/record/1451888>.
- [24] B. Abbott et al., *Production and integration of the ATLAS Insertable B-Layer*, JINST **13** (2018) T05008, arXiv: [1803.00844 \[physics.ins-det\]](#).
- [25] ATLAS Collaboration, *Performance of the ATLAS trigger system in 2015*, Eur. Phys. J. C **77** (2017) 317, arXiv: [1611.09661 \[hep-ex\]](#).
- [26] ATLAS Collaboration, *Luminosity Determination in pp Collisions at $\sqrt{s} = 13$ TeV using the ATLAS Detector at the LHC*, ATLAS-CONF-2019-021, 2019, URL: <https://cdsweb.cern.ch/record/2677054>.
- [27] G. Avoni et al., *The new LUCID-2 detector for luminosity measurement and monitoring in ATLAS*, JINST **13** (2018) P07017.
- [28] S. Agostinelli et al., *GEANT4 - a simulation toolkit*, Nucl. Instrum. Meth. A **506** (2003) 250.
- [29] ATLAS Collaboration, *The ATLAS simulation infrastructure*, Eur. Phys. J. C **70** (2010) 823, arXiv: [1005.4568 \[physics.ins-det\]](#).
- [30] T. Sjöstrand, S. Mrenna and P.Z. Skands, *A brief introduction to PYTHIA 8.1*, Comput. Phys. Commun. **178** (2008) 852, arXiv: [0710.3820 \[hep-ph\]](#).
- [31] B. Andersson, G. Gustafson, G. Ingelman and T. Sjöstrand, *Parton Fragmentation and String Dynamics*, Phys. Rept. **97** (1983) 31.

- [32] C. Winter, F. Krauss and G. Soff, *A modified cluster hadronisation model*, *Eur. Phys. J. C* **36** (2004) 381, arXiv: [hep-ph/0311085](#).
- [33] R. D. Ball et al., *Parton distributions with LHC data*, *Nucl. Phys. B* **867** (2013) 244, arXiv: [1207.1303 \[hep-ph\]](#).
- [34] H.-L. Lai et al., *New parton distributions for collider physics*, *Phys. Rev. D* **82** (2010) 074024, arXiv: [1007.2241 \[hep-ph\]](#).
- [35] ATLAS Collaboration, *ATLAS Pythia 8 tunes to 7 TeV data*, ATL-PHYS-PUB-2014-021, 2014, URL: <https://cds.cern.ch/record/1966419>.
- [36] S. Höche, F. Krauss, S. Schumann and F. Siegert, *QCD matrix elements and truncated showers*, *JHEP* **05** (2009) 053, arXiv: [0903.1219 \[hep-ph\]](#).
- [37] S. Frixione, *Isolated photons in perturbative QCD*, *Phys. Lett. B* **429** (1998) 369, arXiv: [hep-ph/9801442](#).
- [38] T. Gleisberg and S. Höche, *Comix, a new matrix element generator*, *JHEP* **12** (2008) 039, arXiv: [0808.3674 \[hep-ph\]](#).
- [39] F. Krauss, R. Kuhn and G. Soff, *AMEGIC++ 1.0: A Matrix element generator in C++*, *JHEP* **02** (2002) 044, arXiv: [hep-ph/0109036](#).
- [40] F. Cascioli, P. Maierhöfer and S. Pozzorini, *Scattering Amplitudes with Open Loops*, *Phys. Rev. Lett.* **108** (2012) 111601, arXiv: [1111.5206 \[hep-ph\]](#).
- [41] S. Schumann and F. Krauss, *A Parton shower algorithm based on Catani-Seymour dipole factorisation*, *JHEP* **03** (2008) 038, arXiv: [0709.1027 \[hep-ph\]](#).
- [42] S. Höche, F. Krauss, M. Schönherr and F. Siegert, *QCD matrix elements + parton showers: The NLO case*, *JHEP* **04** (2013) 027, arXiv: [1207.5030 \[hep-ph\]](#).
- [43] NNPDF Collaboration, R.D. Ball et al., *Parton distributions for the LHC Run II*, *JHEP* **04** (2015) 040, arXiv: [1410.8849 \[hep-ph\]](#).
- [44] ATLAS Collaboration, *Summary of ATLAS Pythia 8 tunes*, ATL-PHYS-PUB-2012-003, 2012, URL: <https://cds.cern.ch/record/1474107>.
- [45] A.D. Martin, W.J. Stirling, R.S. Thorne and G. Watt, *Parton distributions for the LHC*, *Eur. Phys. J. C* **63** (2009) 189, arXiv: [0901.0002 \[hep-ph\]](#).
- [46] ATLAS Collaboration, *Measurement of the photon identification efficiencies with the ATLAS detector using LHC Run 2 data collected in 2015 and 2016*, *Eur. Phys. J. C* **79** (2019) 205, arXiv: [1810.05087 \[hep-ex\]](#).
- [47] ATLAS Collaboration, *Topological cell clustering in the ATLAS calorimeters and its performance in LHC Run 1*, *Eur. Phys. J. C* **77** (2017) 490, arXiv: [1603.02934 \[hep-ex\]](#).
- [48] ATLAS Collaboration, *Measurement of the inclusive isolated prompt photon cross section in pp collisions at $\sqrt{s} = 7$ TeV with the ATLAS detector*, *Phys. Rev. D* **83** (2011) 052005, arXiv: [1012.4389 \[hep-ex\]](#).
- [49] ATLAS Collaboration, *Measurement of the inclusive isolated prompt photon cross-section in pp collisions at $\sqrt{s} = 7$ TeV using 35 pb^{-1} of ATLAS data*, *Phys. Lett. B* **706** (2011) 150, arXiv: [1108.0253 \[hep-ex\]](#).
- [50] M. Cacciari, G.P. Salam and G. Soyez, *The catchment area of Jets*, *JHEP* **04** (2008) 005, arXiv: [0802.1188 \[hep-ph\]](#).

- [51] M. Cacciari, G.P. Salam and S. Sapeta, *On the characterisation of the underlying event*, **JHEP 04** (2010) 065, arXiv: [0912.4926 \[hep-ph\]](#).
- [52] ATLAS Collaboration, *Electron and photon energy calibration with the ATLAS detector using LHC Run 1 data*, **Eur. Phys. J. C 74** (2014) 3071, arXiv: [1407.5063 \[hep-ex\]](#).
- [53] ATLAS Collaboration, *Electron and photon energy calibration with the ATLAS detector using 2015-2016 LHC proton-proton collision data*, **JINST 14** (2019) P03017, arXiv: [1812.03848 \[hep-ex\]](#).
- [54] G. D'Agostini, *A multidimensional unfolding method based on Bayes' theorem*, **Nucl. Instrum. Meth. A 362** (1995) 487.
- [55] G. Bohm and G. Zech, *Introduction to statistics and data analysis for physicists*, Deutsches Elektronen-Synchrotron, Hamburg, Germany, ISBN 9783935702881, 2014.
- [56] ATLAS Collaboration, *Measurement of the Inelastic Proton-Proton Cross Section at $\sqrt{s} = 13$ TeV with the ATLAS Detector at the LHC*, **Phys. Rev. Lett. 117** (2016) 182002, arXiv: [1606.02625 \[hep-ex\]](#).
- [57] L.A. Harland-Lang, A.D. Martin, P. Motylinski and R.S. Thorne, *Parton distributions in the LHC era: MMHT 2014 PDFs*, **Eur. Phys. J. C 75** (2015) 204, arXiv: [1412.3989 \[hep-ph\]](#).
- [58] L. Bourhis, M. Fontannaz and J.Ph. Guillet, *Quark and gluon fragmentation functions into photons*, **Eur. Phys. J. C 2** (1998) 529, arXiv: [hep-ph/9704447](#).
- [59] S. Dulat et al., *New parton distribution functions from a global analysis of quantum chromodynamics*, **Phys. Rev. D 93** (2016) 033006, arXiv: [1506.07443 \[hep-ph\]](#).
- [60] S. Alekhin, J. Blümlein, S. Moch, R. Placakyte, *Parton distribution functions, α_s , and heavy-quark masses for LHC Run II*, **Phys. Rev. D 96** (2017) 014011, arXiv: [1701.05838 \[hep-ph\]](#).
- [61] H1 and ZEUS Collaborations, H. Abramowicz et al., *Combination of measurements of inclusive deep inelastic $e^\pm p$ scattering cross sections and QCD analysis of HERA data*, **Eur. Phys. J. C 75** (2015) 580, arXiv: [1506.06042 \[hep-ex\]](#).
- [62] F. Siegert, *A practical guide to event generation for prompt photon production with Sherpa*, **J. Phys. G 44** (2017) 044007, arXiv: [1611.07226 \[hep-ph\]](#).
- [63] R.D. Ball et al., *Parton distributions from high-precision collider data*, **Eur. Phys. J. C 77** (2017) 663, arXiv: [1706.00428 \[hep-ph\]](#).
- [64] S. Dittmaier and M. Huber, *Radiative corrections to the neutral-current Drell-Yan process in the Standard Model and its minimal supersymmetric extension*, **JHEP 01** (2010) 060, arXiv: [0911.2329 \[hep-ph\]](#).
- [65] T. Becher and X. Garcia i Tormo, *Addendum to Electroweak Sudakov effects in W , Z and γ production at large transverse momentum*, **Phys. Rev. D 92** (2015) 073011, arXiv: [1509.01961 \[hep-ph\]](#).
- [66] J. Pumplin et al., *Uncertainties of predictions from parton distribution functions. 2. The Hessian method*, **Phys. Rev. D 65** (2001) 014013, arXiv: [hep-ph/0101032](#).
- [67] L.A. Harland-Lang, A.D. Martin, P. Motylinski and R.S. Thorne, *Uncertainties on α_S in the MMHT2014 global PDF analysis and implications for SM predictions*, **Eur. Phys. J. C 75** (2015) 435, arXiv: [1506.05682 \[hep-ph\]](#).
- [68] ATLAS Collaboration, *ATLAS Computing Acknowledgements*, ATL-GEN-PUB-2016-002, URL: <https://cds.cern.ch/record/2202407>.

The ATLAS Collaboration

G. Aad¹⁰¹, B. Abbott¹²⁸, D.C. Abbott¹⁰², O. Abdinov^{13,*}, A. Abed Abud^{70a,70b}, K. Abeling⁵³, D.K. Abhayasinghe⁹³, S.H. Abidi¹⁶⁷, O.S. AbouZeid⁴⁰, N.L. Abraham¹⁵⁶, H. Abramowicz¹⁶¹, H. Abreu¹⁶⁰, Y. Abulaiti⁶, B.S. Acharya^{66a,66b,q}, B. Achkar⁵³, S. Adachi¹⁶³, L. Adam⁹⁹, C. Adam Bourdarios¹³², L. Adamczyk^{83a}, L. Adamek¹⁶⁷, J. Adelman¹²¹, M. Adersberger¹¹⁴, A. Adiguzel^{12c,am}, S. Adorni⁵⁴, T. Adye¹⁴⁴, A.A. Affolder¹⁴⁶, Y. Afik¹⁶⁰, C. Agapopoulou¹³², M.N. Agaras³⁸, A. Aggarwal¹¹⁹, C. Agheorghiesei^{27c}, J.A. Aguilar-Saavedra^{140f,140a,al}, F. Ahmadov⁷⁹, W.S. Ahmed¹⁰³, X. Ai^{15a}, G. Aielli^{73a,73b}, S. Akatsuka⁸⁵, T.P.A. Åkesson⁹⁶, E. Akilli⁵⁴, A.V. Akimov¹¹⁰, K. Al Khoury¹³², G.L. Alberghi^{23b,23a}, J. Albert¹⁷⁶, M.J. Alconada Verzini¹⁶¹, S. Alderweireldt³⁶, M. Alekso³⁶, I.N. Aleksandrov⁷⁹, C. Alexa^{27b}, D. Alexandre¹⁹, T. Alexopoulos¹⁰, A. Alfonsi¹²⁰, M. Alhroob¹²⁸, B. Ali¹⁴², G. Alimonti^{68a}, J. Alison³⁷, S.P. Alkire¹⁴⁸, C. Allaire¹³², B.M.M. Allbrooke¹⁵⁶, B.W. Allen¹³¹, P.P. Allport²¹, A. Aloisio^{69a,69b}, A. Alonso⁴⁰, F. Alonso⁸⁸, C. Alpigiani¹⁴⁸, A.A. Alshehri⁵⁷, M. Alvarez Estevez⁹⁸, D. Álvarez Piqueras¹⁷⁴, M.G. Alviggi^{69a,69b}, Y. Amaral Coutinho^{80b}, A. Ambler¹⁰³, L. Ambroz¹³⁵, C. Amelung²⁶, D. Amidei¹⁰⁵, S.P. Amor Dos Santos^{140a}, S. Amoroso⁴⁶, C.S. Amrouche⁵⁴, F. An⁷⁸, C. Anastopoulos¹⁴⁹, N. Andari¹⁴⁵, T. Andeen¹¹, C.F. Anders^{61b}, J.K. Anders²⁰, A. Andreazza^{68a,68b}, V. Andrei^{61a}, C.R. Anelli¹⁷⁶, S. Angelidakis³⁸, A. Angerami³⁹, A.V. Anisenkov^{122b,122a}, A. Annovi^{71a}, C. Antel^{61a}, M.T. Anthony¹⁴⁹, M. Antonelli⁵¹, D.J.A. Antrim¹⁷¹, F. Anulli^{72a}, M. Aoki⁸¹, J.A. Aparisi Pozo¹⁷⁴, L. Aperio Bella³⁶, G. Arabidze¹⁰⁶, J.P. Araque^{140a}, V. Araujo Ferraz^{80b}, R. Araujo Pereira^{80b}, C. Arcangeletti⁵¹, A.T.H. Arce⁴⁹, F.A. Arduh⁸⁸, J-F. Arguin¹⁰⁹, S. Argyropoulos⁷⁷, J.-H. Arling⁴⁶, A.J. Armbruster³⁶, L.J. Armitage⁹², A. Armstrong¹⁷¹, O. Arnaez¹⁶⁷, H. Arnold¹²⁰, A. Artamonov^{111,*}, G. Artoni¹³⁵, S. Artz⁹⁹, S. Asai¹⁶³, N. Asbah⁵⁹, E.M. Asimakopoulou¹⁷², L. Asquith¹⁵⁶, K. Assamagan²⁹, R. Astalos^{28a}, R.J. Atkin^{33a}, M. Atkinson¹⁷³, N.B. Atlay¹⁵¹, H. Atmani¹³², K. Augsten¹⁴², G. Avolio³⁶, R. Avramidou^{60a}, M.K. Ayoub^{15a}, A.M. Azoulay^{168b}, G. Azuelos^{109,bb}, M.J. Baca²¹, H. Bachacou¹⁴⁵, K. Bachas^{67a,67b}, M. Backes¹³⁵, F. Backman^{45a,45b}, P. Bagnaia^{72a,72b}, M. Bahmani⁸⁴, H. Bahrasemani¹⁵², A.J. Bailey¹⁷⁴, V.R. Bailey¹⁷³, J.T. Baines¹⁴⁴, M. Bajic⁴⁰, C. Bakalis¹⁰, O.K. Baker¹⁸³, P.J. Bakker¹²⁰, D. Bakshi Gupta⁸, S. Balaji¹⁵⁷, E.M. Baldin^{122b,122a}, P. Balek¹⁸⁰, F. Balli¹⁴⁵, W.K. Balunas¹³⁵, J. Balz⁹⁹, E. Banas⁸⁴, A. Bandyopadhyay²⁴, Sw. Banerjee^{181,k}, A.A.E. Bannoura¹⁸², L. Barak¹⁶¹, W.M. Barbe³⁸, E.L. Barberio¹⁰⁴, D. Barberis^{55b,55a}, M. Barbero¹⁰¹, T. Barillari¹¹⁵, M-S. Barisits³⁶, J. Barkeloo¹³¹, T. Barklow¹⁵³, R. Barnea¹⁶⁰, S.L. Barnes^{60c}, B.M. Barnett¹⁴⁴, R.M. Barnett¹⁸, Z. Barnovska-Blenessy^{60a}, A. Baroncelli^{60a}, G. Barone²⁹, A.J. Barr¹³⁵, L. Barranco Navarro^{45a,45b}, F. Barreiro⁹⁸, J. Barreiro Guimarães da Costa^{15a}, S. Barsov¹³⁸, R. Bartoldus¹⁵³, G. Bartolini¹⁰¹, A.E. Barton⁸⁹, P. Bartos^{28a}, A. Basalaev⁴⁶, A. Bassalat^{132,au}, R.L. Bates⁵⁷, S.J. Batista¹⁶⁷, S. Batlamous^{35e}, J.R. Batley³², B. Batool¹⁵¹, M. Battaglia¹⁴⁶, M. Bauce^{72a,72b}, F. Bauer¹⁴⁵, K.T. Bauer¹⁷¹, H.S. Bawa^{31,o}, J.B. Beacham⁴⁹, T. Beau¹³⁶, P.H. Beauchemin¹⁷⁰, F. Becherer⁵², P. Bechtle²⁴, H.C. Beck⁵³, H.P. Beck^{20,u}, K. Becker⁵², M. Becker⁹⁹, C. Becot⁴⁶, A. Beddall^{12d}, A.J. Beddall^{12a}, V.A. Bednyakov⁷⁹, M. Bedognetti¹²⁰, C.P. Bee¹⁵⁵, T.A. Beermann⁷⁶, M. Begalli^{80b}, M. Begel²⁹, A. Behera¹⁵⁵, J.K. Behr⁴⁶, F. Beisiegel²⁴, A.S. Bell⁹⁴, G. Bella¹⁶¹, L. Bellagamba^{23b}, A. Bellerive³⁴, P. Bellos⁹, K. Beloborodov^{122b,122a}, K. Belotskiy¹¹², N.L. Belyaev¹¹², D. Benchekroun^{35a}, N. Benekos¹⁰, Y. Benhammou¹⁶¹, D.P. Benjamin⁶, M. Benoit⁵⁴, J.R. Bensinger²⁶, S. Bentvelsen¹²⁰, L. Beresford¹³⁵, M. Beretta⁵¹, D. Berge⁴⁶, E. Bergeaas Kuutmann¹⁷², N. Berger⁵, B. Bergmann¹⁴², L.J. Bergsten²⁶, J. Beringer¹⁸, S. Berlendis⁷, N.R. Bernard¹⁰², G. Bernardi¹³⁶, C. Bernius¹⁵³, T. Berry⁹³, P. Berta⁹⁹, C. Bertella^{15a}, I.A. Bertram⁸⁹, G.J. Besjes⁴⁰, O. Bessidskaia Bylund¹⁸², N. Besson¹⁴⁵, A. Bethani¹⁰⁰, S. Bethke¹¹⁵, A. Betti²⁴, A.J. Bevan⁹², J. Beyer¹¹⁵, R. Bi¹³⁹, R.M. Bianchi¹³⁹, O. Biebel¹¹⁴, D. Biedermann¹⁹, R. Bielski³⁶, K. Bierwagen⁹⁹, N.V. Biesuz^{71a,71b}, M. Biglietti^{74a}, T.R.V. Billoud¹⁰⁹, M. Bindi⁵³, A. Bingul^{12d},

C. Bini^{72a,72b}, S. Biondi^{23b,23a}, M. Birman¹⁸⁰, T. Bisanz⁵³, J.P. Biswal¹⁶¹, A. Bitadze¹⁰⁰, C. Bitrich⁴⁸, K. Bjørke¹³⁴, K.M. Black²⁵, T. Blazek^{28a}, I. Bloch⁴⁶, C. Blocker²⁶, A. Blue⁵⁷, U. Blumenschein⁹², G.J. Bobbink¹²⁰, V.S. Bobrovnikov^{122b,122a}, S.S. Bocchetta⁹⁶, A. Bocci⁴⁹, D. Boerner⁴⁶, D. Bogavac¹⁴, A.G. Bogdanchikov^{122b,122a}, C. Bohm^{45a}, V. Boisvert⁹³, P. Bokan^{53,172}, T. Bold^{83a}, A.S. Boldyrev¹¹³, A.E. Bolz^{61b}, M. Bomben¹³⁶, M. Bona⁹², J.S. Bonilla¹³¹, M. Boonekamp¹⁴⁵, H.M. Borecka-Bielska⁹⁰, A. Borisov¹²³, G. Borissov⁸⁹, J. Bortfeldt³⁶, D. Bortoletto¹³⁵, V. Bortolotto^{73a,73b}, D. Boscherini^{23b}, M. Bosman¹⁴, J.D. Bossio Sola¹⁰³, K. Bouaouda^{35a}, J. Boudreau¹³⁹, E.V. Bouhova-Thacker⁸⁹, D. Boumediene³⁸, S.K. Boutle⁵⁷, A. Boveia¹²⁶, J. Boyd³⁶, D. Boye^{33b,av}, I.R. Boyko⁷⁹, A.J. Bozon⁹³, J. Bracinik²¹, N. Brahimi¹⁰¹, G. Brandt¹⁸², O. Brandt^{61a}, F. Braren⁴⁶, B. Brau¹⁰², J.E. Brau¹³¹, W.D. Breaden Madden⁵⁷, K. Brendlinger⁴⁶, L. Brenner⁴⁶, R. Brenner¹⁷², S. Bressler¹⁸⁰, B. Brickwedde⁹⁹, D.L. Briglin²¹, D. Britton⁵⁷, D. Britzger¹¹⁵, I. Brock²⁴, R. Brock¹⁰⁶, G. Brooijmans³⁹, W.K. Brooks^{147b}, E. Brost¹²¹, J.H Broughton²¹, P.A. Bruckman de Renstrom⁸⁴, D. Bruncko^{28b}, A. Bruni^{23b}, G. Bruni^{23b}, L.S. Bruni¹²⁰, S. Bruno^{73a,73b}, B.H. Brunt³², M. Bruschi^{23b}, N. Bruscino¹³⁹, P. Bryant³⁷, L. Bryngemark⁹⁶, T. Buanes¹⁷, Q. Buat³⁶, P. Buchholz¹⁵¹, A.G. Buckley⁵⁷, I.A. Budagov⁷⁹, M.K. Bugge¹³⁴, F. Bührer⁵², O. Bulekov¹¹², T.J. Burch¹²¹, S. Burdin⁹⁰, C.D. Burgard¹²⁰, A.M. Burger¹²⁹, B. Burghgrave⁸, K. Burka⁸⁴, J.T.P. Burr⁴⁶, J.C. Burzynski¹⁰², V. Büscher⁹⁹, E. Buschmann⁵³, P.J. Bussey⁵⁷, J.M. Butler²⁵, C.M. Buttar⁵⁷, J.M. Butterworth⁹⁴, P. Butti³⁶, W. Buttlinger³⁶, A. Buzatu¹⁵⁸, A.R. Buzykaev^{122b,122a}, G. Cabras^{23b,23a}, S. Cabrera Urbán¹⁷⁴, D. Caforio⁵⁶, H. Cai¹⁷³, V.M.M. Cairo¹⁵³, O. Cakir^{4a}, N. Calace³⁶, P. Calafiura¹⁸, A. Calandri¹⁰¹, G. Calderini¹³⁶, P. Calfayan⁶⁵, G. Callea⁵⁷, L.P. Caloba^{80b}, S. Calvente Lopez⁹⁸, D. Calvet³⁸, S. Calvet³⁸, T.P. Calvet¹⁵⁵, M. Calvetti^{71a,71b}, R. Camacho Toro¹³⁶, S. Camarda³⁶, D. Camarero Munoz⁹⁸, P. Camarri^{73a,73b}, D. Cameron¹³⁴, R. Caminal Armadans¹⁰², C. Camincher³⁶, S. Campana³⁶, M. Campanelli⁹⁴, A. Camplani⁴⁰, A. Campoverde¹⁵¹, V. Canale^{69a,69b}, A. Canesse¹⁰³, M. Cano Bret^{60c}, J. Cantero¹²⁹, T. Cao¹⁶¹, Y. Cao¹⁷³, M.D.M. Capeans Garrido³⁶, M. Capua^{41b,41a}, R. Cardarelli^{73a}, F. Cardillo¹⁴⁹, G. Carducci^{41b,41a}, I. Carli¹⁴³, T. Carli³⁶, G. Carlino^{69a}, B.T. Carlson¹³⁹, L. Carminati^{68a,68b}, R.M.D. Carney^{45a,45b}, S. Caron¹¹⁹, E. Carquin^{147b}, S. Carrá⁴⁶, J.W.S. Carter¹⁶⁷, M.P. Casado^{14,f}, A.F. Casha¹⁶⁷, D.W. Casper¹⁷¹, R. Castelijn¹²⁰, F.L. Castillo¹⁷⁴, V. Castillo Gimenez¹⁷⁴, N.F. Castro^{140a,140e}, A. Catinaccio³⁶, J.R. Catmore¹³⁴, A. Cattai³⁶, J. Caudron²⁴, V. Cavalieri²⁹, E. Cavallaro¹⁴, M. Cavalli-Sforza¹⁴, V. Cavasinni^{71a,71b}, E. Celebi^{12b}, F. Ceradini^{74a,74b}, L. Cerdà Alberich¹⁷⁴, K. Cerny¹³⁰, A.S. Cerqueira^{80a}, A. Cerri¹⁵⁶, L. Cerrito^{73a,73b}, F. Cerutti¹⁸, A. Cervelli^{23b,23a}, S.A. Cetin^{12b}, D. Chakraborty¹²¹, S.K. Chan⁵⁹, W.S. Chan¹²⁰, W.Y. Chan⁹⁰, J.D. Chapman³², B. Chargeishvili^{159b}, D.G. Charlton²¹, T.P. Charman⁹², C.C. Chau³⁴, S. Che¹²⁶, A. Chegwidden¹⁰⁶, S. Chekanov⁶, S.V. Chekulaev^{168a}, G.A. Chelkov^{79,ba}, M.A. Chelstowska³⁶, B. Chen⁷⁸, C. Chen^{60a}, C.H. Chen⁷⁸, H. Chen²⁹, J. Chen^{60a}, J. Chen³⁹, S. Chen¹³⁷, S.J. Chen^{15c}, X. Chen^{15b,az}, Y. Chen⁸², Y-H. Chen⁴⁶, H.C. Cheng^{63a}, H.J. Cheng^{15a,15d}, A. Cheplakov⁷⁹, E. Cheremushkina¹²³, R. Cherkaoui El Moursli^{35e}, E. Cheu⁷, K. Cheung⁶⁴, T.J.A. Chevaléries¹⁴⁵, L. Chevalier¹⁴⁵, V. Chiarella⁵¹, G. Chiarelli^{71a}, G. Chiodini^{67a}, A.S. Chisholm^{36,21}, A. Chitan^{27b}, I. Chiu¹⁶³, Y.H. Chiu¹⁷⁶, M.V. Chizhov⁷⁹, K. Choi⁶⁵, A.R. Chomont^{72a,72b}, S. Chouridou¹⁶², Y.S. Chow¹²⁰, M.C. Chu^{63a}, X. Chu^{15a}, J. Chudoba¹⁴¹, A.J. Chuinard¹⁰³, J.J. Chwastowski⁸⁴, L. Chytka¹³⁰, K.M. Ciesla⁸⁴, D. Cinca⁴⁷, V. Cindro⁹¹, I.A. Cioară^{27b}, A. Ciocio¹⁸, F. Cirotto^{69a,69b}, Z.H. Citron^{180,m}, M. Citterio^{68a}, D.A. Ciubotaru^{27b}, B.M. Ciungu¹⁶⁷, A. Clark⁵⁴, M.R. Clark³⁹, P.J. Clark⁵⁰, C. Clement^{45a,45b}, Y. Coadou¹⁰¹, M. Cobal^{66a,66c}, A. Coccaro^{55b}, J. Cochran⁷⁸, H. Cohen¹⁶¹, A.E.C. Coimbra³⁶, L. Colasurdo¹¹⁹, B. Cole³⁹, A.P. Colijn¹²⁰, J. Collot⁵⁸, P. Conde Muñoz^{140a,g}, E. Coniavit⁵², S.H. Connell^{33b}, I.A. Connelly⁵⁷, S. Constantinescu^{27b}, F. Conventi^{69a,bc}, A.M. Cooper-Sarkar¹³⁵, F. Cormier¹⁷⁵, K.J.R. Cormier¹⁶⁷, L.D. Corpe⁹⁴, M. Corradi^{72a,72b}, E.E. Corrigan⁹⁶, F. Corriveau^{103,ah}, A. Cortes-Gonzalez³⁶, M.J. Costa¹⁷⁴, F. Costanza⁵, D. Costanzo¹⁴⁹, G. Cowan⁹³, J.W. Cowley³², J. Crane¹⁰⁰, K. Cranmer¹²⁴, S.J. Crawley⁵⁷, R.A. Creager¹³⁷, S. Crépé-Renaudin⁵⁸, F. Crescioli¹³⁶, M. Cristinziani²⁴, V. Croft¹²⁰, G. Crosetti^{41b,41a}, A. Cueto⁵, T. Cuhadar Donszelmann¹⁴⁹,

A.R. Cukierman¹⁵³, S. Czekiera⁸⁴, P. Czodrowski³⁶, M.J. Da Cunha Sargedas De Sousa^{60b},
 J.V. Da Fonseca Pinto^{80b}, C. Da Via¹⁰⁰, W. Dabrowski^{83a}, T. Dado^{28a}, S. Dahbi^{35e}, T. Dai¹⁰⁵,
 C. Dallapiccola¹⁰², M. Dam⁴⁰, G. D'amen^{23b,23a}, V. D'Amico^{74a,74b}, J. Damp⁹⁹, J.R. Dandoy¹³⁷,
 M.F. Daneri³⁰, N.P. Dang^{181,k}, N.S. Dann¹⁰⁰, M. Danninger¹⁷⁵, V. Dao³⁶, G. Darbo^{55b}, O. Dartsi⁵,
 A. Dattagupta¹³¹, T. Daubney⁴⁶, S. D'Auria^{68a,68b}, W. Davey²⁴, C. David⁴⁶, T. Davidek¹⁴³, D.R. Davis⁴⁹,
 I. Dawson¹⁴⁹, K. De⁸, R. De Asmundis^{69a}, M. De Beurs¹²⁰, S. De Castro^{23b,23a}, S. De Cecco^{72a,72b},
 N. De Groot¹¹⁹, P. de Jong¹²⁰, H. De la Torre¹⁰⁶, A. De Maria^{15c}, D. De Pedis^{72a}, A. De Salvo^{72a},
 U. De Sanctis^{73a,73b}, M. De Santis^{73a,73b}, A. De Santo¹⁵⁶, K. De Vasconcelos Corga¹⁰¹,
 J.B. De Vivie De Regie¹³², C. Debenedetti¹⁴⁶, D.V. Dedovich⁷⁹, A.M. Deiana⁴², M. Del Gaudio^{41b,41a},
 J. Del Peso⁹⁸, Y. Delabat Diaz⁴⁶, D. Delgove¹³², F. Deliot^{145,t}, C.M. Delitzsch⁷, M. Della Pietra^{69a,69b},
 D. Della Volpe⁵⁴, A. Dell'Acqua³⁶, L. Dell'Asta^{73a,73b}, M. Delmastro⁵, C. Delporte¹³², P.A. Delsart⁵⁸,
 D.A. DeMarco¹⁶⁷, S. Demers¹⁸³, M. Demichev⁷⁹, G. Demontigny¹⁰⁹, S.P. Denisov¹²³, D. Denysiuk¹²⁰,
 L. D'Eramo¹³⁶, D. Derendarz⁸⁴, J.E. Derkaoui^{35d}, F. Derue¹³⁶, P. Dervan⁹⁰, K. Desch²⁴, C. Deterre⁴⁶,
 K. Dette¹⁶⁷, C. Deutsch²⁴, M.R. Devesa³⁰, P.O. Deviveiros³⁶, A. Dewhurst¹⁴⁴, S. Dhaliwal²⁶,
 F.A. Di Bello⁵⁴, A. Di Ciaccio^{73a,73b}, L. Di Ciaccio⁵, W.K. Di Clemente¹³⁷, C. Di Donato^{69a,69b},
 A. Di Girolamo³⁶, G. Di Gregorio^{71a,71b}, B. Di Micco^{74a,74b}, R. Di Nardo¹⁰², K.F. Di Petrillo⁵⁹,
 R. Di Sipio¹⁶⁷, D. Di Valentino³⁴, C. Diaconu¹⁰¹, F.A. Dias⁴⁰, T. Dias Do Vale^{140a}, M.A. Diaz^{147a},
 J. Dickinson¹⁸, E.B. Diehl¹⁰⁵, J. Dietrich¹⁹, S. Díez Cornell⁴⁶, A. Dimitrievska¹⁸, W. Ding^{15b},
 J. Dingfelder²⁴, F. Dittus³⁶, F. Djama¹⁰¹, T. Djobava^{159b}, J.I. Djuvsland¹⁷, M.A.B. Do Vale^{80c},
 M. Dobre^{27b}, D. Dodsworth²⁶, C. Doglioni⁹⁶, J. Dolejsi¹⁴³, Z. Dolezal¹⁴³, M. Donadelli^{80d}, B. Dong^{60c},
 J. Donini³⁸, A. D'onofrio⁹², M. D'Onofrio⁹⁰, J. Dopke¹⁴⁴, A. Doria^{69a}, M.T. Dova⁸⁸, A.T. Doyle⁵⁷,
 E. Drechsler¹⁵², E. Dreyer¹⁵², T. Dreyer⁵³, A.S. Drobac¹⁷⁰, Y. Duan^{60b}, F. Dubinin¹¹⁰, M. Dubovsky^{28a},
 A. Dubreuil⁵⁴, E. Duchovni¹⁸⁰, G. Duckeck¹¹⁴, A. Ducourthial¹³⁶, O.A. Ducu¹⁰⁹, D. Duda¹¹⁵,
 A. Dudarev³⁶, A.C. Dudder⁹⁹, E.M. Duffield¹⁸, L. Duflot¹³², M. Dührssen³⁶, C. Dülsen¹⁸²,
 M. Dumancic¹⁸⁰, A.E. Dumitriu^{27b}, A.K. Duncan⁵⁷, M. Dunford^{61a}, A. Duperin¹⁰¹, H. Duran Yildiz^{4a},
 M. Düren⁵⁶, A. Durglishvili^{159b}, D. Duschinger⁴⁸, B. Dutta⁴⁶, D. Duvnjak¹, G.I. Dyckes¹³⁷, M. Dyndal³⁶,
 S. Dysch¹⁰⁰, B.S. Dziedzic⁸⁴, K.M. Ecker¹¹⁵, R.C. Edgar¹⁰⁵, T. Eifert³⁶, G. Eigen¹⁷, K. Einsweiler¹⁸,
 T. Ekelof¹⁷², H. El Jarrari^{35e}, M. El Kacimi^{35c}, R. El Kosseifi¹⁰¹, V. Ellajosyula¹⁷², M. Ellert¹⁷²,
 F. Ellinghaus¹⁸², A.A. Elliot⁹², N. Ellis³⁶, J. Elmsheuser²⁹, M. Elsing³⁶, D. Emeliyanov¹⁴⁴,
 A. Emerman³⁹, Y. Enari¹⁶³, J.S. Ennis¹⁷⁸, M.B. Epland⁴⁹, J. Erdmann⁴⁷, A. Ereditato²⁰, M. Errenst³⁶,
 M. Escalier¹³², C. Escobar¹⁷⁴, O. Estrada Pastor¹⁷⁴, E. Etzion¹⁶¹, H. Evans⁶⁵, A. Ezhilov¹³⁸, F. Fabbri⁵⁷,
 L. Fabbri^{23b,23a}, V. Fabiani¹¹⁹, G. Facini⁹⁴, R.M. Faisca Rodrigues Pereira^{140a}, R.M. Fakhruddinov¹²³,
 S. Falciano^{72a}, P.J. Falke⁵, S. Falke⁵, J. Faltova¹⁴³, Y. Fang^{15a}, Y. Fang^{15a}, G. Fanourakis⁴⁴,
 M. Fanti^{68a,68b}, M. Faraj^{66a,66c,w}, A. Farbin⁸, A. Farilla^{74a}, E.M. Farina^{70a,70b}, T. Farooque¹⁰⁶, S. Farrell¹⁸,
 S.M. Farrington⁵⁰, P. Farthouat³⁶, F. Fassi^{35e}, P. Fassnacht³⁶, D. Fassouliotis⁹, M. Faucci Giannelli⁵⁰,
 W.J. Fawcett³², L. Fayard¹³², O.L. Fedin^{138,r}, W. Fedorko¹⁷⁵, M. Feickert⁴², S. Feigl¹³⁴, L. Feligioni¹⁰¹,
 A. Fell¹⁴⁹, C. Feng^{60b}, E.J. Feng³⁶, M. Feng⁴⁹, M.J. Fenton⁵⁷, A.B. Fenyuk¹²³, J. Ferrando⁴⁶,
 A. Ferrante¹⁷³, A. Ferrari¹⁷², P. Ferrari¹²⁰, R. Ferrari^{70a}, D.E. Ferreira de Lima^{61b}, A. Ferrer¹⁷⁴,
 D. Ferrere⁵⁴, C. Ferretti¹⁰⁵, F. Fiedler⁹⁹, A. Filipčič⁹¹, F. Filthaut¹¹⁹, K.D. Finelli²⁵,
 M.C.N. Fiolhais^{140a,140c,a}, L. Fiorini¹⁷⁴, F. Fischer¹¹⁴, W.C. Fisher¹⁰⁶, I. Fleck¹⁵¹, P. Fleischmann¹⁰⁵,
 R.R.M. Fletcher¹³⁷, T. Flick¹⁸², B.M. Flierl¹¹⁴, L. Flores¹³⁷, L.R. Flores Castillo^{63a}, F.M. Follega^{75a,75b},
 N. Fomin¹⁷, J.H. Foo¹⁶⁷, G.T. Forcolin^{75a,75b}, A. Formica¹⁴⁵, F.A. Förster¹⁴, A.C. Forti¹⁰⁰, A.G. Foster²¹,
 M.G. Foti¹³⁵, D. Fournier¹³², H. Fox⁸⁹, P. Francavilla^{71a,71b}, S. Francescato^{72a,72b}, M. Franchini^{23b,23a},
 S. Franchino^{61a}, D. Francis³⁶, L. Franconi²⁰, M. Franklin⁵⁹, A.N. Fray⁹², B. Freund¹⁰⁹, W.S. Freund^{80b},
 E.M. Freundlich⁴⁷, D.C. Frizzell¹²⁸, D. Froidevaux³⁶, J.A. Frost¹³⁵, C. Fukunaga¹⁶⁴,
 E. Fullana Torregrosa¹⁷⁴, E. Fumagalli^{55b,55a}, T. Fusayasu¹¹⁶, J. Fuster¹⁷⁴, A. Gabrielli^{23b,23a},
 A. Gabrielli¹⁸, G.P. Gach^{83a}, S. Gadatsch⁵⁴, P. Gadow¹¹⁵, G. Gagliardi^{55b,55a}, L.G. Gagnon¹⁰⁹,

C. Galea^{27b}, B. Galhardo^{140a}, G.E. Gallardo¹³⁵, E.J. Gallas¹³⁵, B.J. Gallop¹⁴⁴, P. Gallus¹⁴², G. Galster⁴⁰, R. Gamboa Goni⁹², K.K. Gan¹²⁶, S. Ganguly¹⁸⁰, J. Gao^{60a}, Y. Gao⁹⁰, Y.S. Gao^{31,o}, C. García¹⁷⁴, J.E. García Navarro¹⁷⁴, J.A. García Pascual^{15a}, C. Garcia-Argos⁵², M. Garcia-Sciveres¹⁸, R.W. Gardner³⁷, N. Garelli¹⁵³, S. Gargiulo⁵², V. Garonne¹³⁴, A. Gaudiello^{55b,55a}, G. Gaudio^{70a}, I.L. Gavrilenko¹¹⁰, A. Gavrilyuk¹¹¹, C. Gay¹⁷⁵, G. Gaycken²⁴, E.N. Gazis¹⁰, A.A. Geanta^{27b}, C.N.P. Gee¹⁴⁴, J. Geisen⁵³, M. Geisen⁹⁹, M.P. Geisler^{61a}, C. Gemme^{55b}, M.H. Genest⁵⁸, C. Geng¹⁰⁵, S. Gentile^{72a,72b}, S. George⁹³, T. Geralis⁴⁴, L.O. Gerlach⁵³, P. Gessinger-Befurt⁹⁹, G. Gessner⁴⁷, S. Ghasemi¹⁵¹, M. Ghasemi Bostanabad¹⁷⁶, A. Ghosh¹³², A. Ghosh⁷⁷, B. Giacobbe^{23b}, S. Giagu^{72a,72b}, N. Giangiacomi^{23b,23a}, P. Giannetti^{71a}, A. Giannini^{69a,69b}, S.M. Gibson⁹³, M. Gignac¹⁴⁶, D. Gillberg³⁴, G. Gilles¹⁸², D.M. Gingrich^{3,bb}, M.P. Giordani^{66a,66c}, F.M. Giorgi^{23b}, P.F. Giraud¹⁴⁵, G. Giugliarelli^{66a,66c}, D. Giugni^{68a}, F. Giuli^{73a,73b}, S. Gkaitatzis¹⁶², I. Gkialas^{9,i}, E.L. Gkougkousis¹⁴, P. Gkountoumis¹⁰, L.K. Gladilin¹¹³, C. Glasman⁹⁸, J. Glatzer¹⁴, P.C.F. Glaysher⁴⁶, A. Glazov⁴⁶, M. Goblirsch-Kolb²⁶, S. Goldfarb¹⁰⁴, T. Golling⁵⁴, D. Golubkov¹²³, A. Gomes^{140a,140b}, R. Goncalves Gama⁵³, R. Gonçalo^{140a,140b}, G. Gonella⁵², L. Gonella²¹, A. Gongadze⁷⁹, F. Gonnella²¹, J.L. Gonski⁵⁹, S. González de la Hoz¹⁷⁴, S. Gonzalez-Sevilla⁵⁴, G.R. Goncalvo Rodriguez¹⁷⁴, L. Goossens³⁶, P.A. Gorbounov¹¹¹, H.A. Gordon²⁹, B. Gorini³⁶, E. Gorini^{67a,67b}, A. Gorišek⁹¹, A.T. Goshaw⁴⁹, M.I. Gostkin⁷⁹, C.A. Gottardo²⁴, M. Gouighri^{35b}, D. Goujdami^{35c}, A.G. Goussiou¹⁴⁸, N. Govender^{33b,b}, C. Goy⁵, E. Gozani¹⁶⁰, I. Grabowska-Bold^{83a}, E.C. Graham⁹⁰, J. Gramling¹⁷¹, E. Gramstad¹³⁴, S. Grancagnolo¹⁹, M. Grandi¹⁵⁶, V. Gratchev¹³⁸, P.M. Gravila^{27f}, F.G. Gravili^{67a,67b}, C. Gray⁵⁷, H.M. Gray¹⁸, C. Grefe²⁴, K. Gregersen⁹⁶, I.M. Gregor⁴⁶, P. Grenier¹⁵³, K. Grevtsov⁴⁶, C. Grieco¹⁴, N.A. Grieser¹²⁸, J. Griffiths⁸, A.A. Grillo¹⁴⁶, K. Grimm^{31,n}, S. Grinstein^{14,ab}, J.-F. Grivaz¹³², S. Groh⁹⁹, E. Gross¹⁸⁰, J. Grosse-Knetter⁵³, Z.J. Grout⁹⁴, C. Grud¹⁰⁵, A. Grummer¹¹⁸, L. Guan¹⁰⁵, W. Guan¹⁸¹, J. Guenther³⁶, A. Guerguichon¹³², J.G.R. Guerrero Rojas¹⁷⁴, F. Guescini¹¹⁵, D. Guest¹⁷¹, R. Gugel⁵², T. Guillemin⁵, S. Guindon³⁶, U. Gul⁵⁷, J. Guo^{60c}, W. Guo¹⁰⁵, Y. Guo^{60a,v}, Z. Guo¹⁰¹, R. Gupta⁴⁶, S. Gurbuz^{12c}, G. Gustavino¹²⁸, P. Gutierrez¹²⁸, C. Gutschow⁹⁴, C. Guyot¹⁴⁵, M.P. Guzik^{83a}, C. Gwenlan¹³⁵, C.B. Gwilliam⁹⁰, A. Haas¹²⁴, C. Haber¹⁸, H.K. Hadavand⁸, N. Haddad^{35e}, A. Hadef^{60a}, S. Hageböck³⁶, M. Hagihara¹⁶⁹, M. Haleem¹⁷⁷, J. Haley¹²⁹, G. Halladjian¹⁰⁶, G.D. Hallewell¹⁰¹, K. Hamacher¹⁸², P. Hamal¹³⁰, K. Hamano¹⁷⁶, H. Hamdaoui^{35e}, G.N. Hamity¹⁴⁹, K. Han^{60a,ao}, L. Han^{60a}, S. Han^{15a,15d}, K. Hanagaki^{81,z}, M. Hance¹⁴⁶, D.M. Handl¹¹⁴, B. Haney¹³⁷, R. Hankache¹³⁶, E. Hansen⁹⁶, J.B. Hansen⁴⁰, J.D. Hansen⁴⁰, M.C. Hansen²⁴, P.H. Hansen⁴⁰, E.C. Hanson¹⁰⁰, K. Hara¹⁶⁹, A.S. Hard¹⁸¹, T. Harenberg¹⁸², S. Harkusha¹⁰⁷, P.F. Harrison¹⁷⁸, N.M. Hartmann¹¹⁴, Y. Hasegawa¹⁵⁰, A. Hasib⁵⁰, S. Hassani¹⁴⁵, S. Haug²⁰, R. Hauser¹⁰⁶, L.B. Havener³⁹, M. Havranek¹⁴², C.M. Hawkes²¹, R.J. Hawkings³⁶, D. Hayden¹⁰⁶, C. Hayes¹⁵⁵, R.L. Hayes¹⁷⁵, C.P. Hays¹³⁵, J.M. Hays⁹², H.S. Hayward⁹⁰, S.J. Haywood¹⁴⁴, F. He^{60a}, M.P. Heath⁵⁰, V. Hedberg⁹⁶, L. Heelan⁸, S. Heer²⁴, K.K. Heidegger⁵², W.D. Heidorn⁷⁸, J. Heilman³⁴, S. Heim⁴⁶, T. Heim¹⁸, B. Heinemann^{46,aw}, J.J. Heinrich¹³¹, L. Heinrich³⁶, C. Heinz⁵⁶, J. Hejbal¹⁴¹, L. Helary^{61b}, A. Held¹⁷⁵, S. Hellesund¹³⁴, C.M. Helling¹⁴⁶, S. Hellman^{45a,45b}, C. Helsens³⁶, R.C.W. Henderson⁸⁹, Y. Heng¹⁸¹, S. Henkelmann¹⁷⁵, A.M. Henriques Correia³⁶, G.H. Herbert¹⁹, H. Herde²⁶, V. Herget¹⁷⁷, Y. Hernández Jiménez^{33c}, H. Herr⁹⁹, M.G. Herrmann¹¹⁴, T. Herrmann⁴⁸, G. Herten⁵², R. Hertenberger¹¹⁴, L. Hervas³⁶, T.C. Herwig¹³⁷, G.G. Hesketh⁹⁴, N.P. Hessey^{168a}, A. Higashida¹⁶³, S. Higashino⁸¹, E. Higón-Rodriguez¹⁷⁴, K. Hildebrand³⁷, E. Hill¹⁷⁶, J.C. Hill³², K.K. Hill²⁹, K.H. Hiller⁴⁶, S.J. Hillier²¹, M. Hils⁴⁸, I. Hinchliffe¹⁸, F. Hinterkeuser²⁴, M. Hirose¹³³, S. Hirose⁵², D. Hirschbuehl¹⁸², B. Hiti⁹¹, O. Hladík¹⁴¹, D.R. Hlaluku^{33c}, X. Hoad⁵⁰, J. Hobbs¹⁵⁵, N. Hod¹⁸⁰, M.C. Hodgkinson¹⁴⁹, A. Hoecker³⁶, F. Hoenig¹¹⁴, D. Hohn⁵², D. Hohov¹³², T.R. Holmes³⁷, M. Holzbock¹¹⁴, L.B.A.H Hommels³², S. Honda¹⁶⁹, T. Honda⁸¹, T.M. Hong¹³⁹, A. Höhne¹¹⁵, B.H. Hooberman¹⁷³, W.H. Hopkins⁶, Y. Horii¹¹⁷, P. Horn⁴⁸, L.A. Horyn³⁷, J.-Y. Hostachy⁵⁸, A. Hostiuc¹⁴⁸, S. Hou¹⁵⁸, A. Hoummada^{35a}, J. Howarth¹⁰⁰, J. Hoya⁸⁸, M. Hrabovsky¹³⁰, J. Hrdinka⁷⁶, I. Hristova¹⁹, J. Hrivnac¹³², A. Hrynevich¹⁰⁸, T. Hrynn'ova⁵, P.J. Hsu⁶⁴, S.-C. Hsu¹⁴⁸, Q. Hu²⁹, S. Hu^{60c},

Y. Huang^{15a}, Z. Hubacek¹⁴², F. Hubaut¹⁰¹, M. Huebner²⁴, F. Huegging²⁴, T.B. Huffman¹³⁵, M. Huhtinen³⁶, R.F.H. Hunter³⁴, P. Huo¹⁵⁵, A.M. Hupe³⁴, N. Huseynov^{79,aj}, J. Huston¹⁰⁶, J. Huth⁵⁹, R. Hyneman¹⁰⁵, S. Hyrych^{28a}, G. Iacobucci⁵⁴, G. Iakovidis²⁹, I. Ibragimov¹⁵¹, L. Iconomidou-Fayard¹³², Z. Idrissi^{35e}, P. Iengo³⁶, R. Ignazzi⁴⁰, O. Igonkina^{120,ad,*}, R. Iguchi¹⁶³, T. Iizawa⁵⁴, Y. Ikegami⁸¹, M. Ikeno⁸¹, D. Iliadis¹⁶², N. Ilic¹¹⁹, F. Iltzsche⁴⁸, G. Introzzi^{70a,70b}, M. Iodice^{74a}, K. Iordanidou^{168a}, V. Ippolito^{72a,72b}, M.F. Isacson¹⁷², M. Ishino¹⁶³, M. Ishitsuka¹⁶⁵, W. Islam¹²⁹, C. Issever¹³⁵, S. Istin¹⁶⁰, F. Ito¹⁶⁹, J.M. Iturbe Ponce^{63a}, R. Iuppa^{75a,75b}, A. Ivina¹⁸⁰, H. Iwasaki⁸¹, J.M. Izen⁴³, V. Izzo^{69a}, P. Jacka¹⁴¹, P. Jackson¹, R.M. Jacobs²⁴, B.P. Jaeger¹⁵², V. Jain², G. Jäkel¹⁸², K.B. Jakobi⁹⁹, K. Jakobs⁵², S. Jakobsen⁷⁶, T. Jakoubek¹⁴¹, J. Jamieson⁵⁷, K.W. Janas^{83a}, R. Jansky⁵⁴, J. Janssen²⁴, M. Janus⁵³, P.A. Janus^{83a}, G. Jarlskog⁹⁶, N. Javadov^{79,aj}, T. Javůrek³⁶, M. Javurkova⁵², F. Jeanneau¹⁴⁵, L. Jeanty¹³¹, J. Jejelava^{159a,ak}, A. Jelinskas¹⁷⁸, P. Jenni^{52,c}, J. Jeong⁴⁶, N. Jeong⁴⁶, S. Jézéquel⁵, H. Ji¹⁸¹, J. Jia¹⁵⁵, H. Jiang⁷⁸, Y. Jiang^{60a}, Z. Jiang^{153,s}, S. Jiggins⁵², F.A. Jimenez Morales³⁸, J. Jimenez Pena¹⁷⁴, S. Jin^{15c}, A. Jinaru^{27b}, O. Jinnouchi¹⁶⁵, H. Jivan^{33c}, P. Johansson¹⁴⁹, K.A. Johns⁷, C.A. Johnson⁶⁵, K. Jon-And^{45a,45b}, R.W.L. Jones⁸⁹, S.D. Jones¹⁵⁶, S. Jones⁷, T.J. Jones⁹⁰, J. Jongmanns^{61a}, P.M. Jorge^{140a}, J. Jovicevic³⁶, X. Ju¹⁸, J.J. Junggeburth¹¹⁵, A. Juste Rozas^{14,ab}, A. Kaczmarska⁸⁴, M. Kado^{72a,72b}, H. Kagan¹²⁶, M. Kagan¹⁵³, C. Kahra⁹⁹, T. Kaji¹⁷⁹, E. Kajomovitz¹⁶⁰, C.W. Kalderon⁹⁶, A. Kaluza⁹⁹, A. Kamenshchikov¹²³, L. Kanjir⁹¹, Y. Kano¹⁶³, V.A. Kantserov¹¹², J. Kanzaki⁸¹, L.S. Kaplan¹⁸¹, D. Kar^{33c}, M.J. Kareem^{168b}, E. Karentzos¹⁰, S.N. Karpov⁷⁹, Z.M. Karpova⁷⁹, V. Kartvelishvili⁸⁹, A.N. Karyukhin¹²³, L. Kashif¹⁸¹, R.D. Kass¹²⁶, A. Kastanas^{45a,45b}, Y. Kataoka¹⁶³, C. Kato^{60d,60c}, J. Katzy⁴⁶, K. Kawade⁸², K. Kawagoe⁸⁷, T. Kawaguchi¹¹⁷, T. Kawamoto¹⁶³, G. Kawamura⁵³, E.F. Kay¹⁷⁶, V.F. Kazanin^{122b,122a}, R. Keeler¹⁷⁶, R. Kehoe⁴², J.S. Keller³⁴, E. Kellermann⁹⁶, D. Kelsey¹⁵⁶, J.J. Kempster²¹, J. Kendrick²¹, O. Kepka¹⁴¹, S. Kersten¹⁸², B.P. Kerševan⁹¹, S. Ketabchi Haghigat¹⁶⁷, M. Khader¹⁷³, F. Khalil-Zada¹³, M. Khandoga¹⁴⁵, A. Khanov¹²⁹, A.G. Kharlamov^{122b,122a}, T. Kharlamova^{122b,122a}, E.E. Khoda¹⁷⁵, A. Khodinov¹⁶⁶, T.J. Khoo⁵⁴, E. Khramov⁷⁹, J. Khubua^{159b}, S. Kido⁸², M. Kiehn⁵⁴, C.R. Kilby⁹³, Y.K. Kim³⁷, N. Kimura^{66a,66c}, O.M. Kind¹⁹, B.T. King^{90,*}, D. Kirchmeier⁴⁸, J. Kirk¹⁴⁴, A.E. Kiryunin¹¹⁵, T. Kishimoto¹⁶³, D.P. Kisliuk¹⁶⁷, V. Kitali⁴⁶, O. Kivernyk⁵, E. Kladiva^{28b,*}, T. Klapdor-Kleingrothaus⁵², M. Klassen^{61a}, M.H. Klein¹⁰⁵, M. Klein⁹⁰, U. Klein⁹⁰, K. Kleinknecht⁹⁹, P. Klimek¹²¹, A. Klimentov²⁹, T. Klingl²⁴, T. Klioutchnikova³⁶, F.F. Klitzner¹¹⁴, P. Kluit¹²⁰, S. Kluth¹¹⁵, E. Kneringer⁷⁶, E.B.F.G. Knoops¹⁰¹, A. Knue⁵², D. Kobayashi⁸⁷, T. Kobayashi¹⁶³, M. Kobel⁴⁸, M. Kocian¹⁵³, P. Kodys¹⁴³, P.T. Koenig²⁴, T. Koffas³⁴, N.M. Köhler¹¹⁵, T. Koi¹⁵³, M. Kolb^{61b}, I. Koletsou⁵, T. Komarek¹³⁰, T. Kondo⁸¹, N. Kondrashova^{60c}, K. Köneke⁵², A.C. König¹¹⁹, T. Kono¹²⁵, R. Konoplich^{124,ar}, V. Konstantinides⁹⁴, N. Konstantinidis⁹⁴, B. Konya⁹⁶, R. Kopeliansky⁶⁵, S. Koperny^{83a}, K. Korcyl⁸⁴, K. Kordas¹⁶², G. Koren¹⁶¹, A. Korn⁹⁴, I. Korolkov¹⁴, E.V. Korolkova¹⁴⁹, N. Korotkova¹¹³, O. Kortner¹¹⁵, S. Kortner¹¹⁵, T. Kosek¹⁴³, V.V. Kostyukhin²⁴, A. Kotwal⁴⁹, A. Koulouris¹⁰, A. Kourkoumeli-Charalampidi^{70a,70b}, C. Kourkoumelis⁹, E. Kourlitis¹⁴⁹, V. Kouskoura²⁹, A.B. Kowalewska⁸⁴, R. Kowalewski¹⁷⁶, C. Kozakai¹⁶³, W. Kozanecki¹⁴⁵, A.S. Kozhin¹²³, V.A. Kramarenko¹¹³, G. Kramberger⁹¹, D. Krasnopol'tsev^{60a}, M.W. Krasny¹³⁶, A. Krasznahorkay³⁶, D. Krauss¹¹⁵, J.A. Kremer^{83a}, J. Kretzschmar⁹⁰, P. Krieger¹⁶⁷, F. Krieter¹¹⁴, A. Krishnan^{61b}, K. Krizka¹⁸, K. Kroeninger⁴⁷, H. Kroha¹¹⁵, J. Kroll¹⁴¹, J. Kroll¹³⁷, J. Krstic¹⁶, U. Kruchonak⁷⁹, H. Krüger²⁴, N. Krumnack⁷⁸, M.C. Kruse⁴⁹, J.A. Krzysiak⁸⁴, T. Kubota¹⁰⁴, O. Kuchinskaia¹⁶⁶, S. Kuday^{4b}, J.T. Kuechler⁴⁶, S. Kuehn³⁶, A. Kugel^{61a}, T. Kuhl⁴⁶, V. Kukhtin⁷⁹, R. Kukla¹⁰¹, Y. Kulchitsky^{107,an}, S. Kuleshov^{147b}, Y.P. Kulinich¹⁷³, M. Kuna⁵⁸, T. Kunigo⁸⁵, A. Kupco¹⁴¹, T. Kupfer⁴⁷, O. Kuprash⁵², H. Kurashige⁸², L.L. Kurchaninov^{168a}, Y.A. Kurochkin¹⁰⁷, A. Kurova¹¹², M.G. Kurth^{15a,15d}, E.S. Kuwertz³⁶, M. Kuze¹⁶⁵, A.K. Kvam¹⁴⁸, J. Kvita¹³⁰, T. Kwan¹⁰³, A. La Rosa¹¹⁵, L. La Rotonda^{41b,41a}, F. La Ruffa^{41b,41a}, C. Lacasta¹⁷⁴, F. Lacava^{72a,72b}, D.P.J. Lack¹⁰⁰, H. Lacker¹⁹, D. Lacour¹³⁶, E. Ladygin⁷⁹, R. Lafaye⁵, B. Laforge¹³⁶, T. Lagouri^{33c}, S. Lai⁵³, S. Lammers⁶⁵, W. Lampl⁷, C. Lampoudis¹⁶², E. Lançon²⁹, U. Landgraf⁵², M.P.J. Landon⁹², M.C. Lanfermann⁵⁴, V.S. Lang⁴⁶, J.C. Lange⁵³,

R.J. Langenberg³⁶, A.J. Lankford¹⁷¹, F. Lanni²⁹, K. Lantzsch²⁴, A. Lanza^{70a}, A. Lapertosa^{55b,55a}, S. Laplace¹³⁶, J.F. Laporte¹⁴⁵, T. Lari^{68a}, F. Lasagni Manghi^{23b,23a}, M. Lassnig³⁶, T.S. Lau^{63a}, A. Laudrain¹³², A. Laurier³⁴, M. Lavorgna^{69a,69b}, M. Lazzaroni^{68a,68b}, B. Le¹⁰⁴, E. Le Guirriec¹⁰¹, M. LeBlanc⁷, T. LeCompte⁶, F. Ledroit-Guillon⁵⁸, C.A. Lee²⁹, G.R. Lee¹⁷, L. Lee⁵⁹, S.C. Lee¹⁵⁸, S.J. Lee³⁴, B. Lefebvre^{168a}, M. Lefebvre¹⁷⁶, F. Legger¹¹⁴, C. Leggett¹⁸, K. Lehmann¹⁵², N. Lehmann¹⁸², G. Lehmann Miotto³⁶, W.A. Leight⁴⁶, A. Leisos^{162,aa}, M.A.L. Leite^{80d}, C.E. Leitgeb¹¹⁴, R. Leitner¹⁴³, D. Lellouch^{180,*}, K.J.C. Leney⁴², T. Lenz²⁴, B. Lenzi³⁶, R. Leone⁷, S. Leone^{71a}, C. Leonidopoulos⁵⁰, A. Leopold¹³⁶, G. Lerner¹⁵⁶, C. Leroy¹⁰⁹, R. Les¹⁶⁷, C.G. Lester³², M. Levchenko¹³⁸, J. Levêque⁵, D. Levin¹⁰⁵, L.J. Levinson¹⁸⁰, D.J. Lewis²¹, B. Li^{15b}, B. Li¹⁰⁵, C-Q. Li^{60a}, F. Li^{60c}, H. Li^{60a}, H. Li^{60b}, J. Li^{60c}, K. Li¹⁵³, L. Li^{60c}, M. Li^{15a}, Q. Li^{15a,15d}, Q.Y. Li^{60a}, S. Li^{60d,60c}, X. Li⁴⁶, Y. Li⁴⁶, Z. Li^{60b}, Z. Liang^{15a}, B. Liberti^{73a}, A. Liblong¹⁶⁷, K. Lie^{63c}, S. Liem¹²⁰, C.Y. Lin³², K. Lin¹⁰⁶, T.H. Lin⁹⁹, R.A. Linck⁶⁵, J.H. Lindon²¹, A.L. Lioni⁵⁴, E. Lipeles¹³⁷, A. Lipniacka¹⁷, M. Lisovyi^{61b}, T.M. Liss^{173,ay}, A. Lister¹⁷⁵, A.M. Litke¹⁴⁶, J.D. Little⁸, B. Liu^{78,ag}, B.L. Liu⁶, H.B. Liu²⁹, H. Liu¹⁰⁵, J.B. Liu^{60a}, J.K.K. Liu¹³⁵, K. Liu¹³⁶, M. Liu^{60a}, P. Liu¹⁸, Y. Liu^{15a,15d}, Y.L. Liu¹⁰⁵, Y.W. Liu^{60a}, M. Livan^{70a,70b}, A. Lleres⁵⁸, J. Llorente Merino^{15a}, S.L. Lloyd⁹², C.Y. Lo^{63b}, F. Lo Sterzo⁴², E.M. Lobodzinska⁴⁶, P. Loch⁷, S. Loffredo^{73a,73b}, T. Lohse¹⁹, K. Lohwasser¹⁴⁹, M. Lokajicek¹⁴¹, J.D. Long¹⁷³, R.E. Long⁸⁹, L. Longo³⁶, K.A. Looper¹²⁶, J.A. Lopez^{147b}, I. Lopez Paz¹⁰⁰, A. Lopez Solis¹⁴⁹, J. Lorenz¹¹⁴, N. Lorenzo Martinez⁵, M. Losada²², P.J. Lösel¹¹⁴, A. Lösle⁵², X. Lou⁴⁶, X. Lou^{15a}, A. Lounis¹³², J. Love⁶, P.A. Love⁸⁹, J.J. Lozano Bahilo¹⁷⁴, M. Lu^{60a}, Y.J. Lu⁶⁴, H.J. Lubatti¹⁴⁸, C. Luci^{72a,72b}, A. Lucotte⁵⁸, C. Luedtke⁵², F. Luehring⁶⁵, I. Luise¹³⁶, L. Luminari^{72a}, B. Lund-Jensen¹⁵⁴, M.S. Lutz¹⁰², D. Lynn²⁹, R. Lysak¹⁴¹, E. Lytken⁹⁶, F. Lyu^{15a}, V. Lyubushkin⁷⁹, T. Lyubushkina⁷⁹, H. Ma²⁹, L.L. Ma^{60b}, Y. Ma^{60b}, G. Maccarrone⁵¹, A. Macchiolo¹¹⁵, C.M. Macdonald¹⁴⁹, J. Machado Miguens¹³⁷, D. Madaffari¹⁷⁴, R. Madar³⁸, W.F. Mader⁴⁸, N. Madysa⁴⁸, J. Maeda⁸², K. Maekawa¹⁶³, S. Maeland¹⁷, T. Maeno²⁹, M. Maerker⁴⁸, A.S. Maevskiy¹¹³, V. Magerl⁵², N. Magini⁷⁸, D.J. Mahon³⁹, C. Maidantchik^{80b}, T. Maier¹¹⁴, A. Maio^{140a,140b,140d}, O. Majersky^{28a}, S. Majewski¹³¹, Y. Makida⁸¹, N. Makovec¹³², B. Malaescu¹³⁶, Pa. Malecki⁸⁴, V.P. Maleev¹³⁸, F. Malek⁵⁸, U. Mallik⁷⁷, D. Malon⁶, C. Malone³², S. Maltezos¹⁰, S. Malyukov⁷⁹, J. Mamuzic¹⁷⁴, G. Mancini⁵¹, I. Mandic⁹¹, L. Manhaes de Andrade Filho^{80a}, I.M. Maniatis¹⁶², J. Manjarres Ramos⁴⁸, K.H. Mankinen⁹⁶, A. Mann¹¹⁴, A. Manousos⁷⁶, B. Mansoulie¹⁴⁵, I. Manthos¹⁶², S. Manzoni¹²⁰, A. Marantis¹⁶², G. Marcea³⁰, L. Marchese¹³⁵, G. Marchiori¹³⁶, M. Marcisovsky¹⁴¹, C. Marcon⁹⁶, C.A. Marin Tobon³⁶, M. Marjanovic³⁸, Z. Marshall¹⁸, M.U.F Martensson¹⁷², S. Marti-Garcia¹⁷⁴, C.B. Martin¹²⁶, T.A. Martin¹⁷⁸, V.J. Martin⁵⁰, B. Martin dit Latour¹⁷, L. Martinelli^{74a,74b}, M. Martinez^{14,ab}, V.I. Martinez Outschoorn¹⁰², S. Martin-Haugh¹⁴⁴, V.S. Martoiu^{27b}, A.C. Martyniuk⁹⁴, A. Marzin³⁶, S.R. Maschek¹¹⁵, L. Masetti⁹⁹, T. Mashimo¹⁶³, R. Mashinistov¹¹⁰, J. Masik¹⁰⁰, A.L. Maslenikov^{122b,122a}, L.H. Mason¹⁰⁴, L. Massa^{73a,73b}, P. Massarotti^{69a,69b}, P. Mastrandrea^{71a,71b}, A. Mastroberardino^{41b,41a}, T. Masubuchi¹⁶³, A. Matic¹¹⁴, P. Mättig²⁴, J. Maurer^{27b}, B. Maček⁹¹, D.A. Maximov^{122b,122a}, R. Mazini¹⁵⁸, I. Maznas¹⁶², S.M. Mazza¹⁴⁶, S.P. Mc Kee¹⁰⁵, T.G. McCarthy¹¹⁵, L.I. McClymont⁹⁴, W.P. McCormack¹⁸, E.F. McDonald¹⁰⁴, J.A. McFayden³⁶, M.A. McKay⁴², K.D. McLean¹⁷⁶, S.J. McMahon¹⁴⁴, P.C. McNamara¹⁰⁴, C.J. McNicol¹⁷⁸, R.A. McPherson^{176,ah}, J.E. Mdhluli^{33c}, Z.A. Meadows¹⁰², S. Meehan¹⁴⁸, T. Megy⁵², S. Mehlhase¹¹⁴, A. Mehta⁹⁰, T. Meideck⁵⁸, B. Meirose⁴³, D. Melini¹⁷⁴, B.R. Mellado Garcia^{33c}, J.D. Mellenthin⁵³, M. Melo^{28a}, F. Meloni⁴⁶, A. Melzer²⁴, S.B. Menary¹⁰⁰, E.D. Mendes Gouveia^{140a,140e}, L. Meng³⁶, X.T. Meng¹⁰⁵, S. Menke¹¹⁵, E. Meoni^{41b,41a}, S. Mergelmeyer¹⁹, S.A.M. Merkt¹³⁹, C. Merlassino²⁰, P. Mermod⁵⁴, L. Merola^{69a,69b}, C. Meroni^{68a}, O. Meshkov^{113,110}, J.K.R. Meshreki¹⁵¹, A. Messina^{72a,72b}, J. Metcalfe⁶, A.S. Mete¹⁷¹, C. Meyer⁶⁵, J. Meyer¹⁶⁰, J.-P. Meyer¹⁴⁵, H. Meyer Zu Theenhausen^{61a}, F. Miano¹⁵⁶, M. Michetti¹⁹, R.P. Middleton¹⁴⁴, L. Mijovic⁵⁰, G. Mikenberg¹⁸⁰, M. Mikestikova¹⁴¹, M. Mikuž⁹¹, H. Mildner¹⁴⁹, M. Milesi¹⁰⁴, A. Milic¹⁶⁷, D.A. Millar⁹², D.W. Miller³⁷, A. Milov¹⁸⁰, D.A. Milstead^{45a,45b}, R.A. Mina^{153,s}, A.A. Minaenko¹²³,

M. Miñano Moya¹⁷⁴, I.A. Minashvili^{159b}, A.I. Mincer¹²⁴, B. Mindur^{83a}, M. Mineev⁷⁹, Y. Minegishi¹⁶³, Y. Ming¹⁸¹, L.M. Mir¹⁴, A. Mirto^{67a,67b}, K.P. Mistry¹³⁷, T. Mitani¹⁷⁹, J. Mitrevski¹¹⁴, V.A. Mitsou¹⁷⁴, M. Mittal^{60c}, A. Miucci²⁰, P.S. Miyagawa¹⁴⁹, A. Mizukami⁸¹, J.U. Mjörnmark⁹⁶, T. Mkrtchyan¹⁸⁴, M. Mlynarikova¹⁴³, T. Moa^{45a,45b}, K. Mochizuki¹⁰⁹, P. Mogg⁵², S. Mohapatra³⁹, R. Moles-Valls²⁴, M.C. Mondragon¹⁰⁶, K. Mönig⁴⁶, J. Monk⁴⁰, E. Monnier¹⁰¹, A. Montalbano¹⁵², J. Montejo Berlingen³⁶, M. Montella⁹⁴, F. Monticelli⁸⁸, S. Monzani^{68a}, N. Morange¹³², D. Moreno²², M. Moreno Llácer³⁶, C. Moreno Martinez¹⁴, P. Morettini^{55b}, M. Morgenstern¹²⁰, S. Morgenstern⁴⁸, D. Mori¹⁵², M. Morii⁵⁹, M. Morinaga¹⁷⁹, V. Morisbak¹³⁴, A.K. Morley³⁶, G. Mornacchi³⁶, A.P. Morris⁹⁴, L. Morvaj¹⁵⁵, P. Moschovakos³⁶, B. Moser¹²⁰, M. Mosidze^{159b}, T. Moskalets¹⁴⁵, H.J. Moss¹⁴⁹, J. Moss^{31,p}, K. Motohashi¹⁶⁵, E. Mountricha³⁶, E.J.W. Moyse¹⁰², S. Muanza¹⁰¹, J. Mueller¹³⁹, R.S.P. Mueller¹¹⁴, D. Muenstermann⁸⁹, G.A. Mullier⁹⁶, J.L. Munoz Martinez¹⁴, F.J. Munoz Sanchez¹⁰⁰, P. Murin^{28b}, W.J. Murray^{178,144}, A. Murrone^{68a,68b}, M. Muškinja¹⁸, C. Mwewa^{33a}, A.G. Myagkov^{123,as}, J. Myers¹³¹, M. Myska¹⁴², B.P. Nachman¹⁸, O. Nackenhorst⁴⁷, A.Nag Nag⁴⁸, K. Nagai¹³⁵, K. Nagano⁸¹, Y. Nagasaka⁶², M. Nagel⁵², E. Nagy¹⁰¹, A.M. Nairz³⁶, Y. Nakahama¹¹⁷, K. Nakamura⁸¹, T. Nakamura¹⁶³, I. Nakano¹²⁷, H. Nanjo¹³³, F. Napolitano^{61a}, R.F. Naranjo Garcia⁴⁶, R. Narayan⁴², D.I. Narrias Villar^{61a}, I. Naryshkin¹³⁸, T. Naumann⁴⁶, G. Navarro²², H.A. Neal^{105,*}, P.Y. Nechaeva¹¹⁰, F. Nechansky⁴⁶, T.J. Neep²¹, A. Negri^{70a,70b}, M. Negrini^{23b}, C. Nellist⁵³, M.E. Nelson¹³⁵, S. Nemecek¹⁴¹, P. Nemethy¹²⁴, M. Nessi^{36,e}, M.S. Neubauer¹⁷³, M. Neumann¹⁸², P.R. Newman²¹, Y.S. Ng¹⁹, Y.W.Y. Ng¹⁷¹, H.D.N. Nguyen¹⁰¹, T. Nguyen Manh¹⁰⁹, E. Nibigira³⁸, R.B. Nickerson¹³⁵, R. Nicolaïdou¹⁴⁵, D.S. Nielsen⁴⁰, J. Nielsen¹⁴⁶, N. Nikiforou¹¹, V. Nikolaenko^{123,as}, I. Nikolic-Audit¹³⁶, K. Nikolopoulos²¹, P. Nilsson²⁹, H.R. Nindhito⁵⁴, Y. Ninomiya⁸¹, A. Nisati^{72a}, N. Nishu^{60c}, R. Nisius¹¹⁵, I. Nitsche⁴⁷, T. Nitta¹⁷⁹, T. Nobe¹⁶³, Y. Noguchi⁸⁵, I. Nomidis¹³⁶, M.A. Nomura²⁹, M. Nordberg³⁶, N. Norjoharuddeen¹³⁵, T. Novak⁹¹, O. Novgorodova⁴⁸, R. Novotny¹⁴², L. Nozka¹³⁰, K. Ntekas¹⁷¹, E. Nurse⁹⁴, F.G. Oakham^{34,bb}, H. Oberlack¹¹⁵, J. Ocariz¹³⁶, A. Ochi⁸², I. Ochoa³⁹, J.P. Ochoa-Ricoux^{147a}, K. O'Connor²⁶, S. Oda⁸⁷, S. Odaka⁸¹, S. Oerdekk⁵³, A. Ogodnik^{83a}, A. Oh¹⁰⁰, S.H. Oh⁴⁹, C.C. Ohm¹⁵⁴, H. Oide^{55b,55a}, M.L. Ojeda¹⁶⁷, H. Okawa¹⁶⁹, Y. Okazaki⁸⁵, Y. Okumura¹⁶³, T. Okuyama⁸¹, A. Olariu^{27b}, L.F. Oleiro Seabra^{140a}, S.A. Olivares Pino^{147a}, D. Oliveira Damazio²⁹, J.L. Oliver¹, M.J.R. Olsson¹⁷¹, A. Olszewski⁸⁴, J. Olszowska⁸⁴, D.C. O'Neil¹⁵², A. Onofre^{140a,140e}, K. Onogi¹¹⁷, P.U.E. Onyisi¹¹, H. Oppen¹³⁴, M.J. Oreglia³⁷, G.E. Orellana⁸⁸, D. Orestano^{74a,74b}, N. Orlando¹⁴, R.S. Orr¹⁶⁷, V. O'Shea⁵⁷, R. Ospanov^{60a}, G. Otero y Garzon³⁰, H. Otono⁸⁷, M. Ouchrif^{35d}, J. Ouellette²⁹, F. Ould-Saada¹³⁴, A. Ouraou¹⁴⁵, Q. Ouyang^{15a}, M. Owen⁵⁷, R.E. Owen²¹, V.E. Ozcan^{12c}, N. Ozturk⁸, J. Pacalt¹³⁰, H.A. Pacey³², K. Pachal⁴⁹, A. Pacheco Pages¹⁴, C. Padilla Aranda¹⁴, S. Pagan Griso¹⁸, M. Paganini¹⁸³, G. Palacino⁶⁵, S. Palazzo⁵⁰, S. Palestini³⁶, M. Palka^{83b}, D. Pallin³⁸, I. Panagoulias¹⁰, C.E. Pandini³⁶, J.G. Panduro Vazquez⁹³, P. Pani⁴⁶, G. Panizzo^{66a,66c}, L. Paolozzi⁵⁴, C. Papadatos¹⁰⁹, K. Papageorgiou^{9,i}, A. Paramonov⁶, D. Paredes Hernandez^{63b}, S.R. Paredes Saenz¹³⁵, B. Parida¹⁶⁶, T.H. Park¹⁶⁷, A.J. Parker⁸⁹, M.A. Parker³², F. Parodi^{55b,55a}, E.W.P. Parrish¹²¹, J.A. Parsons³⁹, U. Parzefall⁵², L. Pascual Dominguez¹³⁶, V.R. Pascuzzi¹⁶⁷, J.M.P. Pasner¹⁴⁶, E. Pasqualucci^{72a}, S. Passaggio^{55b}, F. Pastore⁹³, P. Pasuwan^{45a,45b}, S. Pataraia⁹⁹, J.R. Pater¹⁰⁰, A. Pathak¹⁸¹, T. Pauly³⁶, B. Pearson¹¹⁵, M. Pedersen¹³⁴, L. Pedraza Diaz¹¹⁹, R. Pedro^{140a}, T. Peiffer⁵³, S.V. Peleganchuk^{122b,122a}, O. Penc¹⁴¹, H. Peng^{60a}, B.S. Peralva^{80a}, M.M. Perego¹³², A.P. Pereira Peixoto^{140a}, D.V. Perepelitsa²⁹, F. Peri¹⁹, L. Perini^{68a,68b}, H. Pernegger³⁶, S. Perrella^{69a,69b}, K. Peters⁴⁶, R.F.Y. Peters¹⁰⁰, B.A. Petersen³⁶, T.C. Petersen⁴⁰, E. Petit¹⁰¹, A. Petridis¹, C. Petridou¹⁶², P. Petroff¹³², M. Petrov¹³⁵, F. Petrucci^{74a,74b}, M. Pettee¹⁸³, N.E. Pettersson¹⁰², K. Petukhova¹⁴³, A. Peyaud¹⁴⁵, R. Pezoa^{147b}, L. Pezzotti^{70a,70b}, T. Pham¹⁰⁴, F.H. Phillips¹⁰⁶, P.W. Phillips¹⁴⁴, M.W. Phipps¹⁷³, G. Piacquadio¹⁵⁵, E. Pianori¹⁸, A. Picazio¹⁰², R.H. Pickles¹⁰⁰, R. Piegaia³⁰, D. Pietreanu^{27b}, J.E. Pilcher³⁷, A.D. Pilkington¹⁰⁰, M. Pinamonti^{73a,73b}, J.L. Pinfold³, M. Pitt¹⁸⁰, L. Pizzimento^{73a,73b}, M.-A. Pleier²⁹, V. Pleskot¹⁴³, E. Plotnikova⁷⁹, D. Pluth⁷⁸, P. Podberezko^{122b,122a}, R. Poettgen⁹⁶, R. Poggi⁵⁴, L. Poggiali¹³²,

I. Pogrebnyak¹⁰⁶, D. Pohl²⁴, I. Pokharel⁵³, G. Polesello^{70a}, A. Poley¹⁸, A. Policicchio^{72a,72b}, R. Polifka¹⁴³,
 A. Polini^{23b}, C.S. Pollard⁴⁶, V. Polychronakos²⁹, D. Ponomarenko¹¹², L. Pontecorvo³⁶, S. Popa^{27a},
 G.A. Popeneciu^{27d}, D.M. Portillo Quintero⁵⁸, S. Pospisil¹⁴², K. Potamianos⁴⁶, I.N. Potrap⁷⁹, C.J. Potter³²,
 H. Potti¹¹, T. Poulsen⁹⁶, J. Poveda³⁶, T.D. Powell¹⁴⁹, G. Pownall⁴⁶, M.E. Pozo Astigarraga³⁶,
 P. Pralavorio¹⁰¹, S. Prell⁷⁸, D. Price¹⁰⁰, M. Primavera^{67a}, S. Prince¹⁰³, M.L. Proffitt¹⁴⁸, N. Proklova¹¹²,
 K. Prokofiev^{63c}, F. Prokoshin⁷⁹, S. Protopopescu²⁹, J. Proudfoot⁶, M. Przybycien^{83a}, D. Pudzha¹³⁸,
 A. Puri¹⁷³, P. Puzo¹³², J. Qian¹⁰⁵, Y. Qin¹⁰⁰, A. Quadt⁵³, M. Queitsch-Maitland⁴⁶, A. Qureshi¹,
 P. Rados¹⁰⁴, F. Ragusa^{68a,68b}, G. Rahal⁹⁷, J.A. Raine⁵⁴, S. Rajagopalan²⁹, A. Ramirez Morales⁹²,
 K. Ran^{15a,15d}, T. Rashid¹³², S. Raspovov⁵, D.M. Rauch⁴⁶, F. Rauscher¹¹⁴, S. Rave⁹⁹, B. Ravina¹⁴⁹,
 I. Ravinovich¹⁸⁰, J.H. Rawling¹⁰⁰, M. Raymond³⁶, A.L. Read¹³⁴, N.P. Readloff⁵⁸, M. Reale^{67a,67b},
 D.M. Rebuzzi^{70a,70b}, A. Redelbach¹⁷⁷, G. Redlinger²⁹, K. Reeves⁴³, L. Rehnisch¹⁹, J. Reichert¹³⁷,
 D. Reikher¹⁶¹, A. Reiss⁹⁹, A. Rej¹⁵¹, C. Rembser³⁶, M. Renda^{27b}, M. Rescigno^{72a}, S. Resconi^{68a},
 E.D. Resseguei¹³⁷, S. Rettie¹⁷⁵, E. Reynolds²¹, O.L. Rezanova^{122b,122a}, P. Reznicek¹⁴³, E. Ricci^{75a,75b},
 R. Richter¹¹⁵, S. Richter⁴⁶, E. Richter-Was^{83b}, O. Ricken²⁴, M. Ridel¹³⁶, P. Rieck¹¹⁵, C.J. Riegel¹⁸²,
 O. Rifki⁴⁶, M. Rijssenbeek¹⁵⁵, A. Rimoldi^{70a,70b}, M. Rimoldi⁴⁶, L. Rinaldi^{23b}, G. Ripellino¹⁵⁴, B. Ristic⁸⁹,
 E. Ritsch³⁶, I. Riu¹⁴, J.C. Rivera Vergara¹⁷⁶, F. Rizatdinova¹²⁹, E. Rizvi⁹², C. Rizzi³⁶, R.T. Roberts¹⁰⁰,
 S.H. Robertson^{103,ah}, M. Robin⁴⁶, D. Robinson³², J.E.M. Robinson⁴⁶, C.M. Robles Gajardo^{147b},
 A. Robson⁵⁷, E. Rocco⁹⁹, C. Roda^{71a,71b}, S. Rodriguez Bosca¹⁷⁴, A. Rodriguez Perez¹⁴,
 D. Rodriguez Rodriguez¹⁷⁴, A.M. Rodríguez Vera^{168b}, S. Roe³⁶, O. Røhne¹³⁴, R. Röhrlig¹¹⁵,
 C.P.A. Roland⁶⁵, J. Roloff⁵⁹, A. Romaniouk¹¹², M. Romano^{23b,23a}, N. Rompotis⁹⁰, M. Ronzani¹²⁴,
 L. Roos¹³⁶, S. Rosati^{72a}, K. Rosbach⁵², G. Rosin¹⁰², B.J. Rosser¹³⁷, E. Rossi⁴⁶, E. Rossi^{74a,74b},
 E. Rossi^{69a,69b}, L.P. Rossi^{55b}, L. Rossini^{68a,68b}, R. Rosten¹⁴, M. Rotaru^{27b}, J. Rothberg¹⁴⁸, D. Rousseau¹³²,
 G. Rovelli^{70a,70b}, A. Roy¹¹, D. Roy^{33c}, A. Rozanov¹⁰¹, Y. Rozen¹⁶⁰, X. Ruan^{33c}, F. Rubbo¹⁵³, F. Rühr⁵²,
 A. Ruiz-Martinez¹⁷⁴, A. Rummller³⁶, Z. Rurikova⁵², N.A. Rusakovich⁷⁹, H.L. Russell¹⁰³, L. Rustige^{38,47},
 J.P. Rutherford⁷, E.M. Rüttinger^{46,1}, M. Rybar³⁹, G. Rybkin¹³², A. Ryzhov¹²³, G.F. Rzehorz⁵³,
 P. Sabatini⁵³, G. Sabato¹²⁰, S. Sacerdoti¹³², H.F-W. Sadrozinski¹⁴⁶, R. Sadykov⁷⁹, F. Safai Tehrani^{72a},
 B. Safarzadeh Samani¹⁵⁶, P. Saha¹²¹, S. Saha¹⁰³, M. Sahinsoy^{61a}, A. Sahu¹⁸², M. Saimpert⁴⁶, M. Saito¹⁶³,
 T. Saito¹⁶³, H. Sakamoto¹⁶³, A. Sakharov^{124,ar}, D. Salamani⁵⁴, G. Salamanna^{74a,74b},
 J.E. Salazar Loyola^{147b}, P.H. Sales De Bruin¹⁷², A. Salnikov¹⁵³, J. Salt¹⁷⁴, D. Salvatore^{41b,41a},
 F. Salvatore¹⁵⁶, A. Salvucci^{63a,63b,63c}, A. Salzburger³⁶, J. Samarati³⁶, D. Sammel⁵², D. Sampsonidis¹⁶²,
 D. Sampsonidou¹⁶², J. Sánchez¹⁷⁴, A. Sanchez Pineda^{66a,66c}, H. Sandaker¹³⁴, C.O. Sander⁴⁶,
 I.G. Sanderswood⁸⁹, M. Sandhoff¹⁸², C. Sandoval²², D.P.C. Sankey¹⁴⁴, M. Sannino^{55b,55a}, Y. Sano¹¹⁷,
 A. Sansoni⁵¹, C. Santoni³⁸, H. Santos^{140a,140b}, S.N. Santpur¹⁸, A. Santra¹⁷⁴, A. Sapronov⁷⁹,
 J.G. Saraiva^{140a,140d}, O. Sasaki⁸¹, K. Sato¹⁶⁹, E. Sauvan⁵, P. Savard^{167,bb}, N. Savic¹¹⁵, R. Sawada¹⁶³,
 C. Sawyer¹⁴⁴, L. Sawyer^{95,ap}, C. Sbarra^{23b}, A. Sbrizzi^{23a}, T. Scanlon⁹⁴, J. Schaarschmidt¹⁴⁸, P. Schacht¹¹⁵,
 B.M. Schachtner¹¹⁴, D. Schaefer³⁷, L. Schaefer¹³⁷, J. Schaeffer⁹⁹, S. Schaepe³⁶, U. Schäfer⁹⁹,
 A.C. Schaffer¹³², D. Schaile¹¹⁴, R.D. Schamberger¹⁵⁵, N. Scharmburg¹⁰⁰, V.A. Schegelsky¹³⁸,
 D. Scheirich¹⁴³, F. Schenck¹⁹, M. Schernau¹⁷¹, C. Schiavi^{55b,55a}, S. Schier¹⁴⁶, L.K. Schildgen²⁴,
 Z.M. Schillaci²⁶, E.J. Schioppa³⁶, M. Schioppa^{41b,41a}, K.E. Schleicher⁵², S. Schlenker³⁶,
 K.R. Schmidt-Sommerfeld¹¹⁵, K. Schmieden³⁶, C. Schmitt⁹⁹, S. Schmitt⁴⁶, S. Schmitz⁹⁹,
 J.C. Schmoeckel⁴⁶, U. Schnoor⁵², L. Schoeffel¹⁴⁵, A. Schoening^{61b}, P.G. Scholer⁵², E. Schopf¹³⁵,
 M. Schott⁹⁹, J.F.P. Schouwenberg¹¹⁹, J. Schovancova³⁶, S. Schramm⁵⁴, F. Schroeder¹⁸², A. Schulte⁹⁹,
 H-C. Schultz-Coulon^{61a}, M. Schumacher⁵², B.A. Schumm¹⁴⁶, Ph. Schune¹⁴⁵, A. Schwartzman¹⁵³,
 T.A. Schwarz¹⁰⁵, Ph. Schwemling¹⁴⁵, R. Schwienhorst¹⁰⁶, A. Sciandra¹⁴⁶, G. Sciolla²⁶, M. Scodeggio⁴⁶,
 M. Scornajenghi^{41b,41a}, F. Scuri^{71a}, F. Scutti¹⁰⁴, L.M. Scyboz¹¹⁵, C.D. Sebastiani^{72a,72b}, P. Seema¹⁹,
 S.C. Seidel¹¹⁸, A. Seiden¹⁴⁶, T. Seiss³⁷, J.M. Seixas^{80b}, G. Sekhniaidze^{69a}, K. Sekhon¹⁰⁵, S.J. Sekula⁴²,
 N. Semprini-Cesari^{23b,23a}, S. Sen⁴⁹, S. Senkin³⁸, C. Serfon⁷⁶, L. Serin¹³², L. Serkin^{66a,66b}, M. Sessa^{60a},

H. Severini¹²⁸, T. Šfiligoj⁹¹, F. Sforza¹⁷⁰, A. Sfyrla⁵⁴, E. Shabalina⁵³, J.D. Shahinian¹⁴⁶,
 N.W. Shaikh^{45a,45b}, D. Shaked Renous¹⁸⁰, L.Y. Shan^{15a}, R. Shang¹⁷³, J.T. Shank²⁵, M. Shapiro¹⁸,
 A. Sharma¹³⁵, A.S. Sharma¹, P.B. Shatalov¹¹¹, K. Shaw¹⁵⁶, S.M. Shaw¹⁰⁰, A. Shcherbakova¹³⁸,
 Y. Shen¹²⁸, N. Sherafati³⁴, A.D. Sherman²⁵, P. Sherwood⁹⁴, L. Shi^{158,ax}, S. Shimizu⁸¹, C.O. Shimmin¹⁸³,
 Y. Shimogama¹⁷⁹, M. Shimojima¹¹⁶, I.P.J. Shipsey¹³⁵, S. Shirabe⁸⁷, M. Shiyakova^{79,ae}, J. Shlomi¹⁸⁰,
 A. Shmeleva¹¹⁰, M.J. Shochet³⁷, J. Shojaei¹⁰⁴, D.R. Shope¹²⁸, S. Shrestha¹²⁶, E.M. Shrif^{33c}, E. Shulga¹⁸⁰,
 P. Sicho¹⁴¹, A.M. Sickles¹⁷³, P.E. Sidebo¹⁵⁴, E. Sideras Haddad^{33c}, O. Sidiropoulou³⁶, A. Sidoti^{23b,23a},
 F. Siegert⁴⁸, Dj. Sijacki¹⁶, M.Jr. Silva¹⁸¹, M.V. Silva Oliveira^{80a}, S.B. Silverstein^{45a}, S. Simion¹³²,
 E. Simioni⁹⁹, R. Simoniello⁹⁹, S. Simsek^{12b}, P. Sinervo¹⁶⁷, V. Sinetckii^{113,110}, N.B. Sinev¹³¹,
 M. Sioli^{23b,23a}, I. Siral¹⁰⁵, S.Yu. Sivoklokov¹¹³, J. Sjölin^{45a,45b}, E. Skorda⁹⁶, P. Skubic¹²⁸, M. Slawinska⁸⁴,
 K. Sliwa¹⁷⁰, R. Slovak¹⁴³, V. Smakhtin¹⁸⁰, B.H. Smart¹⁴⁴, J. Smiesko^{28a}, N. Smirnov¹¹²,
 S.Yu. Smirnov¹¹², Y. Smirnov¹¹², L.N. Smirnova^{113,x}, O. Smirnova⁹⁶, J.W. Smith⁵³, M. Smizanska⁸⁹,
 K. Smolek¹⁴², A. Smykiewicz⁸⁴, A.A. Snesarev¹¹⁰, H.L. Snoek¹²⁰, I.M. Snyder¹³¹, S. Snyder²⁹,
 R. Sobie^{176,ah}, A.M. Soffa¹⁷¹, A. Soffer¹⁶¹, A. Søgaard⁵⁰, F. Sohns⁵³, C.A. Solans Sanchez³⁶,
 E.Yu. Soldatov¹¹², U. Soldevila¹⁷⁴, A.A. Solodkov¹²³, A. Soloshenko⁷⁹, O.V. Solovyanov¹²³,
 V. Solovyev¹³⁸, P. Sommer¹⁴⁹, H. Son¹⁷⁰, W. Song¹⁴⁴, W.Y. Song^{168b}, A. Sopczak¹⁴², F. Sopkova^{28b},
 C.L. Sotiropoulou^{71a,71b}, S. Sottocornola^{70a,70b}, R. Soualah^{66a,66c,h}, A.M. Soukharev^{122b,122a}, D. South⁴⁶,
 S. Spagnolo^{67a,67b}, M. Spalla¹¹⁵, M. Spangenberg¹⁷⁸, F. Spanò⁹³, D. Sperlich⁵², T.M. Speker^{61a},
 R. Spighi^{23b}, G. Spigo³⁶, M. Spina¹⁵⁶, D.P. Spiteri⁵⁷, M. Spousta¹⁴³, A. Stabile^{68a,68b}, B.L. Stamas¹²¹,
 R. Stamen^{61a}, M. Stamenkovic¹²⁰, E. Stanecka⁸⁴, R.W. Stanek⁶, B. Stanislaus¹³⁵, M.M. Stanitzki⁴⁶,
 M. Stankaityte¹³⁵, B. Stapf¹²⁰, E.A. Starchenko¹²³, G.H. Stark¹⁴⁶, J. Stark⁵⁸, S.H. Stark⁴⁰, P. Staroba¹⁴¹,
 P. Starovoitov^{61a}, S. Stärz¹⁰³, R. Staszewski⁸⁴, G. Stavropoulos⁴⁴, M. Stegler⁴⁶, P. Steinberg²⁹,
 A.L. Steinhebel¹³¹, B. Stelzer¹⁵², H.J. Stelzer¹³⁹, O. Stelzer-Chilton^{168a}, H. Stenzel⁵⁶, T.J. Stevenson¹⁵⁶,
 G.A. Stewart³⁶, M.C. Stockton³⁶, G. Stoica^{27b}, M. Stolarski^{140a}, P. Stolte⁵³, S. Stonjek¹¹⁵,
 A. Straessner⁴⁸, J. Strandberg¹⁵⁴, S. Strandberg^{45a,45b}, M. Strauss¹²⁸, P. Strizenec^{28b}, R. Ströhmer¹⁷⁷,
 D.M. Strom¹³¹, R. Stroynowski⁴², A. Strubig⁵⁰, S.A. Stucci²⁹, B. Stugu¹⁷, J. Stupak¹²⁸, N.A. Styles⁴⁶,
 D. Su¹⁵³, S. Suchek^{61a}, V.V. Sulin¹¹⁰, M.J. Sullivan⁹⁰, D.M.S. Sultan⁵⁴, S. Sultansoy^{4c}, T. Sumida⁸⁵,
 S. Sun¹⁰⁵, X. Sun³, K. Suruliz¹⁵⁶, C.J.E. Suster¹⁵⁷, M.R. Sutton¹⁵⁶, S. Suzuki⁸¹, M. Svatos¹⁴¹,
 M. Swiatlowski³⁷, S.P. Swift², T. Swirski¹⁷⁷, A. Sydorenko⁹⁹, I. Sykora^{28a}, M. Sykora¹⁴³, T. Sykora¹⁴³,
 D. Ta⁹⁹, K. Tackmann^{46,ac}, J. Taenzer¹⁶¹, A. Taffard¹⁷¹, R. Tafirout^{168a}, H. Takai²⁹, R. Takashima⁸⁶,
 K. Takeda⁸², T. Takeshita¹⁵⁰, E.P. Takeva⁵⁰, Y. Takubo⁸¹, M. Talby¹⁰¹, A.A. Talyshev^{122b,122a},
 N.M. Tamir¹⁶¹, J. Tanaka¹⁶³, M. Tanaka¹⁶⁵, R. Tanaka¹³², S. Tapia Araya¹⁷³, S. Tapprogge⁹⁹,
 A. Tarek Abouelfadl Mohamed¹³⁶, S. Tarem¹⁶⁰, G. Tarna^{27b,d}, G.F. Tartarelli^{68a}, P. Tas¹⁴³, M. Tasevsky¹⁴¹,
 T. Tashiro⁸⁵, E. Tassi^{41b,41a}, A. Tavares Delgado^{140a,140b}, Y. Tayalati^{35e}, A.J. Taylor⁵⁰, G.N. Taylor¹⁰⁴,
 W. Taylor^{168b}, A.S. Tee⁸⁹, R. Teixeira De Lima¹⁵³, P. Teixeira-Dias⁹³, H. Ten Kate³⁶, J.J. Teoh¹²⁰,
 S. Terada⁸¹, K. Terashi¹⁶³, J. Terron⁹⁸, S. Terzo¹⁴, M. Testa⁵¹, R.J. Teuscher^{167,ah}, S.J. Thais¹⁸³,
 T. Theveneaux-Pelzer⁴⁶, F. Thiele⁴⁰, D.W. Thomas⁹³, J.O. Thomas⁴², J.P. Thomas²¹, A.S. Thompson⁵⁷,
 P.D. Thompson²¹, L.A. Thomsen¹⁸³, E. Thomson¹³⁷, E.J. Thorpe⁹², Y. Tian³⁹, R.E. Ticse Torres⁵³,
 V.O. Tikhomirov^{110,at}, Yu.A. Tikhonov^{122b,122a}, S. Timoshenko¹¹², P. Tipton¹⁸³, S. Tisserant¹⁰¹,
 K. Todome^{23b,23a}, S. Todorova-Nova⁵, S. Todt⁴⁸, J. Tojo⁸⁷, S. Tokár^{28a}, K. Tokushuku⁸¹, E. Tolley¹²⁶,
 K.G. Tomiwa^{33c}, M. Tomoto¹¹⁷, L. Tompkins^{153,s}, B. Tong⁵⁹, P. Tornambe¹⁰², E. Torrence¹³¹, H. Torres⁴⁸,
 E. Torró Pastor¹⁴⁸, C. Tosciri¹³⁵, J. Toth^{101,af}, D.R. Tovey¹⁴⁹, A. Traeet¹⁷, C.J. Treado¹²⁴, T. Trefzger¹⁷⁷,
 F. Tresoldi¹⁵⁶, A. Tricoli²⁹, I.M. Trigger^{168a}, S. Trincaz-Duvold¹³⁶, W. Trischuk¹⁶⁷, B. Trocmé⁵⁸,
 A. Trofymov¹⁴⁵, C. Troncon^{68a}, M. Trovatelli¹⁷⁶, F. Trovato¹⁵⁶, L. Truong^{33b}, M. Trzebinski⁸⁴,
 A. Trzupek⁸⁴, F. Tsai⁴⁶, J.C.-L. Tseng¹³⁵, P.V. Tsiareshka^{107,an}, A. Tsirigotis¹⁶², N. Tsirintanis⁹,
 V. Tsiskaridze¹⁵⁵, E.G. Tskhadadze^{159a}, M. Tsopoulou¹⁶², I.I. Tsukerman¹¹¹, V. Tsulaia¹⁸, S. Tsuno⁸¹,
 D. Tsybychev¹⁵⁵, Y. Tu^{63b}, A. Tudorache^{27b}, V. Tudorache^{27b}, T.T. Tulbure^{27a}, A.N. Tuna⁵⁹,

S. Turchikhin⁷⁹, D. Turgeman¹⁸⁰, I. Turk Cakir^{4b,y}, R.J. Turner²¹, R.T. Turra^{68a}, P.M. Tuts³⁹,
 S. Tzamarias¹⁶², E. Tzovara⁹⁹, G. Ucchielli⁴⁷, K. Uchida¹⁶³, I. Ueda⁸¹, M. Ughetto^{45a,45b}, F. Ukegawa¹⁶⁹,
 G. Unal³⁶, A. Undrus²⁹, G. Unel¹⁷¹, F.C. Ungaro¹⁰⁴, Y. Unno⁸¹, K. Uno¹⁶³, J. Urban^{28b}, P. Urquijo¹⁰⁴,
 G. Usai⁸, J. Usui⁸¹, Z. Uysal^{12d}, L. Vacavant¹⁰¹, V. Vacek¹⁴², B. Vachon¹⁰³, K.O.H. Vadla¹³⁴, A. Vaidya⁹⁴,
 C. Valderanis¹¹⁴, E. Valdes Santurio^{45a,45b}, M. Valente⁵⁴, S. Valentinetto^{23b,23a}, A. Valero¹⁷⁴, L. Valéry⁴⁶,
 R.A. Vallance²¹, A. Vallier³⁶, J.A. Valls Ferrer¹⁷⁴, T.R. Van Daalen¹⁴, P. Van Gemmeren⁶,
 I. Van Vulpen¹²⁰, M. Vanadia^{73a,73b}, W. Vandelli³⁶, A. Vaniachine¹⁶⁶, D. Vannicola^{72a,72b}, R. Vari^{72a},
 E.W. Varnes⁷, C. Varni^{55b,55a}, T. Varol⁴², D. Varouchas¹³², K.E. Varvell¹⁵⁷, M.E. Vasile^{27b},
 G.A. Vasquez¹⁷⁶, J.G. Vasquez¹⁸³, F. Vazeille³⁸, D. Vazquez Furelos¹⁴, T. Vazquez Schroeder³⁶,
 J. Veatch⁵³, V. Vecchio^{74a,74b}, M.J. Veen¹²⁰, L.M. Veloce¹⁶⁷, F. Veloso^{140a,140c}, S. Veneziano^{72a},
 A. Ventura^{67a,67b}, N. Venturi³⁶, A. Verbytskyi¹¹⁵, V. Vercesi^{70a}, M. Verducci^{74a,74b}, C.M. Vergel Infante⁷⁸,
 C. Vergis²⁴, W. Verkerke¹²⁰, A.T. Vermeulen¹²⁰, J.C. Vermeulen¹²⁰, M.C. Vetterli^{152,bb},
 N. Viaux Maira^{147b}, M. Vicente Barreto Pinto⁵⁴, T. Vickey¹⁴⁹, O.E. Vickey Boeriu¹⁴⁹,
 G.H.A. Viehhauser¹³⁵, L. Vigani¹³⁵, M. Villa^{23b,23a}, M. Villaplana Perez^{68a,68b}, E. Vilucchi⁵¹,
 M.G. Vincter³⁴, V.B. Vinogradov⁷⁹, A. Vishwakarma⁴⁶, C. Vittori^{23b,23a}, I. Vivarelli¹⁵⁶, M. Vogel¹⁸²,
 P. Vokac¹⁴², S.E. von Buddenbrock^{33c}, E. Von Toerne²⁴, V. Vorobel¹⁴³, K. Vorobev¹¹², M. Vos¹⁷⁴,
 J.H. Vossebeld⁹⁰, M. Vozak¹⁰⁰, N. Vranjes¹⁶, M. Vranjes Milosavljevic¹⁶, V. Vrba¹⁴², M. Vreeswijk¹²⁰,
 R. Vuillermet³⁶, I. Vukotic³⁷, P. Wagner²⁴, W. Wagner¹⁸², J. Wagner-Kuhr¹¹⁴, S. Wahdan¹⁸²,
 H. Wahlberg⁸⁸, K. Wakamiya⁸², V.M. Walbrecht¹¹⁵, J. Walder⁸⁹, R. Walker¹¹⁴, S.D. Walker⁹³,
 W. Walkowiak¹⁵¹, V. Wallangen^{45a,45b}, A.M. Wang⁵⁹, C. Wang^{60b}, F. Wang¹⁸¹, H. Wang¹⁸, H. Wang³,
 J. Wang¹⁵⁷, J. Wang^{61b}, P. Wang⁴², Q. Wang¹²⁸, R.-J. Wang⁹⁹, R. Wang^{60a}, R. Wang⁶, S.M. Wang¹⁵⁸,
 W.T. Wang^{60a}, W. Wang^{15c,ai}, W.X. Wang^{60a,ai}, Y. Wang^{60a,aq}, Z. Wang^{60c}, C. Wanotayaroj⁴⁶,
 A. Warburton¹⁰³, C.P. Ward³², D.R. Wardrope⁹⁴, N. Warrack⁵⁷, A. Washbrook⁵⁰, A.T. Watson²¹,
 M.F. Watson²¹, G. Watts¹⁴⁸, B.M. Waugh⁹⁴, A.F. Webb¹¹, S. Webb⁹⁹, C. Weber¹⁸³, M.S. Weber²⁰,
 S.A. Weber³⁴, S.M. Weber^{61a}, A.R. Weidberg¹³⁵, J. Weingarten⁴⁷, M. Weirich⁹⁹, C. Weiser⁵², P.S. Wells³⁶,
 T. Wenaus²⁹, T. Wengler³⁶, S. Wenig³⁶, N. Wermes²⁴, M.D. Werner⁷⁸, M. Wessels^{61a}, T.D. Weston²⁰,
 K. Whalen¹³¹, N.L. Whallon¹⁴⁸, A.M. Wharton⁸⁹, A.S. White¹⁰⁵, A. White⁸, M.J. White¹,
 D. Whiteson¹⁷¹, B.W. Whitmore⁸⁹, F.J. Wickens¹⁴⁴, W. Wiedenmann¹⁸¹, M. Wielers¹⁴⁴, N. Wieseotte⁹⁹,
 C. Wiglesworth⁴⁰, L.A.M. Wiik-Fuchs⁵², F. Wilk¹⁰⁰, H.G. Wilkens³⁶, L.J. Wilkins⁹³, H.H. Williams¹³⁷,
 S. Williams³², C. Willis¹⁰⁶, S. Willocq¹⁰², J.A. Wilson²¹, I. Wingerter-Seez⁵, E. Winkels¹⁵⁶,
 F. Winklmeier¹³¹, O.J. Winston¹⁵⁶, B.T. Winter⁵², M. Wittgen¹⁵³, M. Wobisch⁹⁵, A. Wolf⁹⁹,
 T.M.H. Wolf¹²⁰, R. Wolff¹⁰¹, R.W. Wölker¹³⁵, J. Wollrath⁵², M.W. Wolter⁸⁴, H. Wolters^{140a,140c},
 V.W.S. Wong¹⁷⁵, N.L. Woods¹⁴⁶, S.D. Worm²¹, B.K. Wosiek⁸⁴, K.W. Woźniak⁸⁴, K. Wraight⁵⁷,
 S.L. Wu¹⁸¹, X. Wu⁵⁴, Y. Wu^{60a}, T.R. Wyatt¹⁰⁰, B.M. Wynne⁵⁰, S. Xella⁴⁰, Z. Xi¹⁰⁵, L. Xia¹⁷⁸, D. Xu^{15a},
 H. Xu^{60a,d}, L. Xu²⁹, T. Xu¹⁴⁵, W. Xu¹⁰⁵, Z. Xu^{60b}, Z. Xu¹⁵³, B. Yabsley¹⁵⁷, S. Yacoob^{33a}, K. Yajima¹³³,
 D.P. Yallup⁹⁴, D. Yamaguchi¹⁶⁵, Y. Yamaguchi¹⁶⁵, A. Yamamoto⁸¹, T. Yamanaka¹⁶³, F. Yamane⁸²,
 M. Yamatani¹⁶³, T. Yamazaki¹⁶³, Y. Yamazaki⁸², Z. Yan²⁵, H.J. Yang^{60c,60d}, H.T. Yang¹⁸, S. Yang⁷⁷,
 X. Yang^{60b,58}, Y. Yang¹⁶³, W-M. Yao¹⁸, Y.C. Yap⁴⁶, Y. Yasu⁸¹, E. Yatsenko^{60c,60d}, J. Ye⁴², S. Ye²⁹,
 I. Yeletskikh⁷⁹, M.R. Yexley⁸⁹, E. Yigitbasi²⁵, K. Yorita¹⁷⁹, K. Yoshihara¹³⁷, C.J.S. Young³⁶, C. Young¹⁵³,
 J. Yu⁷⁸, R. Yuan^{60b,j}, X. Yue^{61a}, S.P.Y. Yuen²⁴, B. Zabinski⁸⁴, G. Zacharis¹⁰, E. Zaffaroni⁵⁴,
 J. Zahreddine¹³⁶, A.M. Zaitsev^{123,as}, T. Zakareishvili^{159b}, N. Zakharchuk³⁴, S. Zambito⁵⁹, D. Zanzi³⁶,
 D.R. Zaripovas⁵⁷, S.V. Zeißner⁴⁷, C. Zeitnitz¹⁸², G. Zemaityte¹³⁵, J.C. Zeng¹⁷³, O. Zenin¹²³, T. Ženiš^{28a},
 D. Zerwas¹³², M. Zgubić¹³⁵, D.F. Zhang^{15b}, F. Zhang¹⁸¹, G. Zhang^{60a}, G. Zhang^{15b}, H. Zhang^{15c},
 J. Zhang⁶, L. Zhang^{15c}, L. Zhang^{60a}, M. Zhang¹⁷³, R. Zhang^{60a}, R. Zhang²⁴, X. Zhang^{60b}, Y. Zhang^{15a,15d},
 Z. Zhang^{63a}, Z. Zhang¹³², P. Zhao⁴⁹, Y. Zhao^{60b}, Z. Zhao^{60a}, A. Zhemchugov⁷⁹, Z. Zheng¹⁰⁵, D. Zhong¹⁷³,
 B. Zhou¹⁰⁵, C. Zhou¹⁸¹, M.S. Zhou^{15a,15d}, M. Zhou¹⁵⁵, N. Zhou^{60c}, Y. Zhou⁷, C.G. Zhu^{60b}, H.L. Zhu^{60a},
 H. Zhu^{15a}, J. Zhu¹⁰⁵, Y. Zhu^{60a}, X. Zhuang^{15a}, K. Zhukov¹¹⁰, V. Zhulanov^{122b,122a}, D. Ziemińska⁶⁵,

N.I. Zimine⁷⁹, S. Zimmermann⁵², Z. Zinonos¹¹⁵, M. Ziolkowski¹⁵¹, L. Živković¹⁶, G. Zobernig¹⁸¹, A. Zoccoli^{23b,23a}, K. Zoch⁵³, T.G. Zorbas¹⁴⁹, R. Zou³⁷, L. Zwalski³⁶.

¹Department of Physics, University of Adelaide, Adelaide; Australia.

²Physics Department, SUNY Albany, Albany NY; United States of America.

³Department of Physics, University of Alberta, Edmonton AB; Canada.

^{4(a)}Department of Physics, Ankara University, Ankara; ^(b)Istanbul Aydin University, Istanbul; ^(c)Division of Physics, TOBB University of Economics and Technology, Ankara; Turkey.

⁵LAPP, Université Grenoble Alpes, Université Savoie Mont Blanc, CNRS/IN2P3, Annecy; France.

⁶High Energy Physics Division, Argonne National Laboratory, Argonne IL; United States of America.

⁷Department of Physics, University of Arizona, Tucson AZ; United States of America.

⁸Department of Physics, University of Texas at Arlington, Arlington TX; United States of America.

⁹Physics Department, National and Kapodistrian University of Athens, Athens; Greece.

¹⁰Physics Department, National Technical University of Athens, Zografou; Greece.

¹¹Department of Physics, University of Texas at Austin, Austin TX; United States of America.

^{12(a)}Bahcesehir University, Faculty of Engineering and Natural Sciences, Istanbul; ^(b)Istanbul Bilgi University, Faculty of Engineering and Natural Sciences, Istanbul; ^(c)Department of Physics, Bogazici University, Istanbul; ^(d)Department of Physics Engineering, Gaziantep University, Gaziantep; Turkey.

¹³Institute of Physics, Azerbaijan Academy of Sciences, Baku; Azerbaijan.

¹⁴Institut de Física d'Altes Energies (IFAE), Barcelona Institute of Science and Technology, Barcelona; Spain.

^{15(a)}Institute of High Energy Physics, Chinese Academy of Sciences, Beijing; ^(b)Physics Department, Tsinghua University, Beijing; ^(c)Department of Physics, Nanjing University, Nanjing; ^(d)University of Chinese Academy of Science (UCAS), Beijing; China.

¹⁶Institute of Physics, University of Belgrade, Belgrade; Serbia.

¹⁷Department for Physics and Technology, University of Bergen, Bergen; Norway.

¹⁸Physics Division, Lawrence Berkeley National Laboratory and University of California, Berkeley CA; United States of America.

¹⁹Institut für Physik, Humboldt Universität zu Berlin, Berlin; Germany.

²⁰Albert Einstein Center for Fundamental Physics and Laboratory for High Energy Physics, University of Bern, Bern; Switzerland.

²¹School of Physics and Astronomy, University of Birmingham, Birmingham; United Kingdom.

²²Facultad de Ciencias y Centro de Investigaciones, Universidad Antonio Nariño, Bogota; Colombia.

^{23(a)}INFN Bologna and Universita' di Bologna, Dipartimento di Fisica; ^(b)INFN Sezione di Bologna; Italy.

²⁴Physikalisches Institut, Universität Bonn, Bonn; Germany.

²⁵Department of Physics, Boston University, Boston MA; United States of America.

²⁶Department of Physics, Brandeis University, Waltham MA; United States of America.

^{27(a)}Transilvania University of Brasov, Brasov; ^(b)Horia Hulubei National Institute of Physics and Nuclear Engineering, Bucharest; ^(c)Department of Physics, Alexandru Ioan Cuza University of Iasi, Iasi; ^(d)National Institute for Research and Development of Isotopic and Molecular Technologies, Physics Department, Cluj-Napoca; ^(e)University Politehnica Bucharest, Bucharest; ^(f)West University in Timisoara, Timisoara; Romania.

^{28(a)}Faculty of Mathematics, Physics and Informatics, Comenius University, Bratislava; ^(b)Department of Subnuclear Physics, Institute of Experimental Physics of the Slovak Academy of Sciences, Kosice; Slovak Republic.

²⁹Physics Department, Brookhaven National Laboratory, Upton NY; United States of America.

³⁰Departamento de Física, Universidad de Buenos Aires, Buenos Aires; Argentina.

- ³¹California State University, CA; United States of America.
- ³²Cavendish Laboratory, University of Cambridge, Cambridge; United Kingdom.
- ^{33(a)}Department of Physics, University of Cape Town, Cape Town;^(b)Department of Mechanical Engineering Science, University of Johannesburg, Johannesburg;^(c)School of Physics, University of the Witwatersrand, Johannesburg; South Africa.
- ³⁴Department of Physics, Carleton University, Ottawa ON; Canada.
- ^{35(a)}Faculté des Sciences Ain Chock, Réseau Universitaire de Physique des Hautes Energies - Université Hassan II, Casablanca;^(b)Faculté des Sciences, Université Ibn-Tofail, Kénitra;^(c)Faculté des Sciences Semlalia, Université Cadi Ayyad, LPHEA-Marrakech;^(d)Faculté des Sciences, Université Mohamed Premier and LPTPM, Oujda;^(e)Faculté des sciences, Université Mohammed V, Rabat; Morocco.
- ³⁶CERN, Geneva; Switzerland.
- ³⁷Enrico Fermi Institute, University of Chicago, Chicago IL; United States of America.
- ³⁸LPC, Université Clermont Auvergne, CNRS/IN2P3, Clermont-Ferrand; France.
- ³⁹Nevis Laboratory, Columbia University, Irvington NY; United States of America.
- ⁴⁰Niels Bohr Institute, University of Copenhagen, Copenhagen; Denmark.
- ^{41(a)}Dipartimento di Fisica, Università della Calabria, Rende;^(b)INFN Gruppo Collegato di Cosenza, Laboratori Nazionali di Frascati; Italy.
- ⁴²Physics Department, Southern Methodist University, Dallas TX; United States of America.
- ⁴³Physics Department, University of Texas at Dallas, Richardson TX; United States of America.
- ⁴⁴National Centre for Scientific Research "Demokritos", Agia Paraskevi; Greece.
- ^{45(a)}Department of Physics, Stockholm University;^(b)Oskar Klein Centre, Stockholm; Sweden.
- ⁴⁶Deutsches Elektronen-Synchrotron DESY, Hamburg and Zeuthen; Germany.
- ⁴⁷Lehrstuhl für Experimentelle Physik IV, Technische Universität Dortmund, Dortmund; Germany.
- ⁴⁸Institut für Kern- und Teilchenphysik, Technische Universität Dresden, Dresden; Germany.
- ⁴⁹Department of Physics, Duke University, Durham NC; United States of America.
- ⁵⁰SUPA - School of Physics and Astronomy, University of Edinburgh, Edinburgh; United Kingdom.
- ⁵¹INFN e Laboratori Nazionali di Frascati, Frascati; Italy.
- ⁵²Physikalisch Institut, Albert-Ludwigs-Universität Freiburg, Freiburg; Germany.
- ⁵³II. Physikalisch Institut, Georg-August-Universität Göttingen, Göttingen; Germany.
- ⁵⁴Département de Physique Nucléaire et Corpusculaire, Université de Genève, Genève; Switzerland.
- ^{55(a)}Dipartimento di Fisica, Università di Genova, Genova;^(b)INFN Sezione di Genova; Italy.
- ⁵⁶II. Physikalisch Institut, Justus-Liebig-Universität Giessen, Giessen; Germany.
- ⁵⁷SUPA - School of Physics and Astronomy, University of Glasgow, Glasgow; United Kingdom.
- ⁵⁸LPSC, Université Grenoble Alpes, CNRS/IN2P3, Grenoble INP, Grenoble; France.
- ⁵⁹Laboratory for Particle Physics and Cosmology, Harvard University, Cambridge MA; United States of America.
- ^{60(a)}Department of Modern Physics and State Key Laboratory of Particle Detection and Electronics, University of Science and Technology of China, Hefei;^(b)Institute of Frontier and Interdisciplinary Science and Key Laboratory of Particle Physics and Particle Irradiation (MOE), Shandong University, Qingdao;^(c)School of Physics and Astronomy, Shanghai Jiao Tong University, KLPPAC-MoE, SKLPPC, Shanghai;^(d)Tsung-Dao Lee Institute, Shanghai; China.
- ^{61(a)}Kirchhoff-Institut für Physik, Ruprecht-Karls-Universität Heidelberg, Heidelberg;^(b)Physikalisches Institut, Ruprecht-Karls-Universität Heidelberg, Heidelberg; Germany.
- ⁶²Faculty of Applied Information Science, Hiroshima Institute of Technology, Hiroshima; Japan.
- ^{63(a)}Department of Physics, Chinese University of Hong Kong, Shatin, N.T., Hong Kong;^(b)Department of Physics, University of Hong Kong, Hong Kong;^(c)Department of Physics and Institute for Advanced Study, Hong Kong University of Science and Technology, Clear Water Bay, Kowloon, Hong Kong; China.

- ⁶⁴Department of Physics, National Tsing Hua University, Hsinchu; Taiwan.
- ⁶⁵Department of Physics, Indiana University, Bloomington IN; United States of America.
- ^{66(a)}INFN Gruppo Collegato di Udine, Sezione di Trieste, Udine;^(b)ICTP, Trieste;^(c)Dipartimento Politecnico di Ingegneria e Architettura, Università di Udine, Udine; Italy.
- ^{67(a)}INFN Sezione di Lecce;^(b)Dipartimento di Matematica e Fisica, Università del Salento, Lecce; Italy.
- ^{68(a)}INFN Sezione di Milano;^(b)Dipartimento di Fisica, Università di Milano, Milano; Italy.
- ^{69(a)}INFN Sezione di Napoli;^(b)Dipartimento di Fisica, Università di Napoli, Napoli; Italy.
- ^{70(a)}INFN Sezione di Pavia;^(b)Dipartimento di Fisica, Università di Pavia, Pavia; Italy.
- ^{71(a)}INFN Sezione di Pisa;^(b)Dipartimento di Fisica E. Fermi, Università di Pisa, Pisa; Italy.
- ^{72(a)}INFN Sezione di Roma;^(b)Dipartimento di Fisica, Sapienza Università di Roma, Roma; Italy.
- ^{73(a)}INFN Sezione di Roma Tor Vergata;^(b)Dipartimento di Fisica, Università di Roma Tor Vergata, Roma; Italy.
- ^{74(a)}INFN Sezione di Roma Tre;^(b)Dipartimento di Matematica e Fisica, Università Roma Tre, Roma; Italy.
- ^{75(a)}INFN-TIFPA;^(b)Università degli Studi di Trento, Trento; Italy.
- ⁷⁶Institut für Astro- und Teilchenphysik, Leopold-Franzens-Universität, Innsbruck; Austria.
- ⁷⁷University of Iowa, Iowa City IA; United States of America.
- ⁷⁸Department of Physics and Astronomy, Iowa State University, Ames IA; United States of America.
- ⁷⁹Joint Institute for Nuclear Research, Dubna; Russia.
- ^{80(a)}Departamento de Engenharia Elétrica, Universidade Federal de Juiz de Fora (UFJF), Juiz de Fora;^(b)Universidade Federal do Rio De Janeiro COPPE/EE/IF, Rio de Janeiro;^(c)Universidade Federal de São João del Rei (UFSJ), São João del Rei;^(d)Instituto de Física, Universidade de São Paulo, São Paulo; Brazil.
- ⁸¹KEK, High Energy Accelerator Research Organization, Tsukuba; Japan.
- ⁸²Graduate School of Science, Kobe University, Kobe; Japan.
- ^{83(a)}AGH University of Science and Technology, Faculty of Physics and Applied Computer Science, Krakow;^(b)Marian Smoluchowski Institute of Physics, Jagiellonian University, Krakow; Poland.
- ⁸⁴Institute of Nuclear Physics Polish Academy of Sciences, Krakow; Poland.
- ⁸⁵Faculty of Science, Kyoto University, Kyoto; Japan.
- ⁸⁶Kyoto University of Education, Kyoto; Japan.
- ⁸⁷Research Center for Advanced Particle Physics and Department of Physics, Kyushu University, Fukuoka ; Japan.
- ⁸⁸Instituto de Física La Plata, Universidad Nacional de La Plata and CONICET, La Plata; Argentina.
- ⁸⁹Physics Department, Lancaster University, Lancaster; United Kingdom.
- ⁹⁰Oliver Lodge Laboratory, University of Liverpool, Liverpool; United Kingdom.
- ⁹¹Department of Experimental Particle Physics, Jožef Stefan Institute and Department of Physics, University of Ljubljana, Ljubljana; Slovenia.
- ⁹²School of Physics and Astronomy, Queen Mary University of London, London; United Kingdom.
- ⁹³Department of Physics, Royal Holloway University of London, Egham; United Kingdom.
- ⁹⁴Department of Physics and Astronomy, University College London, London; United Kingdom.
- ⁹⁵Louisiana Tech University, Ruston LA; United States of America.
- ⁹⁶Fysiska institutionen, Lunds universitet, Lund; Sweden.
- ⁹⁷Centre de Calcul de l’Institut National de Physique Nucléaire et de Physique des Particules (IN2P3), Villeurbanne; France.
- ⁹⁸Departamento de Física Teorica C-15 and CIAFF, Universidad Autónoma de Madrid, Madrid; Spain.
- ⁹⁹Institut für Physik, Universität Mainz, Mainz; Germany.
- ¹⁰⁰School of Physics and Astronomy, University of Manchester, Manchester; United Kingdom.
- ¹⁰¹CPPM, Aix-Marseille Université, CNRS/IN2P3, Marseille; France.

- ¹⁰²Department of Physics, University of Massachusetts, Amherst MA; United States of America.
- ¹⁰³Department of Physics, McGill University, Montreal QC; Canada.
- ¹⁰⁴School of Physics, University of Melbourne, Victoria; Australia.
- ¹⁰⁵Department of Physics, University of Michigan, Ann Arbor MI; United States of America.
- ¹⁰⁶Department of Physics and Astronomy, Michigan State University, East Lansing MI; United States of America.
- ¹⁰⁷B.I. Stepanov Institute of Physics, National Academy of Sciences of Belarus, Minsk; Belarus.
- ¹⁰⁸Research Institute for Nuclear Problems of Byelorussian State University, Minsk; Belarus.
- ¹⁰⁹Group of Particle Physics, University of Montreal, Montreal QC; Canada.
- ¹¹⁰P.N. Lebedev Physical Institute of the Russian Academy of Sciences, Moscow; Russia.
- ¹¹¹Institute for Theoretical and Experimental Physics of the National Research Centre Kurchatov Institute, Moscow; Russia.
- ¹¹²National Research Nuclear University MEPhI, Moscow; Russia.
- ¹¹³D.V. Skobeltsyn Institute of Nuclear Physics, M.V. Lomonosov Moscow State University, Moscow; Russia.
- ¹¹⁴Fakultät für Physik, Ludwig-Maximilians-Universität München, München; Germany.
- ¹¹⁵Max-Planck-Institut für Physik (Werner-Heisenberg-Institut), München; Germany.
- ¹¹⁶Nagasaki Institute of Applied Science, Nagasaki; Japan.
- ¹¹⁷Graduate School of Science and Kobayashi-Maskawa Institute, Nagoya University, Nagoya; Japan.
- ¹¹⁸Department of Physics and Astronomy, University of New Mexico, Albuquerque NM; United States of America.
- ¹¹⁹Institute for Mathematics, Astrophysics and Particle Physics, Radboud University Nijmegen/Nikhef, Nijmegen; Netherlands.
- ¹²⁰Nikhef National Institute for Subatomic Physics and University of Amsterdam, Amsterdam; Netherlands.
- ¹²¹Department of Physics, Northern Illinois University, DeKalb IL; United States of America.
- ^{122(a)}Budker Institute of Nuclear Physics and NSU, SB RAS, Novosibirsk;^(b)Novosibirsk State University Novosibirsk; Russia.
- ¹²³Institute for High Energy Physics of the National Research Centre Kurchatov Institute, Protvino; Russia.
- ¹²⁴Department of Physics, New York University, New York NY; United States of America.
- ¹²⁵Ochanomizu University, Otsuka, Bunkyo-ku, Tokyo; Japan.
- ¹²⁶Ohio State University, Columbus OH; United States of America.
- ¹²⁷Faculty of Science, Okayama University, Okayama; Japan.
- ¹²⁸Homer L. Dodge Department of Physics and Astronomy, University of Oklahoma, Norman OK; United States of America.
- ¹²⁹Department of Physics, Oklahoma State University, Stillwater OK; United States of America.
- ¹³⁰Palacký University, RCPTM, Joint Laboratory of Optics, Olomouc; Czech Republic.
- ¹³¹Center for High Energy Physics, University of Oregon, Eugene OR; United States of America.
- ¹³²LAL, Université Paris-Sud, CNRS/IN2P3, Université Paris-Saclay, Orsay; France.
- ¹³³Graduate School of Science, Osaka University, Osaka; Japan.
- ¹³⁴Department of Physics, University of Oslo, Oslo; Norway.
- ¹³⁵Department of Physics, Oxford University, Oxford; United Kingdom.
- ¹³⁶LPNHE, Sorbonne Université, Université de Paris, CNRS/IN2P3, Paris; France.
- ¹³⁷Department of Physics, University of Pennsylvania, Philadelphia PA; United States of America.
- ¹³⁸Konstantinov Nuclear Physics Institute of National Research Centre "Kurchatov Institute", PNPI, St. Petersburg; Russia.
- ¹³⁹Department of Physics and Astronomy, University of Pittsburgh, Pittsburgh PA; United States of

America.

¹⁴⁰(^a)Laboratório de Instrumentação e Física Experimental de Partículas - LIP, Lisbon;(^b)Departamento de Física, Faculdade de Ciências, Universidade de Lisboa, Lisbon;(^c)Departamento de Física, Universidade de Coimbra, Coimbra;(^d)Centro de Física Nuclear da Universidade de Lisboa, Lisbon;(^e)Departamento de Física, Universidade do Minho, Braga;(^f)Universidad de Granada, Granada (Spain);(^g)Dep Física and CEFITEC of Faculdade de Ciências e Tecnologia, Universidade Nova de Lisboa, Caparica;(^h)Av. Rovisco Pais, 1 1049-001 Lisbon, Portugal; Portugal.

¹⁴¹Institute of Physics of the Czech Academy of Sciences, Prague; Czech Republic.

¹⁴²Czech Technical University in Prague, Prague; Czech Republic.

¹⁴³Charles University, Faculty of Mathematics and Physics, Prague; Czech Republic.

¹⁴⁴Particle Physics Department, Rutherford Appleton Laboratory, Didcot; United Kingdom.

¹⁴⁵IRFU, CEA, Université Paris-Saclay, Gif-sur-Yvette; France.

¹⁴⁶Santa Cruz Institute for Particle Physics, University of California Santa Cruz, Santa Cruz CA; United States of America.

¹⁴⁷(^a)Departamento de Física, Pontificia Universidad Católica de Chile, Santiago;(^b)Departamento de Física, Universidad Técnica Federico Santa María, Valparaíso; Chile.

¹⁴⁸Department of Physics, University of Washington, Seattle WA; United States of America.

¹⁴⁹Department of Physics and Astronomy, University of Sheffield, Sheffield; United Kingdom.

¹⁵⁰Department of Physics, Shinshu University, Nagano; Japan.

¹⁵¹Department Physik, Universität Siegen, Siegen; Germany.

¹⁵²Department of Physics, Simon Fraser University, Burnaby BC; Canada.

¹⁵³SLAC National Accelerator Laboratory, Stanford CA; United States of America.

¹⁵⁴Physics Department, Royal Institute of Technology, Stockholm; Sweden.

¹⁵⁵Departments of Physics and Astronomy, Stony Brook University, Stony Brook NY; United States of America.

¹⁵⁶Department of Physics and Astronomy, University of Sussex, Brighton; United Kingdom.

¹⁵⁷School of Physics, University of Sydney, Sydney; Australia.

¹⁵⁸Institute of Physics, Academia Sinica, Taipei; Taiwan.

¹⁵⁹(^a)E. Andronikashvili Institute of Physics, Iv. Javakhishvili Tbilisi State University, Tbilisi;(^b)High Energy Physics Institute, Tbilisi State University, Tbilisi; Georgia.

¹⁶⁰Department of Physics, Technion, Israel Institute of Technology, Haifa; Israel.

¹⁶¹Raymond and Beverly Sackler School of Physics and Astronomy, Tel Aviv University, Tel Aviv; Israel.

¹⁶²Department of Physics, Aristotle University of Thessaloniki, Thessaloniki; Greece.

¹⁶³International Center for Elementary Particle Physics and Department of Physics, University of Tokyo, Tokyo; Japan.

¹⁶⁴Graduate School of Science and Technology, Tokyo Metropolitan University, Tokyo; Japan.

¹⁶⁵Department of Physics, Tokyo Institute of Technology, Tokyo; Japan.

¹⁶⁶Tomsk State University, Tomsk; Russia.

¹⁶⁷Department of Physics, University of Toronto, Toronto ON; Canada.

¹⁶⁸(^a)TRIUMF, Vancouver BC;(^b)Department of Physics and Astronomy, York University, Toronto ON; Canada.

¹⁶⁹Division of Physics and Tomonaga Center for the History of the Universe, Faculty of Pure and Applied Sciences, University of Tsukuba, Tsukuba; Japan.

¹⁷⁰Department of Physics and Astronomy, Tufts University, Medford MA; United States of America.

¹⁷¹Department of Physics and Astronomy, University of California Irvine, Irvine CA; United States of America.

¹⁷²Department of Physics and Astronomy, University of Uppsala, Uppsala; Sweden.

- ¹⁷³Department of Physics, University of Illinois, Urbana IL; United States of America.
- ¹⁷⁴Instituto de Física Corpuscular (IFIC), Centro Mixto Universidad de Valencia - CSIC, Valencia; Spain.
- ¹⁷⁵Department of Physics, University of British Columbia, Vancouver BC; Canada.
- ¹⁷⁶Department of Physics and Astronomy, University of Victoria, Victoria BC; Canada.
- ¹⁷⁷Fakultät für Physik und Astronomie, Julius-Maximilians-Universität Würzburg, Würzburg; Germany.
- ¹⁷⁸Department of Physics, University of Warwick, Coventry; United Kingdom.
- ¹⁷⁹Waseda University, Tokyo; Japan.
- ¹⁸⁰Department of Particle Physics, Weizmann Institute of Science, Rehovot; Israel.
- ¹⁸¹Department of Physics, University of Wisconsin, Madison WI; United States of America.
- ¹⁸²Fakultät für Mathematik und Naturwissenschaften, Fachgruppe Physik, Bergische Universität Wuppertal, Wuppertal; Germany.
- ¹⁸³Department of Physics, Yale University, New Haven CT; United States of America.
- ¹⁸⁴Yerevan Physics Institute, Yerevan; Armenia.
- ^a Also at Borough of Manhattan Community College, City University of New York, New York NY; United States of America.
- ^b Also at Centre for High Performance Computing, CSIR Campus, Rosebank, Cape Town; South Africa.
- ^c Also at CERN, Geneva; Switzerland.
- ^d Also at CPPM, Aix-Marseille Université, CNRS/IN2P3, Marseille; France.
- ^e Also at Département de Physique Nucléaire et Corpusculaire, Université de Genève, Genève; Switzerland.
- ^f Also at Departament de Fisica de la Universitat Autònoma de Barcelona, Barcelona; Spain.
- ^g Also at Departamento de Física, Instituto Superior Técnico, Universidade de Lisboa, Lisboa; Portugal.
- ^h Also at Department of Applied Physics and Astronomy, University of Sharjah, Sharjah; United Arab Emirates.
- ⁱ Also at Department of Financial and Management Engineering, University of the Aegean, Chios; Greece.
- ^j Also at Department of Physics and Astronomy, Michigan State University, East Lansing MI; United States of America.
- ^k Also at Department of Physics and Astronomy, University of Louisville, Louisville, KY; United States of America.
- ^l Also at Department of Physics and Astronomy, University of Sheffield, Sheffield; United Kingdom.
- ^m Also at Department of Physics, Ben Gurion University of the Negev, Beer Sheva; Israel.
- ⁿ Also at Department of Physics, California State University, East Bay; United States of America.
- ^o Also at Department of Physics, California State University, Fresno; United States of America.
- ^p Also at Department of Physics, California State University, Sacramento; United States of America.
- ^q Also at Department of Physics, King's College London, London; United Kingdom.
- ^r Also at Department of Physics, St. Petersburg State Polytechnical University, St. Petersburg; Russia.
- ^s Also at Department of Physics, Stanford University, Stanford CA; United States of America.
- ^t Also at Department of Physics, University of Adelaide, Adelaide; Australia.
- ^u Also at Department of Physics, University of Fribourg, Fribourg; Switzerland.
- ^v Also at Department of Physics, University of Michigan, Ann Arbor MI; United States of America.
- ^w Also at Dipartimento di Matematica, Informatica e Fisica, Università di Udine, Udine; Italy.
- ^x Also at Faculty of Physics, M.V. Lomonosov Moscow State University, Moscow; Russia.
- ^y Also at Giresun University, Faculty of Engineering, Giresun; Turkey.
- ^z Also at Graduate School of Science, Osaka University, Osaka; Japan.
- ^{aa} Also at Hellenic Open University, Patras; Greece.
- ^{ab} Also at Institutio Catalana de Recerca i Estudis Avancats, ICREA, Barcelona; Spain.
- ^{ac} Also at Institut für Experimentalphysik, Universität Hamburg, Hamburg; Germany.

- ad* Also at Institute for Mathematics, Astrophysics and Particle Physics, Radboud University Nijmegen/Nikhef, Nijmegen; Netherlands.
- ae* Also at Institute for Nuclear Research and Nuclear Energy (INRNE) of the Bulgarian Academy of Sciences, Sofia; Bulgaria.
- af* Also at Institute for Particle and Nuclear Physics, Wigner Research Centre for Physics, Budapest; Hungary.
- ag* Also at Institute of High Energy Physics, Chinese Academy of Sciences, Beijing; China.
- ah* Also at Institute of Particle Physics (IPP), Vancouver; Canada.
- ai* Also at Institute of Physics, Academia Sinica, Taipei; Taiwan.
- aj* Also at Institute of Physics, Azerbaijan Academy of Sciences, Baku; Azerbaijan.
- ak* Also at Institute of Theoretical Physics, Ilia State University, Tbilisi; Georgia.
- al* Also at Instituto de Fisica Teorica, IFT-UAM/CSIC, Madrid; Spain.
- am* Also at Istanbul University, Dept. of Physics, Istanbul; Turkey.
- an* Also at Joint Institute for Nuclear Research, Dubna; Russia.
- ao* Also at LAL, Université Paris-Sud, CNRS/IN2P3, Université Paris-Saclay, Orsay; France.
- ap* Also at Louisiana Tech University, Ruston LA; United States of America.
- aq* Also at LPNHE, Sorbonne Université, Université de Paris, CNRS/IN2P3, Paris; France.
- ar* Also at Manhattan College, New York NY; United States of America.
- as* Also at Moscow Institute of Physics and Technology State University, Dolgoprudny; Russia.
- at* Also at National Research Nuclear University MEPhI, Moscow; Russia.
- au* Also at Physics Department, An-Najah National University, Nablus; Palestine.
- av* Also at Physics Dept, University of South Africa, Pretoria; South Africa.
- aw* Also at Physikalisches Institut, Albert-Ludwigs-Universität Freiburg, Freiburg; Germany.
- ax* Also at School of Physics, Sun Yat-sen University, Guangzhou; China.
- ay* Also at The City College of New York, New York NY; United States of America.
- az* Also at The Collaborative Innovation Center of Quantum Matter (CICQM), Beijing; China.
- ba* Also at Tomsk State University, Tomsk, and Moscow Institute of Physics and Technology State University, Dolgoprudny; Russia.
- bb* Also at TRIUMF, Vancouver BC; Canada.
- bc* Also at Universita di Napoli Parthenope, Napoli; Italy.

* Deceased